

# **STUDIES ON FIREBALL FORMATION ASSOCIATED WITH AIRCRAFT CRASH**

*By*  
**ASHISH V. SHELKE**  
**ENGG 01201304011**

**Bhabha Atomic Research Centre, Mumbai**

*A thesis submitted to the  
Board of Studies in Engineering Sciences*

*In partial fulfillment of requirements  
for the Degree of*

**DOCTOR OF PHILOSOPHY**

*of*

**HOMI BHABHA NATIONAL INSTITUTE**



**August 2019**



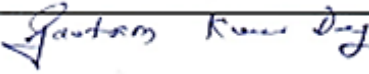
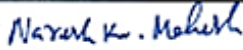
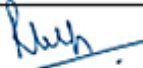
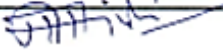
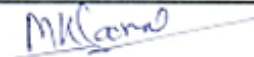
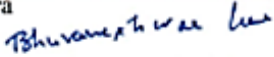
# Homi Bhabha National Institute<sup>1</sup>

## Recommendations of the Viva Voce Committee

As members of the Viva Voce Committee, we certify that we have read the dissertation prepared by *Ashish V. Shelke* entitled *Studies on Fireball Formation Associated with Aircraft crash* and recommend that it may be accepted as fulfilling the thesis requirement for the award of Degree of Doctor of Philosophy.

Final approval and acceptance of this thesis is contingent upon the candidate's submission of the final copies of the thesis to HBNI.

I/We hereby certify that I/we have read this thesis prepared under my/our direction and recommend that it may be accepted as fulfilling the thesis requirement.

Chairman – Dr. G. K. Dey		Date: 9/8/2019
Guide / Convener – Dr. N. K. Maheshwari		Date: 9/8/2019
Co-guide - Dr. R. K. Singh		Date: 9/8/19
Examiner - Prof. A. Patwardhan		Date: 9/8/19
Member 1- Dr. A. P. Tiwari		Date: 09-8-19
Member 2- Dr. J. Chattopadhyay		Date: 9/8/19
Member 3- Dr. M. K. Samal		Date: 09.08.2019
Member 4- Dr. A. Chakravarty		Date: 9/8/19
Tech. Adviser:-Mr. B. Gera		Date: 09/08/2019

Final approval and acceptance of this thesis is contingent upon the candidate's submission of the final copies of the thesis to HBNI.

We hereby certify that we have read this thesis prepared under our direction and recommend that it may be accepted as fulfilling the thesis requirement.

Date: 09/08/2019

Place: MUMBAI

  
Guide

Dr. N. K. Maheshwari

<sup>1</sup> This page is to be included only for final submission after successful completion of viva voce.



## **STATEMENT BY AUTHOR**

This dissertation has been submitted in partial fulfilment of requirements for an advanced degree at Homi Bhabha National Institute (HBNI) and is deposited in the Library to be made available to borrowers under rules of the HBNI.

Brief quotations from this dissertation are allowable without special permission, provided that accurate acknowledgement of source is made. Requests for permission for extended quotation from or reproduction of this manuscript in whole or in part may be granted by the Competent Authority of HBNI when in his or her judgment the proposed use of the material is in the interests of scholarship. In all other instances, however, permission must be obtained from the author.

ASHISH V. SHELKE



## **DECLARATION**

---

I, hereby declare that the investigation presented in the thesis has been carried out by me. The work is original and has not been submitted earlier as a whole or in part for a degree / diploma at this or any other Institution / University.

ASHISH V. SHELKE



## LIST OF PUBLICATIONS ARISING FROM THE THESIS

---

### Journals:

1. **A. V. Shelke**, N. K. Maheshwari, B. Gera, and R. K. Singh, “CFD Analysis of Hydrocarbon Fireballs”, **Combustion Science and Technology**, 2017 Vol. 189, Issue 8; page 1440-1466. <https://doi.org/10.1080/00102202.2017.1296433>
2. **A. V. Shelke**, B. Gera, N. K. Maheshwari, R. K. Singh. “Theoretical Studies on Fuel dispersion and fireball formation associated with aircraft crash”. **Combustion Science and Technology**, 2018, Vol. 190, Issue: 12, pages 2134 – 2163  
<https://doi.org/10.1080/00102202.2018.1494164>
3. **A. V. Shelke**, B. Gera, N. K. Maheshwari, R. K. Singh. “Mathematical model for prediction of droplet sizes and distribution associated with impact of liquid-containing projectile” **KERNTECHNIK** (2018) Vol. 83 Issue 1; page 15-27  
<https://doi.org/10.3139/124.110850>
4. **A. V. Shelke**, B. Gera, N. K. Maheshwari, R. K. Singh. “Parametric studies on hydrocarbon fireball using Large Eddy Simulations.” **Combustion Theory And Modelling**(2018) Vol. 23, Issue 03, page 387-413  
<https://doi.org/10.1080/13647830.2018.1536806>
5. **A. V. Shelke**, B. Gera, N. K. Maheshwari, R. K. Singh “CFD Simulation of fuel dispersion and fireball formation associated to aircraft crash with nuclear power plant”. **Combustion Science and Technology** (2019)  
<https://doi.org/10.1080/00102202.2019.1612383>

## Conferences:

1. **A. V. Shelke**, B. Gera, N. K. Maheshwari, R. K. Singh, “CFD Analysis Fireball Associated with an Aircraft Crash”, International Conference on Ideas, Impact and Innovation in Mechanical Engineering, June 1-2, 2017 (**ICIIME 2017**) Available on: [http://www.ijritcc.org/download/conferences/ICIIME\\_2017/ICIIME\\_2017\\_Track/1497081352\\_10-06-2017.pdf](http://www.ijritcc.org/download/conferences/ICIIME_2017/ICIIME_2017_Track/1497081352_10-06-2017.pdf)
2. **A. V. Shelke**, B. Gera, N. K. Maheshwari, R. K. Singh, " Modelling Of Formation And Combustion Of Fireball Formed In An Air Ambulance Accident", Proceedings of 2<sup>nd</sup> International Conference on Thermal, Energy and Environment, March 25-26, 2016. (**INCOTEE-2016**) **Submission 09.**
3. **A. V. Shelke**, B. Gera, R. K. Singh, “Prediction of droplets sizes formed due to impact of slug of liquid on solid surface”, 23<sup>rd</sup> National Heat and Mass Transfer Conference and 1st International ISHMT-ASTFE Heat and Mass Transfer Conference, December 17-20, 2015.(**ISHMTC-2015**) **Submission 249.**
4. **A. V. Shelke**, B. Gera, R. K. Singh, “Theoretical and Numerical Study of Mist Formation due to Impact of Slug of Liquid on Solid Surface”, 5<sup>th</sup> International and 41<sup>st</sup> National conference on Fluid Mechanics and Fluid Power , IIT Kanpur, December 12-14, 2014. (**FMFP-2014**) **Submission 583.**

## Book Chapter:

Contribution in the Chapter (7) “*CFD simulation for containment safety assessment*” in the *Advances of Computational Fluid Dynamics in Nuclear Reactor Design and Safety Assessment*, 1st Edition”, Elsevier, ISBN: 9780081023372, Editors: Jyeshtharaj Joshi, Arun Nayak

<https://www.elsevier.com/books/advances-of-computational-fluid-dynamics-in-nuclear-reactor-design-and-safety-assessment/joshi/978-0-08-102337-2>

ASHISH V. SHELKE

*Dedicated to my family and teachers*



## ACKNOWLEDGEMENTS

---

I would like to express my deepest gratitude to my supervisors **Dr. N. K. Maheshwari** and **Dr. R. K. Singh**, for their valuable guidance, patience, encouragement and the freedom given to me in carrying out research. Apart from the technical knowledge, the discipline, which I learned from my supervisors is indispensable to my growth as an engineer and as a person. I considered myself to be honoured and fortunate to be associated with them.

Besides my guide, I would like to thank the rest of my thesis committee: Chairman of the committee, Dr. G K Dey, Dr. A. P. Tiwari, Dr. J. Chattopadhyay, Dr. M. K. Samal and Dr. A. Chakravarty for their insightful comments and encouragement, but also for the hard questions, which incited me to widen my research from various perspectives.

I would like to express thanks to Mr Bhuvaneshwar Gera, for his valuable inputs during my work at Reactor Safety Division and Advance Heavy Water Reactor Division, Bhabha Atomic Research Centre, Mumbai. He was being there for a technical guidance and subjective inputs whenever I needed him. Without his precious support, it would not have been a wonderful journey for me to conduct this research. He has been a great inspiration throughout this work.

I would like to thank my friends and fellow graduate students Dr. Ravi D, Dr. Somenath C, Dr. Vinod B, Mr. Anuj S, Dr. Vineet V, Ms. Paridhi G, Dr. Parul G, Dr. Megha T, Ms. Aruna S, Ms. Deepa K and Dr. Abhishek T for the many fruitful discussions and merry memories.

I would also like to thank all Homi Bhabha National Institute, Dean, Academic Dean, administration and staff members for their constant cooperation in all administrative activities related to my PhD.

Last but not the least, is my family. Whosoever I am today, it is because of them only. It was my parents who first instilled in me the motivation for learning and their hard work made me have the chance for higher education. Special thank goes to my wife Mrs. Anupama Shelke. It is impossible for me to finish this thesis without her support, encouragement and sacrifice. Thanks to my brother Mr. Chetan Shelke and my dear friends for their constant support, love and care. I would like to thank my entire family for supporting me spiritually and emotionally throughout this journey and my life in general.

Thanks for all your encouragement and motivation. This journey would not have been completed without each and every one of you.

## SYNOPSIS

---

The safety of nuclear reactor is affected by both internal and external events. The external events can be of natural or human-induced origin. One of such events is the accidental impact of aircraft on nuclear containment. After the events of 9/11, the impact of fast flying commercial aircraft can be a major hazard threatening to Nuclear Power Plant's (NPP) safety. Such an aircraft crash can potentially affect the integrity of Nuclear Power Plants through mechanical destructions and thermal damage due to ignited fuel onboard. During the impact of an aircraft, the fuel tank can get ruptured which causes fuel leakage. At lower impact velocity the fuel may form liquid chunks and rained out. At higher impact velocity the fuel vapour-droplet mixture remains in atmosphere and remaining liquid chunk may rain out on the structures. The vapour-droplet mixture may form a fireball if a source of ignition is available. The liquid fuel collected in the vicinity of structures may also cause pool fire.

The fireball is a rapid turbulent combustion of fuel released into the atmosphere by means of an expanding radiant ball of flame. Occurrences of fireball close to plant buildings due to the release of flammable hydrocarbon fuel caused by the formation of fuel vapour cloud poses severe safety concerns by direct contact, radiation and/or convection of hot combustion products through the opening of air intakes and ducts. This fireball is large enough to engulf the entire NPP. The engulfment may lead to a local rise in temperature, which causes the spallation of concrete structure and fatalities to the human being. This may affect the integrity of NPP structures and has safety implications. The building structures influence the spatial evolution of fireball due to the generation of large turbulent structures.

Many researchers have performed the experiments on fireball using a gram to many tons of fuel to measure the parameters like mass involved in the fireball formation, its resulting

diameter, lifting height and heat radiated from the fireball. Due to the short duration and inherent transient associated with combustion in a fireball, the experimental studies of accident scenarios are found to be difficult. Hence, very little information can be inferred from the experiments about the internal structure formation, evolution, combustion, and explosion of fireballs. To study the internal parameters of fireball such as combustion processes involved in the formation and development of fireball, there is need of computational method. The knowledge about heat released and thermal hazard can be assisted further using CFD simulations in a more definite and detail manner.

Three-dimensional computational fluid dynamics (CFD) simulations of hydrocarbon fireballs have been performed for their detailed characterization, including diameter, lifetime, flame, and internal fireball structure. The fireball analysed using Eddy Dissipation Concept (EDC) with single-step reaction, Large Eddy Simulation (LES) and finite volume discrete ordinate radiation models. The analysis has been performed with hydrocarbon fuel in the vapour form at inlet. The fireball diameter and lifting height computed from the numerical analysis are found in good agreement with experimental data of Droste et al. (1999). To illustrate transient behaviour, developed pressure and flame structures are studied during the evolution of a fireball. The parametric studies are conducted by varying the mass of fuel, inlet velocity and inlet diameter. New correlations for fireball diameter and duration have been proposed based on the parametric studies performed using CFD code. The incident radiation from the fireball is calculated at different locations to assess thermal hazard.

During the literature survey, it has been felt that many phenomena will be taking place during the impact of the fuel tank. The fuel tank will get first crushed and all the fuel inside the tank will spread out. During the process of spreading of liquid fuel, the fuel will get vaporize and also break into smaller droplets. In view of this there is a need to develop a model to study

these phenomena. It is also felt that initial condition in the form of vapour-liquid droplet for analysing the fireball in CFD analysis is required. The complex processes of crushing fuel tank, liquid emerging out and droplet formation with breakup and evaporation have been analysed sequentially using analytical models. A Mathematical model is developed for prediction of droplet sizes and distribution associated with the impact of a liquid-container. The complex processes of crushing fuel tank, liquid emerging out and droplet formation with breakup and evaporation have been analysed sequentially using analytical models. The model can predict the transient behaviour of the droplet cloud. The model is validated with experimental data available in the literature. Further, the analysis has been performed using water and kerosene. The data obtained from this model can be utilized as boundary and initial condition for CFD analysis of aircraft crash.

The fireball arising from the aircraft crash has been studied and analysed in the computational fluid dynamic (CFD) using two methods. In first method, the fuel is injected in complete vapour form and in the second method; fuel is injected as dynamic fuel spray. The input to analyse fireball by dynamic spray model has been obtained from the above developed mathematical model for droplet sizes and distribution. The diameter and lift-off height obtained in CFD analyses are compared with a video footage reported in the literature and it is found to be in good agreement. It has been found that both methods give similar predictions for fireball diameter and lifting height but other parameters like pressure developed, radioactive heat flux, and time-averaged temperature are predicted differently.

Further, the evolution of fireball following fuel dispersion due to the aircraft crash upon NPP has been analysed. Numerical simulation to study the effect of fireball on the target NPP structure and its surrounding has been performed in a three-dimensional CFD code. The inputs to analyse the fireball using dynamic fuel spray have been obtained from a theoretical model

developed above to determine droplet sizes and distribution. This analysis is used to study the evolution of fireball and thermal hazard associated with the radiated heat. It is found that the highest temperature inside the fireball reaches when it lifts above containment building and leaves the structure.

# TABLE OF CONTENTS

---

<b>DECLARATION.....</b>	<b>v</b>
<b>LIST OF PUBLICATIONS ARISING FROM THE THESIS .....</b>	<b>vii</b>
<b>ACKNOWLEDGEMENTS .....</b>	<b>xi</b>
<b>SYNOPSIS .....</b>	<b>xiii</b>
<b>TABLE OF CONTENTS .....</b>	<b>xvii</b>
<b>NOMENCLATURES .....</b>	<b>xxiii</b>
<b>LIST OF FIGURES .....</b>	<b>xxix</b>
<b>LIST OF TABLES .....</b>	<b>xxxv</b>
<b>CHAPTER 1: INTRODUCTION.....</b>	<b>1</b>
1.1. Objective of thesis.....	5
1.2. Accomplishment of the present project .....	5
1.3. Organization of thesis .....	6
<b>CHAPTER 2: REVIEW OF LITERATURE .....</b>	<b>9</b>
2.1. Regulatory approach to the safety assessment of aircraft impact on nuclear containment .....	11
2.1.1. Atomic Energy Regulatory Board (AERB).....	11
2.1.2. International Atomic Energy Agency (IAEA): .....	11
2.2. Aircraft Crash.....	12
2.2.1. Impact with ground .....	13

---

2.2.2. Impact on a small structure .....	13
2.2.3. Impact on Tall structures .....	14
2.2.4. Experiments of aircraft crash .....	16
2.3. Hydrocarbon Fireball .....	17
2.3.1. Small-scale experiments .....	18
2.3.2. Large-scale experiments .....	19
2.3.3. Formation of fireball in various accidents and major hazard .....	21
2.4. Theoretical Studies of Fireball .....	22
2.4.1. Mass of fuel involved .....	24
2.4.2. Fireball Diameter, duration and lifting height .....	24
2.4.3. Heat Release Rate (HRR) .....	27
2.4.4. Radiation effect from the fireball .....	28
2.4.5. Thermal dose .....	29
2.5. Fuel dispersion study .....	29
2.6. Computational Fluid Dynamics (CFD) Studies .....	31
2.6.1. CFD Studies on fireball .....	31
2.6.2. CFD Studies on fireball associated with aircraft crash .....	33
2.6.3. CFD studies with fuel dispersion .....	34
2.7. Gap areas .....	35
2.8. Scope of the work .....	36

---

<b>CHAPTER 3: CFD ANALYSIS OF HYDROCARBON FIREBALLS.....</b>	<b>39</b>
3.1. Introduction.....	39
3.2. Need of Computational Fluid Dynamics (CFD).....	40
3.2.1. Advantages of CFD.....	41
3.3. Mathematical model and numerical method.....	42
3.3.1. Governing Equations.....	42
3.3.2. Turbulence Modelling.....	44
3.3.3. Combustion Model.....	46
3.3.4. Radiation Model.....	49
3.3.5. Soot Model.....	50
3.3.6. Eulerian-Lagrangian model.....	51
3.4. Numerical Method.....	54
3.5. Grid resolution and Time step selection.....	55
3.6. Grid independence and Model Validation.....	56
3.6.1. Computational Domain.....	56
3.6.2. Initial and Boundary Conditions.....	58
3.6.3. Study of grid independency.....	58
3.6.4. Lifting velocity of fireball.....	60
3.7. Effect of Turbulence model.....	61
3.8. Effect of Radiation Model.....	61
3.9. Internal Structure of fireball.....	64

3.10. Thermal Hazard from the fireball ..... 67

3.11. Parametric studies on fireball..... 68

    3.11.1. Effect of fuel mass..... 69

    3.11.2. Effect of initial velocity..... 74

    3.11.3. Effect of inlet diameter..... 77

    3.11.4. Correlations based on CFD Simulation Data ..... 80

3.12. Closure ..... 83

**CHAPTER 4: IMPACT OF LIQUID CONTAINING PROJECTILE AND FUEL  
DISPERSION/ MIST FORMATION ..... 85**

4.1. Introduction..... 85

4.2. Mathematical model..... 86

    4.2.1. Energy balance in impacting container ..... 86

    4.2.2. Water Hammer Effect ..... 88

    4.2.3. Dynamic Spreading Model..... 89

    4.2.4. Breakup of Spreading Film ..... 90

    4.2.5. Aerodynamic Breakup/ Splashing..... 92

    4.2.6. Drop acceleration ..... 93

    4.2.7. Secondary breakup ..... 95

    4.2.8. Droplet evaporation model..... 97

    4.2.9. Characteristic Diameters ..... 99

    4.2.10. Mass involved in Fireball ..... 99

---

4.3. Solution Methodology .....	100
4.4. Application of model .....	102
4.5. Parametric study using water and hydrocarbon fuel.....	104
4.6. Computational Fluid Dynamics (CFD).....	110
4.6.1. Computational Domain .....	110
4.6.2. Initial and Boundary conditions .....	110
4.6.3. CFD Results .....	112
4.7. Closure .....	114
<b>CHAPTER 5: STUDIES ON FIREBALL FORMATION USING FUEL VAPOUR AND DYNAMIC SPRAY AT INLET .....</b>	<b>115</b>
5.1. Introduction.....	115
5.2. Case study: aircraft Boeing 747-400 accident .....	116
5.3. Analysis for calculating fuel dispersion.....	118
5.3.1. Vapour fuel inlet method.....	119
5.3.2. Dynamic spray method.....	119
5.4. Computational domain.....	121
5.4.1. Initial and Boundary Conditions .....	122
5.4.2. Numerical Method.....	122
5.5. Simulation Results .....	123
5.5.1. Vapour inlet method.....	123
5.5.2. Dynamic spray method.....	124

5.5.3. Comparison of models: ..... 125

5.5.4. Local Parameter measurements ..... 128

5.6. Further studies with vapour inlet and dynamic spray methods..... 132

5.7. Closure ..... 135

**CHAPTER 6: SAFETY ASSESSMENT OF NPP STRUCTURE ..... 137**

6.1. Introduction..... 137

6.2. Safety Assessment of NPP for aircraft crash-induced fireball loads ..... 138

6.3. Primary analysis..... 139

6.4. Results of fuel dispersion analysis ..... 140

6.5. Initial and Boundary Conditions ..... 141

6.6. Numerical Method ..... 143

6.7. Results of Impact analysis ..... 145

6.8. Effect of structures on fireball evolution ..... 152

6.9. Closure ..... 154

**CHAPTER 7: CONCLUSION AND FUTURE WORK ..... 155**

7.1. Summary, conclusions and recommendations ..... 155

**APPENDIX A ..... 159**

**REFERENCES..... 171**

# NOMENCLATURES

---

## Nomenclatures:

$A_d$	surface area of the droplet ( $m^2$ )
$C_d$	drag coefficient
$c_g$	speed of sound in gas ( $m\ s^{-1}$ )
$C_p$	specific heat capacity ( $kJ\ kg^{-1}\ K^{-1}$ )
$c_t$	speed of sound in liquid ( $m\ s^{-1}$ )
$D_f$	diffusion coefficient ( $m^2s^{-1}$ )
$d$	depth of computational domain (m)
$D_{slug}$	diameter of impacting slug (m)
$D^*$	characteristic fire diameter (m)
$D_{cyl}$	inner diameter of the cylinder (m)
$d_{drop}$	droplet diameter (m)
$D_f$	diffusivity of vapour in the air( $m^2s^{-1}$ )
$D_{FB}$	fireball diameter (m)
$d_{lig}$	diameter of the ligament (m)
$E_s$	surface energy (J)
$f$	fraction of fuel released entering the fireball
$F$	configuration factor
$F_{crush}$	crushing force (N)
$h$	convection coefficient ( $w\ m^{-2}\ K^{-1}$ )
$h_l$	film thickness (m)
$H_{FB}$	lifting height of fireball (m)
$H^\circ(T)$	absolute enthalpy ( $kJ\ mol^{-1}$ )
$h_s$	sensible enthalpy ( $kJ/kg$ )
$H_v$	latent heat of vaporization ( $kJ\ mol^{-1}$ )
$I$	radiation intensity ( $W\ sr^{-1}$ )
$k$	turbulent kinetic energy ( $m^2\ s^{-2}$ )
$K_s$	wave number of fastest-growing surface wave
$L$	distance from the target (m)

---

$L_{slug}$	length of impacting slug (m)
$L_{cyl}$	length of the cylinder (m)
$L_{wing}$	length of wing tank (m)
$M$	mass of fuel (kg)
$M_{involved}$	mass of fuel in a fireball (kg)
$M_{released}$	mass of liquid released (kg)
$P$	pressure generated as a shock ( $\text{N m}^{-2}$ )
$\dot{Q}$	Heat Release rate of fire (W)
$r_{drop}$	radius of the droplet (m)
$R_{max}$	the maximum spreading radius (m)
$r_{iDiff}$	reciprocal of diffusion timescale ( $\text{s}^{-1}$ )
$rt_{Turb}$	reciprocal of turbulent mixing timescale ( $\text{s}^{-1}$ )
$S_{wing}$	span of wing tank (m)
$s$	path length (m)
$S_{rad}$	source term for thermal radiation
$t$	time (s)
$T_{wing}$	height wing tank (m)
$T$	temperature (K)
$t_c$	characteristic spread time (s)
$t_{cyl}$	thickness of cylinder (m)
$t_{wing}$	thickness of wing tank (m)
$U_{lift}$	uplifting velocity ( $\text{m s}^{-1}$ )
$U_{rel}$	relative drop velocity ( $\text{m s}^{-1}$ )
$V$	velocity of aircraft impact ( $\text{m s}^{-1}$ )
$v$	liquid slug impact velocity ( $\text{m s}^{-1}$ )
$\vec{v}_n$	velocity normal to the impact surface ( $\text{m s}^{-1}$ )
$v_s$	spreading velocity after droplet impact ( $\text{m s}^{-1}$ )
$w$	width of computational domain (m)
$X_V$	vapour mole fraction
$Y$	mass fraction
$Y_{f,R}$	vapour mass fraction at the droplet surface
$Y_{f,\infty}$	vapour mass fraction outside the boundary layer

$\Delta H_c$	Heat of combustion ( $\text{kJ mol}^{-1}$ )
$\Delta t$	integration time step (s)
$\vec{r}$	radius vector
$\vec{S}$	direction vector
$\vec{S}'$	scattering vector

**Subscripts:**

$a$	ambient
$d, \text{drop}$	liquid droplet
$FB$	fireball
$\text{fuel}$	fuel
$h$	enthalpy
$in$	inlet
$k$	species
$lift$	lifting
$max$	maximum
$min$	minimum
$mix$	mixing
$n$	number
$ox$	oxidizer
$r.m.s$	root mean square
$slug$	liquid slug
$t$	turbulent
$wing$	wing of aircraft

**Superscripts:**

“_”	Spatial filter
“~”	Favre filter
$St$	Stokes flow

**Greek Symbols:**

$\mu$	dynamic viscosity ( $\text{N s m}^{-2}$ )
$\alpha$	absorption coefficient
$\beta$	evaporation parameter
$\gamma^*$	mass fraction
$\delta$	grid spacing (m)
$\varepsilon$	dissipation rate ( $\text{m}^2\text{s}^{-3}$ )
$\eta$	refractive index
$\theta$	angle of contact of liquid (rad)
$\xi_{max}$	Ratio of maximum film diameter to initial diameter
$\rho$	density ( $\text{kg m}^{-3}$ )
$\sigma$	Stefan-Boltzmann constant ( $\text{W m}^{-2} \text{K}^{-4}$ )
$\sigma_l$	Surface tension ( $\text{N m}^{-1}$ )
$\sigma_{cyl}$	stress induced in the cylinder ( $\text{N m}^{-2}$ )
$\sigma_s$	scattering coefficient
$\tau$	transmissivity
$\tau_{break}$	breakup time (s)
$\tau_{mix}$	turbulent mixing time (s)
$\tau_d^{st}$	droplet relaxation time (s)
$\nu$	laminar dynamic viscosity ( $\text{N s m}^{-2}$ )
$\phi$	scattering phase function ( $\text{sr}^{-1}$ )
$\chi_R$	radiative heat fraction
$\omega$	reaction rate ( $\text{mol L}^{-1} \text{s}^{-1}$ )
$\Omega'$	spatial angle (sr)

**Abbreviations:**

BAM	Bundesanstalt für Materialforschung (The Federal Institute Of Material Research And Testing)
BLEVE	Boiling Liquid Expanding Vapor Explosion
CCPS	Center for Chemical Process Safety
CFD	Computation Fluid Dynamics

CID	Controlled Impact Demonstration
CSB	Chemical Safety Board
DO	Discrete Ordinates
EDC	Eddy Dissipation Concept
EDC	Eddy Dissipation Concept
FAA	Federal Aviation Administration
FVDOM	Finite Volume Discrete Ordinate Method
HRR	Heat Release Rate
IAEA	International Atomic Energy Agency
NIST	National Institute of Standards and Technology
NPP	Nuclear Power Plant
NTSB	National Transport Safety Board
OpenFOAM	Open Field Operation And Manipulation
PBiCG	Preconditioned Bi-Conjugated Gradient
PHAST	Process Hazard Analysis Software
PISO	Pressure Implicit with Splitting of Operator
PPC	Partially Premixed Combustion
RTE	Radiative Transfer Equation
SEP	Surface Emissive Power
SGS	Sub Grid Scale
SMD	Sauter Mean Diameter
TNO	The Netherlands Organization of applied scientific research
VTT	Technical Research Centre of Finland
WTC	World Trade Centre

**Dimensionless Numbers used:**

$Bi$	Biot Number	$Bi = \frac{h d_{drop}}{6k}$
$B_M$	Spalding Number	$B_M = \frac{X_{v,s} - X_v}{1 - X_{v,s}}$
$Nu$	Nusselt Number	$Nu = \frac{h d_{drop}}{k}$
$Oh$	Ohnesorg Number	$Oh = \frac{\sqrt{We}}{Re}$
$Pr$	Prandtl Number	$Pr = \frac{\mu C_p}{k}$
$Re$	Reynolds Number	$Re_{drop} = \frac{\rho_g U_{rel} d_{drop}}{\mu_g}$
$Sc$	Schmidt Number	$Sc = \frac{\mu}{\rho d_{drop}}$
$Sh$	Sherwood Number	$Sh = 2 + 0.6 Re_{drop}^{1/2} Sc^{1/3}$
$We$	Weber Number	$We = \frac{\rho_l U_{drop}^2 d_{drop}}{\sigma_l}$
$We_g$	gas Weber Number	$We = \frac{\rho_g U_{drop}^2 d_{drop}}{\sigma_l}$

# LIST OF FIGURES

---

Figure 1.1: Generic nuclear power plant.....	4
Figure 2.1: Comparison of NPP with tall structure and small height structure .....	15
Figure 2.2: Comparison of maximum fireball diameter obtained from relationships with accident/experimental observations. ....	26
Figure 2.3: Comparison of fireball duration obtained from relationships with accident/experimental observations. ....	27
Figure 3.1: Schematic of a computational domain showing the fuel inlet at $y=0$ .....	57
Figure 3.2: Profiles obtained from OpenFOAM with 135070 Cells (black solid line), 540280 Cells (dash line) and 2161120 cells (red solid line).....	59
Figure 3.3: Modelling of Diameter and lifting height of fireball from Droste et al. (1999)....	60
Figure 3.4: Temperature profile of gas in a fireball on the plane XY, at $z=0$ (at $t=3.0$ s), LES (left) and $k-\epsilon$ turbulence model (right).....	62
Figure 3.5: Effect of Radiation on flame surface temperature, (XY plane at $z=0$ ) at $t=3.0$ s.	62
Figure 3.6: Effect of Radiation on gas density inside the fireball ( in XY plane at the centre of fireball at $t=3.0$ s).....	63
Figure 3.7: Effect of Radiation on gas density inside the fireball ( in XY plane at the centre of fireball at $t=3.0$ s).....	63
Figure 3.8: Simulation of BAM fireball: $CO_2$ mass fraction, Temperature of gas (K) for vertically inlet velocity of 100 m/s at plane XY, $z=0$ at different time steps .....	64
Figure 3.9: Instantaneous frame on cutting plane ( $z=0$ ) $C_3H_8$ (left) and $CO_2$ (right) at $t=3.0$ s .....	65
Figure 3.10: Time-averaged profile of concentrations along XY plane at $y=50$ .....	65
Figure 3.11: Instantaneous Temperature and Species mass fraction at $t=3.0$ s and $y=50$ m in XY plane ( $z=0$ ) .....	66
Figure 3.12: Pressure developed during combustion of the fireball on XY plane, $z=0$ .....	67
Figure 3.13: Global Heat release rate from BAM fireball .....	67

Figure 3.14: Temperature calculated at ground locations.....	68
Figure 3.15: Comparison of fuel mass with (a) peak Heat Release Rate (HRR) and (b) time of peak HRR.....	70
Figure 3.16: Fraction of heat released during the lifetime of fireball.....	71
Figure 3.17: HRR per unit volume of fireball.....	72
Figure 3.18: Incident radiation flux calculated at 50 m during the fireball.....	72
Figure 3.19: (a) Average Incident radiations calculated at the locations on the ground for various masses (b) Thermal dose calculated at 50 m during the fireball (c) Inverse square law fitting for fireball with fuel mass of $10^3$ kg.....	73
Figure 3.20: Global Heat Release Rate (HRR) from the fireball with different inlet velocities.....	75
Figure 3.21: (a) Position of the upper edge of fireball and (b) expansion of fireball in the horizontal direction for different fuel inlet velocities.....	76
Figure 3.22: (a) Average Incident radiations calculated at the locations on the ground for various fuel inlet velocity. (b) Thermal dose calculated at 20 m on the ground for various fuel inlet velocity.....	77
Figure 3.23: Global heat release rate (HRR) for 1000 kg of propane with different inlet diameters.....	78
Figure 3.24: (a) Position of the upper edge of fireball and (b) expansion of fireball in the horizontal direction for the different inlet opening diameters.....	79
Figure 3.25: (a) Average Incident radiations calculated at the locations on the ground for various inlet opening diameter. (b) Thermal dose calculated at 20 m at the ground for various inlet diameter.....	80
Figure 3.26: (a) mass based correlation developed for the maximum diameter of fireball using CFD results (b) Comparison of maximum fireball diameter obtained using correlation with accidental/experimental observations.....	81
Figure 3.27: (a) mass based correlation developed for the duration of fireball using CFD results (b) Comparison of fireball duration obtained using correlation with accidental/experimental observations.....	82
Figure 4.1: Simplified Model of impacting container.....	88

Figure 4.2: Sketch of spreading after slug mass impact onto the rigid surface (a) before impact, $t=0$ (b) at the intermediate time, $t$ (c) maximum spreading without breaking, $t=tc$ (d) breaking of spreading the film .....	90
Figure 4.3: Breakup of the liquid sheet into ligaments and droplets .....	92
Figure 4.4: Acceleration of droplet and effect of gravity .....	94
Figure 4.5: Schematic view of drop vaporization .....	98
Figure 4.6: Flowchart for calculating the liquid dispersion .....	101
Figure 4.7: Liquid dispersion pattern .....	102
Figure 4.8: Dimensionless numbers and impacting velocities for water (a) and kerosene (b) .....	105
Figure 4.9: Smallest droplet size predicted in a spray .....	106
Figure 4.10: Initial spreading velocity (a) variation as a function of impact velocity (b) velocity ratio .....	106
Figure 4.11: Prediction of droplet size after the primary breakup .....	107
Figure 4.12: Prediction of final droplet size after secondary breakup and evaporation .....	108
Figure 4.13: Percentage evaporation of kerosene .....	108
Figure 4.14: Predicted Droplet distribution (a) droplet number fraction and (b) cumulative fraction .....	109
Figure 4.15: Transient positions of droplet front for impact velocity of 50 and 150 m/s.....	109
Figure 4.16: Two Dimension computational domain used for CFD simulation.....	111
Figure 4.17: Modeling of slug impact in an unsteady state with unstructured mesh with 1006 triangular, 3636 triangular and 14242 triangular elements .....	112
Figure 4.18. Time series of the impact of a slug of water from CFD model .....	113
Figure 4.19. The plot of CFD velocity results with a mathematical model.....	113
Figure 5.1: Images captured from video footage of Boeing 747-400 crash (Daily Mail, 2013). .....	117
Figure 5.2: location of fuel tanks in Boeing 747-400 .....	118
Figure 5.3: Predicted droplet distribution .....	120

Figure 5.4: Schematic of the computational domain showing the fuel inlet at $y=0$ .....	121
Figure 5.5: Fireball evolution during 2, 4, 6 and 8 s in vapour inlet approach.....	124
Figure 5.6: Droplet spray from aircraft wings .....	125
Figure 5.7: Evolution of fireball during 2, 4, 6 and 8 s occasioned from dynamic spray.....	125
Figure 5.8 : Comparison of fireball diameter from video footage and CFD simulations.....	126
Figure 5.9: Comparison of lifting height of fireball centre using video footage and CFD simulation.....	127
Figure 5.10: comparison of heat release rate (HRR) during the evolution of fireball obtained from dynamic spray and vapour inlet methods.....	127
Figure 5.11: The location of probes for calculation of various properties.....	128
Figure 5.12: Fuel mass fraction plotted along the Z axis (centre of wings, 0 m away).....	129
Figure 5.13 $CO_2$ mass fraction calculated at the centre of wings .....	129
Figure 5.14: Pressure Calculated at locations 0 (centre), 10, 20 and 30 m for (a) dynamic spray and (b) vapour inlet methods .....	130
Figure 5.15: Velocity calculated at the locations 0 (centre) and 20 m for (a) dynamic spray, (b) vapour inlet approach.....	131
Figure 5.16: Average radiative flux calculated at the locations on the ground .....	131
Figure 5.17: Time-averaged temperature of ground locations.....	132
Figure 5.18: Global Heat Release Rate (HRR) for fireballs with fuel mass of a) 20 ton and b) 80 ton .....	133
Figure 5.19: Fireball Diameters predicted using dynamic spray and vapour inlet method for fireball with fuel mass of (a) 20 ton and (b) 80 ton. ....	134
Figure 5.20: Average radiative flux calculated at the locations on ground calculated for fireballs with fuel mass of a) 20 ton and b) 80 ton .....	134
Figure 6.1: (a) Predicted droplet sizes distribution and (b) cumulative density function of droplet spray using the model developed in Chapter 4.....	141
Figure 6.2: (a) Schematic of a computational domain showing the fuel inlet (b) aircraft wing (fuel inlet).....	143

---

Figure 6.3: Impact conditions considered for safety assessment.....	146
Figure 6.4: Dispersion of fuel droplet spray at 1, 2 and 3 s for case 1 .....	146
Figure 6.5: Evolution of fireball for case 1 .....	147
Figure 6.6: dispersion of fuel droplet spray at 1.5, 2.5 and 3.5 s for impact condition 2. ....	148
Figure 6.7: Burning of dispersed droplets and fireball evolution at the duration of 1.5, 2.5 and 3.5s for impact condition 2 .....	148
Figure 6.8: the evolution and lifting-up of fireball at time durations of 5, 6 and 10 s in impact condition 2 .....	149
Figure 6.9: dispersion of fuel droplet spray at 1.0 and 4.0 s for impact condition 3. ....	149
Figure 6.10: the evolution and lifting-up of fireball for impact condition 3.....	150
Figure 6.11: Profile of temperature predicted for impact condition 3 .....	151
Figure 6.12: Time history of safety relevant parameters calculated at 30m away from the containment building (at the assumed opening of the building).....	151
Figure 6.13: (a) Global heat release rate (HRR), (b) Average incident radiative heat flux on building surfaces. ....	152
Figure 6.14: local velocity vectors and temperature distribution near containment wall .....	153
Figure A. 1: Transient behaviour of liquid spary fronts .....	169



## LIST OF TABLES

---

Table 2.1: Small scale experiments .....	19
Table 2.2: Fireball accidents reported in the literature .....	22
Table 2.3: Constants for correlations of fireball mass (kg), diameter (m) and duration (s). ...	25
Table 2.4: Correlation for estimating the height of fireball centre from the ground .....	25
Table 2.5: Model estimating the incident radiation on the target .....	28
Table 3.1: Average uplifting velocity of fireball .....	61
Table 3.2: Inlet velocity of 100 m/s for the release time of 1s with varying inlet mass .....	69
Table 3.3: Constant inlet mass of 1000 kg for the release time of 1 s with varying inlet velocity .....	75
Table 3.4: Constant inlet mass of 1000 kg for the release velocity with varying inlet diameters and duration .....	78
Table 4.1: Criteria for the secondary breakup of the droplet (Arcoumanis et al., 1997).....	96
Table 4.2: Specifications of tests (Hostikka et al., 2015) .....	103
Table 4.3: Calculations for the energy of crushing cylinder and velocity of slug impact .....	103
Table 4.4: Comparison of experimental data (Hostikka et al., 2015) and calculated characteristic diameters and velocity .....	104
Table 5.1: Inputs to calculate fuel dispersion using model mentioned in Chapter-4.....	119
Table 5.2: Results of fuel dispersion modelling (for Dynamic spray method).....	120
Table 5.3: Correlations (Abbasi and Abbasi, 2007) for fireball with ~33 tons of kerosene..	122
Table 6.1: Inputs to calculate fuel dispersion using model mentioned in chapter 4 using jet fuel. ....	140
Table 6.2: Results of fuel dispersion modelling .....	141
Table 6.3: Average Uplifting velocity of fireball .....	154
Table A.1: Specifications of tests (Hostikka et al., 2015) .....	159

Table A.2: Criteria for secondary breakup of droplet (Arcoumanis et al., 1997)..... 164

Table A.3: Liquid vapor mass outside the boundary ..... 166

Table A.4: Saturation vapour pressure..... 167

Table A.5: Comparison of experimental and Calculated values..... 168

# CHAPTER 1: INTRODUCTION

---

Nuclear power is one of the leading electricity generation methods with extremely low carbon release into the atmosphere. In India after coal, gas, hydroelectricity and wind power, nuclear power is the fifth-largest source of electricity. In the Nuclear Power Plant (NPP), the energy is released from the nucleus of atoms through the process of nuclear fission that takes place in a reactor, which produces heat. The heat removed from the reactor core using a cooling system is used to generate the steam. This steam drives a steam turbine connected to a generator producing electricity. As of March 2018, India has 22 nuclear reactors in operation in nuclear power plants, having a total installed capacity of 6,780 MW and six more reactors are under construction with a combined generation capacity of 4,300 MW (Utilities, 2018).

Lesson learned from Three Mile, Chernobyl and Fukushima accidents and several other operational incidents in the NPPs, emphasis has been given on design and procedural improvements to enhance safety of NPPs. The safety of nuclear reactor is affected by both internal and external events. The external events can be of natural or human-induced origin. One of such events is accidental impact of aircraft on nuclear containment. Following the impact of aircraft, the aviation fuel may spread in the vicinity of the reactor containment which can lead to formation of fireball. The consequence of this kind of accident is necessary to analyse to understand the effect of formation of fireball on the important structures.

The twin towers of World Trade Centre (WTC) and Pentagon building in the events of 9/11 give an idea about environment created by aircraft crash with building structures (Mlakar et al., 2003). Such an aircraft crash can potentially affect the integrity of Nuclear Power Plants (NPP) through mechanical destructions and thermal damage. In the safety assessment of NPP, direct impact onto reactor containment or related service buildings can lead to serious

radiological consequences. Aftermath the impact, the fire-resistant structural elements (columns, slabs) may suffer the loss of fire protection covers and/or coatings. This may create cracks in the reactor containment.

In the aircraft crash, after impact with cruising velocity, the wing structure fails due to mechanical impact and internal pressure generated by liquid fuel (Forasassi & Lofrano, 2010). The fuel spills out in a large amount from the broken tanks and gets atomized to form a droplet cloud. Due to the availability of heat source either from an electronic circuit (broken) or from hot jet turbine parts, the vaporized portion of dispersed fuel initiates the combustion. A large quantity of the fuel engulfs within the fire in very short duration resulting in a fireball formation. The portion of fuel, which does not involve in fireball formation, spills around and leads to form a local pool fire.

Fireball is formed for a very short duration, radiates a large amount of heat and engulfs surrounding structures during its evolution (Lees, 2012). Studying the parameters of the fireball is an important measure for hazard assessment. Joseph et al. (1969), Fay & Lewis (1977), Hasegawa & Sato (1977), Lihou & Maund (1982), Hardee & Lee (1973), High (1968) and Mishra et al. (2015) performed the experiments on fireball using a gram to several tons of fuel, for measuring the parameters like mass involved in the fireball formation, its resulting diameter and duration, lifting height and heat radiated from the fireball. Researchers also developed correlations to predict these fireball parameters (CCPS, 1999; Hardee et al., 1978; Hardee and Lee, 1975; Marshall, 1987; Pietersen, 1985; TNO Yellow Book, 1989).

The experimental investigation of aircraft accident scenario is difficult due to the short duration and inherent transient associated with combustion of the fireball and cost involved in the experiments to be performed. Very little information may be inferred from the experiments.

Correlations proposed by researchers cannot be applied directly to track these scenarios as these correlations can recognize only maximum diameter and duration of existence of fireballs. To understand the phenomena associated with combustion of fuel and flame structure inside the fireball, it is necessary to analyse fireball using Computational Fluid Dynamics (CFD) codes. In theoretical studies, researchers simulated the fireball with a fuel inlet in vapour form (Baum and Rehm, 2003 and Luther and Müller, 2009).

During the aircraft impact, the fuel spills out from ruptured tanks and disperses in to the surrounding. During the dispersion, primary breakup of liquid occurs due to the destabilizing process of aerodynamic drag and turbulence within the liquid core. The primary breakup phase is followed by secondary breakup phase of flying droplets. Depending on the speed of droplet relative to surrounding gas, the secondary breakup can produce droplets of different sizes.

The consideration of heat of evaporation of droplet cloud during the evolution of fireball with large fuel mass will play a significant role. There is a need to consider droplet evaporation during the simulation of fireball associated with an aircraft crash. The CFD analysis of combustion of droplet clouds arising from ruptured fuel tank requires data related to droplet cloud such as droplet size and distribution as input. Therefore, there is need of theoretical tools, which can deliberate the detailed study of fuel dispersion, droplet size and distribution.

For a hypothetical aircraft crash on NPP structure, the engulfment of fireball and effect of building structures on fireball evolution need to be studied carefully for safety assessment. In the possible consequences of the release of fuel from a crashing aircraft, the fuel may enter the building through normal openings, air intake ducts and/or through perforation caused by the crash lead to the formation of the combustible environment inside the structure. Therefore, there is a need for fuel dispersion study for aircraft impact. Figure 1.1 shows a typical Nuclear

power plant. The containment building is surrounded by building structures that are essential in the working of Nuclear Power plant.

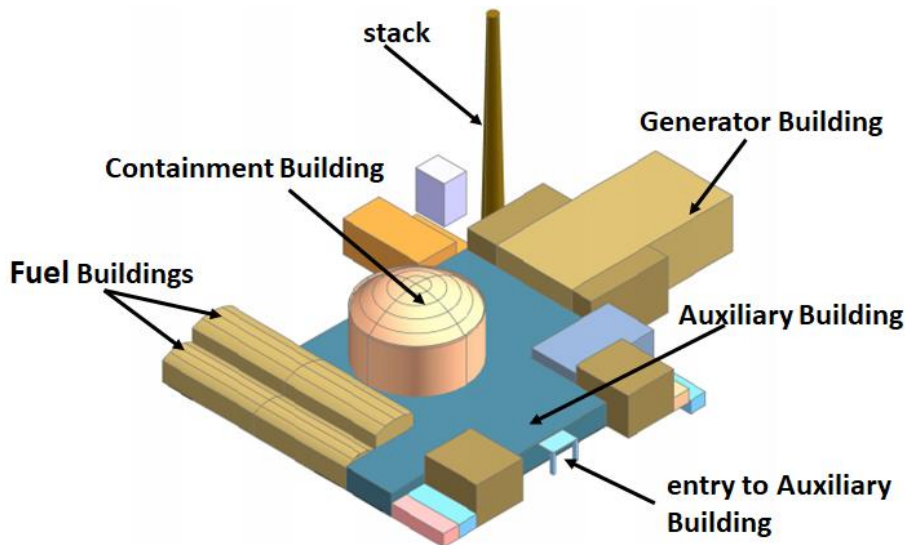


**Figure 1.1: Generic nuclear power plant**

This work should be of interest and beneficial to study the postulated event of aircraft impact with NPP in view of the present day concerns among the nuclear energy communities. It is again difficult to analyse thermal hazard associated with the aircraft crash by accomplishing the experiments due to its complexity and distinct nature. Three-dimensional Computational Fluid Dynamics (CFD) can be the useful tool to deliberate the detailed study of fuel dispersion, combustion of fuel, fireball formation, heat radiation and the thermal hazard from the fireball. The thermal response of the important structures may be predicted for the assessment of fire safety. This will involve estimation of the local rise in the temperature due to incident radiation and/or convection by engulfment due to flame or hot combustion products.

Studies on fireball formation are also useful for preliminary safety assessment of fire and explosions associated with transport and storage of flammable materials in refineries, offshore oil rigs etc.

## **1.1. Objective of thesis**

Based on the above discussions, various phenomena have been identified which are important to study the behaviour of formation and evolution of fireball. The main objective of this thesis is safety assessment of nuclear containment for thermal hazards associated with the impact of aircraft and formation of the fireball.

1. To develop a mathematical model for impacting projectiles with the hydrocarbon fuels which can undergo flashing during splashing of liquid with high speed to predict the transient behaviour of fuel spreading, droplet formation and its associated size distribution as the input data and boundary conditions to study the fire dynamics.
2. To understand the phenomena associated with combustion of fuel and flame structure inside the fireball.
3. To study the effect of inlet fuel mass, inlet velocity and inlet opening diameter on the fireball behaviour.
4. To perform the studies at NPP site and investigate the effect of various parameters associated with the evolution of fireball.

## **1.2. Accomplishment of the present project**

In view of this, the objectives of the present work have been divided into following parts. In the first part, the hydrocarbon fireballs have been analysed for their detailed characterization including diameter, lifetime, flame and internal structure using CFD simulations. The lifetime and diameter of fireball obtained by simulations and available empirical models have been compared with experiments and video footage data to examine inherent assumptions and

limitation made in empirical models in describing internal fireball structures. The parametric studies are also conducted by varying the mass of fuel, inlet velocity and inlet diameter.

In the second part, CFD simulations have been performed with Vapour fuel inlet model and Dynamic fuel spray model. The inputs to the fireball analysis using dynamic spray approach needs the initial droplet sizes and its distribution in the fuel cloud resulting from rupture of an impacting aircraft fuel tank. A Mathematical model is developed for prediction of droplet size and distribution associated with the impact of a liquid-containing projectile. The velocity and droplet distribution of dispersed fuel have been used as inputs to analyse the formation of fireball using OpenFOAM CFD code. In the third part, simulations have been performed to deliberate aircraft impact assessment for NPP structures, using dynamic spray method. The local transient values of parameters relevant to the safety assessment are analysed in details. Effect of NPP structures on the evolution of fireball and radiative heat received has also been studied.

### **1.3. Organization of thesis**

Keeping the research objective in mind, the present thesis is organized into the following chapters.

In **Chapter 2**, the literature review study has been deliberated on the following major parts: aircraft impact, fuel dispersion and hydrocarbon fireball formation. An overview of experiments conducted to analyse liquid dispersion phenomena and spray characterization using liquid-filled metal containers has been given. The accidental and experimental observations of fireball have been summarised. Theoretical studies on fireball diameter, duration, the lifting height of fireball, heat released rate, and the radiative heat flux associated

with fireball are reviewed. The numerical simulations conducted by various authors on aircraft accident and fireball have been discussed in this chapter.

**Chapter 3** describes the mathematical models and numerical methods used in Computational Fluid Dynamics (CFD) analysis of hydrocarbon fireball. The fireball analysed using Eddy Dissipation Concept (EDC) with single-step reaction provides reliable results. LES model for fireball simulation give an idea about instantaneous flame shape in a turbulent cloud. Fireball diameter and lifting height computed from the numerical analysis are found to be in good agreement with experimental data of Droste et al. (1999). The LES model illustrated the large eddies clearly and gives an idea about instantaneous flame shape in the turbulent cloud. To study the effect of inlet fuel mass, inlet velocity and inlet opening diameter on the fireball characteristics such as fireball diameter, lifting height and duration of the fireball, the parametric studies have been accomplished. Correlations for determining the fireball diameter and duration have been developed based on these parametric studies. In this chapter, the radiative flux received from fireball at various places from the safety point of view is also analysed.

In **Chapter 4**, a model has been developed for prediction of droplet sizes and distribution associated with the impact of a liquid-containing projectile. The complex processes of crushing fuel tank, liquid emerging out and droplet formation with breakup and evaporation have been solved sequentially using analytical models. The model has been validated with experimental data available in the literature (Hostikka et al., 2015). Parametric studies are also performed to examine the effect of impacting velocities on primary droplets, secondary droplets, spreading velocities and evaporation using different fluids. The data of droplet cloud formation (droplet sizes distribution and spreading velocities) obtained in calculation has been used as boundary

and initial condition for CFD analysis performed in **Chapter 5** and **6** using dynamic spray method.

In **Chapter 5**, CFD simulations have been performed with vapour fuel inlet model and dynamic fuel spray model, to study the combustion, evolution and heat radiation from the fireball. To understand aircraft impact and dispersion of fuel, an accident case of Boeing 747-400 (available in NTSB, 2015) has been considered for analysis. The velocity and droplet distribution of dispersed fuel used as inputs to analyse the formation of fireball using CFD code has been calculated using a model explained in Chapter 4. The fireball parameters, such as its diameter and lifting in the CFD simulations performed using fuel in vapour form and dynamic spray are found similar once all the liquid fuel evaporates. The heat release rate and incident radiative flux calculated at locations on the ground show difference as the spreading and evaporating droplets may absorb the heat from the fireball during its evolution.

**Chapter 6** contributes the aircraft impact assessment performed with NPP structures. Simulations have been performed to analyse the effect of the fireball on nuclear containment and surrounding building structures using a three-dimensional CFD code. In the worst-case scenario, the maximum aircraft impact velocity and maximum fuel load for the larger commercial airliners in the service near to the NPP site have been considered. Three cases have been analysed to study the effect of impact from the different sides of the containment building. In the initial duration, the temperature of the fireball is found to be low as only small part of the fuel is evaporated and burnt. The fireball evolution is affected by the presence of NPP structure. The structures disturb the flame propagation.

**Chapter 7** provides the summary of the work and conclusions of the current work. Recommendations for future work also described in this chapter. All major findings of the present work have been discussed.

## CHAPTER 2: REVIEW OF LITERATURE

---

NPP safety is defined as the ability of the nuclear reactor to withstand a fixed set of prescribed accident scenarios judged by the International Atomic Energy Agency (IAEA) experts as the most significant adverse events in a nuclear power plant (Keller and Modarres, 2005). The safety of nuclear reactor is affected by both internal and external events. The external event can be of natural or human- induced origin. It is necessary to examine the accidental scenario to understand the consequences of the postulated accidents. There are two methods to analyse the accident scenarios in the nuclear power plants. One of the methods is probabilistic safety assessment and other is deterministic approach. The safety analysis should be performed using suitable combination of probabilistic and deterministic approach. In probabilistic safety assessment, probabilities are assigned to each accident scenario based on the analysis of relevant experimental data and historical incidents and associated frequency is estimated. In probabilistic safety assessment, the accident scenarios are systematically analysed with careful considerations of nuclear components interactions, common caused failure events, operating errors, and success and failure criteria. In the deterministic method, experimental and analytical techniques using a set of conservation equation in addition to conventional empirical correlations or a combination of these are used. The effect of various parameters is examined to understand the accidental scenarios and its consequences for evolving suitable mitigation measures. In this method primarily all input are known.

Following the impact of aircraft on any structures, the aviation fuel may spread in the vicinity of it. This may lead to formation of fireball due to combustion of fuel vapour. A fireball is a sudden ignition and rapid combustion of concentrated flammable vapour of either single fuel or diluted mixtures as an expanding radiant ball (Lees, 2012). The fireball is of relatively short

duration but it passes in its life cycle through several distinct stages which need to be carefully studied (Lees, 2012). These stages are (1) growth, (2) steady burning and (3) burnout. In the growth of fireball, rapid mixing of fuel and air with the rapid combustion of a fuel occurs. In the steady burning stage, the fireball is roughly spherical and changes to mushroom shape with red in colour. In the burnout stage, the size of fireball remains same, but the flame becomes less sooty and more translucent. A number of decisive parameters which helps to know about combustion of droplet or vapour cloud are described by researchers namely Abbott (1990), Cruz et al. (2001), Kuchta (1985) and Pitts (1991) and these are;

- Release direction: vertically released fuels are more probable to produce fireball than horizontal releases due to buoyancy effects,
- Momentum release: high momentum releases ignited quickly will result in a fireball,
- Wind effect: releases in still air are more subject to fireball since the wind tends to disperse the fuel-air mixture and
- Ignition time: earlier ignition is more likely to lead to a fireball,
- Ignition position: ignition sources below the mixture give rise to a fireball than those situated on the side or top of the mixture since buoyancy contributes to fireball formation,

In this chapter, a literature review on aircraft impact, fuel dispersion and fireball formation due to combustion of hydrocarbon fuel has been discussed. An overview of the parameters, which can affect the behaviour of the fireball, has been given. Literature survey on fuel dispersion due to the impact of liquid containing projectiles and characteristics has also been given. In the literature review, theoretical studies on fuel dispersion, fireball formation and heat load associated with it have been also depicted.

## **2.1. Regulatory approach to the safety assessment of aircraft impact on nuclear containment**

### **2.1.1. Atomic Energy Regulatory Board (AERB)**

In AERB regulations the flight frequencies at the nearest airfield and its distance from the site are taken into account. Atomic Energy Regulatory Board (AERB) discusses about the probability of occurrence of an aircraft crashing on nuclear power plant.

For this purpose, data such as the distance of the nearest airport along with the present flight frequency, expected growth, air traffic corridors in the region and the type of aircraft used shall be collected. This data shall be used in conjunction with appropriate formulation to arrive at the annual frequency of aircraft crashing on the category I (one) facility. If this frequency is found to be greater than  $10^{-7}$  per year, the detailed evaluation shall be carried out to assess the impact hazard including secondary consequences such as fire and explosions due to fuel burning.

### **2.1.2. International Atomic Energy Agency (IAEA):**

The analysis of the aircraft impact can be performed as per the regulatory approach given by International Atomic Energy Agency (IAEA) Safety Guides. The IAEA guide for the safety assessment of an NPP, NS-G-3.1 titled “External Human Induced Events in Site Evaluation for Nuclear Power Plants” is published in 2004. The relevant section for Aircraft Crash states the following possible consequences of the release of fuel from a crashing aircraft

- Burning of aircraft fuel outdoors causing damage to exterior plant structures and components important to safety,
- The explosion of part or all of the fuel outside buildings,

- Entry of combustion products into ventilation or air supply systems,
- Entry of fuel into buildings through normal openings, through holes caused by the crash or as vapour or an aerosol through air intake ducts, leading to subsequent fires, explosions or side effects.

The additional details for the type of fuel and the maximum amount of fuel potentially involved in an accident to quantify the fire interaction effects with the potential structural damage have also been given.

## **2.2. Aircraft Crash**

In the aircraft crash, it has been seen that the fuel in the wings is dispersed while crashing. The wings (fuel tanks) of modern commercial aircraft consist of open section beams, ribs and a skin reinforced by stringers made of Aluminium body (Forasassi & Lofrano, 2010). After impact with cruising velocity, the wing structure fails due to mechanical impact and internal pressure generated by liquid fuel. The fuel is expelled out in a large amount from the broken tanks and gets atomized to form a droplet cloud. The remaining fuel is ejected in the form of liquid chunks or may get leaked from the broken tanks. This leaked fuel possibly will lead to the formation of a liquid pool. Due to the availability of heat source either from the electronic circuit (broken) or from hot jet turbine parts, the vaporized portion of dispersed fuel initiates the combustion. The large quantity of the fuel engulfed within fire in very short duration results into a fireball. The portion of fuel, which is not involved in fireball formation, spills around and leads to local pool fire, which is further supplemented with unburnt liquid fuel rain. The fraction of fuel involved in fireball depends on the following

- Aircraft Type, fuel capacity and speed of impact
- Location and direction of impact (height from the ground)

- Type of building structure (size and shape of the building)

Every aircraft crash is unique with respect to parameters such as fuel, cruising velocity and local wind speed, geometry of fuel tank ruptured, fuel dump rate and existence of potential ignition sources. The aircraft accident study is divided into three major parts to understand the consequence of structure with which aircraft crashed. Following subsections explain the crash cases with various impact conditions.

### **2.2.1. Impact with ground**

The impact of aircraft on the ground is known as hard impact, because the aircraft body structure made of Aluminium alloy is softer material than the ground. The aircraft structure gets fully crushed after such an impact. The impact with a hard structure more eventually results in a fireball and rarely results into the case of a pool fire. Pool fire is often observed in the case where aircraft impacts with slower speed or with the soft terrains. Tieszen (1995) carried the experiments with aircraft impact using Lockheed C-141 and found that no liquid pooling occurred for impact velocities greater than 61 m/s. At lower velocities, he found some pooling with a maximum liquid-layer thickness of 5.25 mm.

On December 21<sup>st</sup>, the Lockerbie town suffered from a direct hit from Pan Am Boeing 747 airliner falling from the sky. It was carrying 90 Tons of aviation fuel some of which, upon impact, ignited into a ~100 m diameter fireball setting fire to passing vehicles and burning of buildings (Branch, 1990).

### **2.2.2. Impact on a small structure**

In the case of aircraft impact with small height structures, the approach of impact is horizontal and virtually at ground level. In these accidents, the aviation fuel will play a highly energetic

role immediately after impact and the aviation fuel spills over the structure. The fire from fuel possibly becomes the cause for the destruction of structures.

A hijacked commercial airliner Boeing 757-200 intentionally crashed into the Pentagon building in an act of terrorism (Mlakar et al., 2003). The estimated velocity of aircraft at the time of impact is found to be 156 m/s. One of the wings was sheared-off with the spilling of aircraft fuel and the fireball was generated. According to the National Transportation Safety Board (NTSB), the aircraft was having about 16,000 kg of jet-A fuel on board at the time of impact. Based on images captured by the Pentagon security camera, it was estimated that about 2,200 kg of jet fuel was consumed at the time of impact outside the building. The left about 13,800 kg as the estimated mass of the jet-A fuel entered the building and contributed to fire load within the building burning over 3400 m<sup>2</sup>. The building was damaged by the associated impact, deflagration and fire. The fire caused serious spalling of reinforced concrete.

### **2.2.3. Impact on Tall structures**

In aircraft impact with the tall structures, the cutting and stacking mechanism of skins, frames and spars of light airframes can occur and aircraft wings may cut through columns of the building. The shearing and tearing of the fuel tank will cause the spreading of fuel with a high velocity which aftermath gets atomized to form a combustible droplet cloud. Ignition of such droplet cloud leads to deflagration or detonation.

The hijacked plane, Boeing 767-223 ER hit the north tower of the World Trade Centre (WTC) on 11<sup>th</sup> September 2001. It was estimated by the Federal Emergency Management Agency, (FEMA, 2001) that aircraft was carrying about 34,000 L of fuel and was flying with a speed of about 211 m/s. The second hijacked plane, Boeing 767-222 was carrying about 31,000 L of fuel and travelling at about 265 m/s that hit the south tower of WTC. The large fireballs arising

were of 60 to 100 m in diameter, as mentioned by Federal Emergency Management Agency FEMA (2001). Baum & Rehm (2005) estimated the expansion velocity of the fireball of  $\sim 20$  m/s from the video footages. The remaining fuel flowed down through the building and burned off within a short duration after aircraft impact. The towers were destroyed by a combination of the plane impacts and fire ignited by the fuel available in each plane. Figure 2.1 shows the comparison between tall structures (WTC buildings) and structures with small height (Pentagon, USA and NPP). The aircraft impact velocity in case of tall buildings was higher compared to the case of small building. The maximum aircraft velocity closed to ground surface is limited by stagnation pressure by atmosphere.

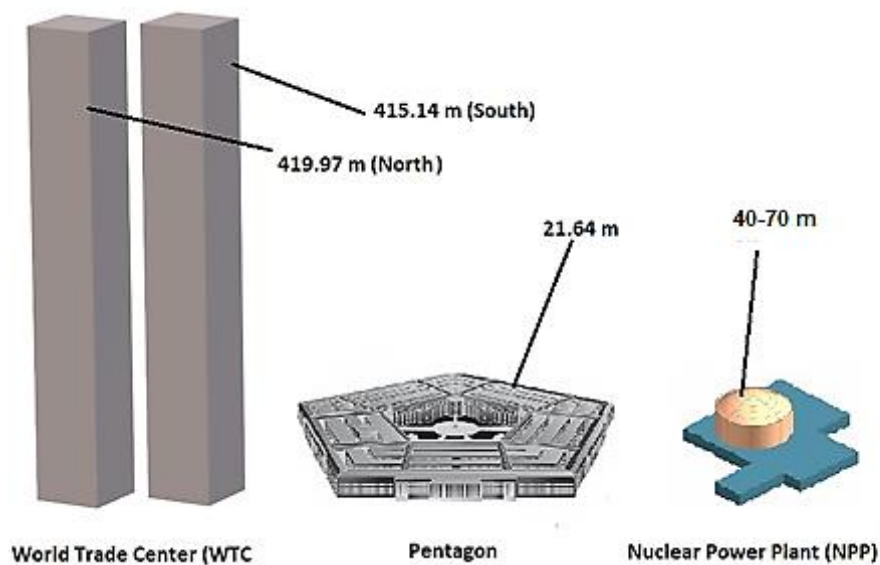


**Figure 2.1: Comparison of NPP with tall structure and small height structure**

It is quite complex to study aircraft crash at actual scale with fuel spillage and ignition phenomena. The aircraft crashes vary with aircraft type, impact velocity, the fuel loading and further, it also depends on the geometry of structure to which aircraft is impacting. To understand the aircraft impact and fuel spillage few experiments reported in the literature are deliberated.

#### **2.2.4. Experiments of aircraft crash**

Miguel (1978), Thomson and Caiafa (1982), Moussa (1990), Wolfson et al. (1990), Piers (1998), Large (2003), Hayden et al. (2005) and Mozingo et al. (2005) studied the fireball associated with aircraft crash.

NASA and the Federal Aviation Administration (FAA) conducted a joint program in 1984 for the acquisition, demonstration and validation of technology for the improvement of transport aircraft occupant crash survivability using a large Boeing 720 (Jackson et al., 2004) in a controlled impact demonstration (CID). The aircraft used in CID is remotely piloted. The aim of this program was to exhibit the use of anti-misting fuel to reduce post-crash fire (Horton & Kempel, 1988). A large fireball enveloping and burning the aircraft is observed in CID.

Tieszen (1995) described the development of a fuel dispersal model for impacting aircraft. He conducted twelve tests using a scaled model with impact velocity ranging from 12 m/s to 91 m/s and angles of impact ranging from 22.5° to 67.5°. He included high-speed cinematography and detailed mass distribution measurements. Tieszen (1995) found that no liquid pooling occurred for impact velocities higher than 61 m/s. At lower velocities, some pooling occurred, but maximum liquid-layer thickness greater than 5.25 mm is found. He noted the occurrence of some atomization of the liquid at all the velocities. These results can be used as initial boundary conditions for analysis of pool fire scenario during aircraft crash.

Muto et al. (1989), Von Rieseemann et al. (1989) and Sugano et al. (1993) reported a crash test conducted by Sandia National Laboratories. They conducted tests with Phantom F-4 aircraft carrying 4.8 Tons of water and hitting a reinforced concrete target at a velocity of 215 m/s. Hostikka et al. (2015) reported the initial liquid discharge velocity of 280 to 330 m/s as observed in their study. Further, they found that the liquid discharge velocity is 1.3 to 1.55

times the impact velocity. The authors detected the final size of droplet cloud diameter of 60 to 80 m. The experimental data obtained from these tests can be used to evaluate fuel dispersion during the impact of aircraft.

Kuchta (1973) reported that, in a survivable crash fire accident, the chance of human survival is greatly reduced when a massive fuel spillage occurs. He illustrated an indication of the fuel dispersion hazard, where the fireball size was plotted against impact velocity for vertical fuel drops with 5 gallons of JP-4 and JP-8 liquid and emulsified fuels. He noticed that the fireball hazard tends to be nearly comparable for the low and high flash point liquid fuels in case the impact velocity is increased sufficiently (e.g. 60 mph). He also observed that the fireball associated with the ignition of a small fuel spillage engulfed a large area in flame. Further, Kuchta (1973) found the dependency of fireball diameter on impact velocity i.e. fireball diameter (ft.) is found to be one half of impact velocity (mph) for 5-gallon metal containers in fuel drops with the JP-4 jet fuel.

During the impact of aircraft with high velocity, the fuel tank can get ruptured which causes fuel leakage. The formation of a large fireball is caused by the ignition of aircraft fuel cloud, which is erupting from the breaking fuel tanks. The liquid chunks or droplets with larger diameters may rain out and contribute to pool fire. The duration of the pool fire depends on the amount of fuel, which has not been burnt in the initial fireball.

### **2.3. Hydrocarbon Fireball**

Following subsections described the literature review carried for the formation of fireballs in experiments and accidents. Researchers performed experiments to study the behaviour of fireballs. These experimental studies are divided into two major categories based on the mass involved in the fireball as small-scale and large-scale experiments.

### 2.3.1. Small-scale experiments

Small-scale fireball experiments include soap bubble experiments in which a spherical gas-air mixture contained by a thin envelope at ambient pressure was released. The released gas was then ignited by a source to form a fireball (Fay and Lewis, 1977; Hardee et al., 1978; Lihou and Maund, 1982 and Roper et al., 1991). The second category includes Boiling Liquid Evaporating Vapour Explosion (BLEVE) (Maurer et al, 1977, Hasegawa and Sato (1977, 1978) and Robert, 1982). The flask containing liquefied fuel was ruptured when vapour pressure reached above its design limit value.

Fay and Lewis (1977) studied the burning of unconfined fuel vapour clouds of volume 200 cm<sup>3</sup>. They performed small-scale experiments with methane, ethane and propane gases at room temperature. Fay and Lewis (1977) used spherical gas samples inside soap bubbles of volumes 20 to 190 cm<sup>3</sup> for fireball experiments. Hasegawa and Sato (1977) used hermetically sealed spherical glass vessels. Each vessel was filled with n-pentane assembled with an electric heater and a thermocouple for measuring the temperature of the liquid. The amount of pentane used was in the range of 0.3 to 6.2 kg. Hardee et al. (1978) investigated pure methane and premixed methane-air fireball reactions. They used balloons filled with 0.1 to 10 kg of pure methane or stoichiometric air-methane mixtures.

Lihou and Maund (1982) used soap bubbles filled with flammable gas to form fireballs. Lihou and Maund (1982) carried out two series of experiments. The first series involved butane-filled bubbles whose masses ranged from  $1.5 \times 10^{-3}$  to  $6 \times 10^{-3}$  kg. The second series was performed with methane and butane in volumes ranging from 100 to 800 cm<sup>3</sup> (For methane of mass range from  $7 \times 10^{-5}$  to  $6 \times 10^{-4}$  kg and for butane it was from  $2.4 \times 10^{-4}$  to  $1.9 \times 10^{-3}$  kg).

Baker et al., (1978) studied the fireball arise from the pressurised tanks filled with Liquefied petroleum Gas (LPG) under high pressure at ambient and elevated temperature. They developed a method to estimate blast yields for unconfined vapour cloud explosions with fuel mass in the range of 7.5-14.5 kg. Roper et al. (1991) studied the effect of release velocity and geometry on burning times for non-premixed fuel gas clouds using propane and methane. They studied the fireballs with release velocities up to 88 m/s and fuel mass in the range of 1.5 to 13 g. Table 2.1 shows the small-scale experiments performed.

**Table 2.1: small scale experiments**

<b>Fuels</b>	<b>Reference</b>	<b>Containment</b>	<b>Fuel mass (kg)</b>	<b>Fireball Duration (s)</b>	<b>Fireball Diameter (m)</b>	<b>Emissive Power (kW/m<sup>2</sup>)</b>
CH <sub>4</sub> ,	Fay and Lewis	Soap	20-190	0.4-0.8	0.2-0.7	20-32
C <sub>2</sub> H <sub>6</sub>	(1977)	Bubble	(cm <sup>3</sup> )			
C <sub>5</sub> H <sub>12</sub>	Hasegawa and Sato (1977, 1978)	Pressurised Glass Spheres	0.3-30	0.8-1.7	2.7-15	110- 413
CH <sub>4</sub>	Hardee et al. (1978)	Polythene bags	0.1-1	1.8-2.4	1.5-2.2	123
C <sub>4</sub> H <sub>10</sub>	Lihou and	Soap	1.5-6 (g)	0.5-1.0	0.4-0.8	-
CH <sub>4</sub>	Maund (1982)	Bubble				
LPG	Baker et al. (1978)	Pressurised Tanks	7.5-14.5	1.0-1.4	12.15	-
C <sub>3</sub> H <sub>8</sub> ,	Roper et al.	toy balloons	1.5-13 (g)	0.5-2.0	0.4-1.2	-
CH <sub>4</sub>	(1991)					

### 2.3.2. Large-scale experiments

With the increased number of severe accidents involving a large mass of fuel, the researchers performed large-scale or full-scale experiments to investigate the behaviour of the fireball. High (1968) reported data on fireball size for rocket propellant systems. He used a kerosene type of fuel and liquid hydrogen with liquid oxygen from 1 kg to 5000 kg of fuel. He expressed

maximum fireball diameter as a function of the total weights of fuel and oxygen. Hardee and Lee (1973) reported experimental data for fireball with propane fuel-containing a mass of 1 kg, 29 kg and 454 kg. They measured total incident heat within the fireballs.

Maurer et al. (1977) performed experiments to study the effects of vapour cloud explosions in which fireballs were generated. These experiments involved vessels of various sizes ranging from 0.226 to 1000 L. The vessels were ruptured, and the released propylene was ignited after a preselected time lag. One of these tests, involving 452 kg of propylene, produced a fireball of 45 m in diameter. Johnson et al. (1991) reported full-scale experiments on the effects of Boiling Liquid Evaporating Vapour Explosions (BLEVE) conducted by British Gas using standard and extended size containers. These experiments involved butane and propane mass 1000 - 2000 kg released under a pressure of 6 to 15 bar gauge. The thermal flux recorded by a radiometer at 50 m from the vessel indicated a peak value of 66 kW/m<sup>2</sup> and the total heat dosage at this point was 115 kJ/m<sup>2</sup>. Li et al. (2015) studied large-scale LPG fireballs during the earthquakes in Japan on 11<sup>th</sup> March 2011. They reported five BLEVEs of LPG occurred resulting in huge fireballs measuring the diameter of about 500 m. They estimated LPG between 400 to 5000 m<sup>3</sup> for each vessel. Droste et al. (1999) performed a fire test with a 45 m<sup>3</sup> rail tank car partially filled with 10 m<sup>3</sup> pressurized liquid propane in Bundesanstalt Für Materialprüfung in Berlin (BAM). In this test, the fireball was formed due to the release of propane at a pressure of 25 bar. The fireball was sustained for 7.6 s. The diameter was about 100 m with the top of fireball about 150 m above ground level.

Mishra et al. (2015) performed an experimental investigation to measure the fireball characteristics using peroxy-fuel (containing 70 % tertabutyl hydro peroxide, ditertabutyl peroxide and water). The container was filled with 900 L of a peroxy-fuel. They measured thermal radiation of 4 kW/m<sup>2</sup> at 100 m from fireball whereas at 225 m it was measured to be

0.8 kW/m<sup>2</sup>. Wang et al. (2017) analysed the consequence of accidental LNG explosions using a full-scale experiment in transmission pipeline of approximately 800 m<sup>3</sup> (76,000 kg). They measured thermal radiation intensity of about 58.8 kW/m<sup>2</sup> at a distance of 100 m. They expected 100% fatality within 1s of exposure at the radial distance of approximately 224 m from the explosive.

### **2.3.3. Formation of fireball in various accidents and major hazard**

Skřínská et al. (2013) reported an explosion of liquefied petroleum gas (LPG) at the Auto-gas filling station. In the accident a car was collided with one of 4 storage tanks containing LPG which followed by gas leak and fire. After the explosion and rupture of the tank, fragments of the tank were scattered at a distance of several meters, causing the rupture of successive tanks nearby. Further, two tanks with a capacity of 3 m<sup>3</sup> each were embraced in the fire.

Park et al. (2006) examined LPG filling station incident occurred in Korea. The faulty joining of the couplings during butane unloading process from tank lorry into an underground storage tank leaked more than 4 tons (4461 kg) of butane resulted in a pool fire. Since, LPG unloading and filling activities were done simultaneously in a congested area, the explosion leads to a fire hazard. Park et al. (2006) studied two Boiling Liquid Evaporating Vapour Explosions (BLEVEs) by comparing with nearby buildings sizes, in which the first fireball observed at the propane tank lorry with the maximum diameter of about 130 m while the second observed maximum diameter of about 90 m at the butane tank lorry.

Pietersen (1985) studied the most tragic gas explosion took place in Mexico City on the 19<sup>th</sup> of November 1984. The storage area consisted of four spherical LPG tanks with a capacity of 1600 m<sup>3</sup> each, two spherical tanks of 2400 m<sup>3</sup> each and 48 cylindrical tanks of different diameters stored horizontally. At the moment of explosion, the total amount of LPG in the

refinery was within the range of 11000 to 12000 m<sup>3</sup>. As a consequence of the explosion about 5000 people were killed, and 7000 were injured. Only 4 out of 48 tanks remained at their original locations after the explosion. Twelve of them were thrown at a distance of 100 m, and one even as far as 1200 m. Pietersen (1985) reported the diameter of the fireball of 200-300 m and its duration of approximately 20 seconds.

**Table 2.2: Fireball accidents reported in the literature**

<b>Location and Year</b>	<b>Mass of Fuel (kg)</b>	<b>Fireball diameter (m)</b>	<b>Fireball duration (s)</b>	<b>Description</b>	<b>Reference</b>
<b>Greece, 1999</b>	41002	200	-	a road accident and tanker explosion containing LPG	(Skřinský et al., 2013)
<b>Korea, 1998</b>	4416	90	-	LPG filling station incident, unloading and filling activities done simultaneously	(Park et al., 2006)
<b>Mexico, 1984</b>	385170	350	25	Bursting of spherical LPG tanks	Pietersen (1985)
<b>Spain, 1978</b>	40000	200	-	a road accident and tanker explosion containing liquefied propylene	(Arturson, 1981)
<b>Spain, 2002</b>	19600	150	12	explosion of a road tanker transporting 19,000 kg of LNG	Planas-Cuchi et al. (2004)

Arturson (1981) reported a tanker explosion in a road accident occurred disaster on 11th July 1978 in Los Alfaques, Spain. The tanker was loaded with 23 tons of highly flammable liquefied propylene. Around 157 people died on site because of the initial explosion and the subsequent fires and explosions of cars nearby. In this consequence, total 217 people were killed and 200 more severely burned. The blast and fireball destroyed cars, trailers and buildings within a 300 m radius.

Planas-Cuchi et al. (2004) analysed the explosion of a road tanker, which was transporting LNG in Spain. All the 19,000 kg of LNG contained in the tank was involved in the fireball.

They estimated the corresponding size, duration and height of the fireball as 150 m, 12 s and 113 m respectively. At a distance of 200 m from the road tanker, two persons were injured (first and second-degree burns) in this accident. The fireball accidents in which major hazard have happened are summarized in Table 2.2.

## **2.4. Theoretical Studies of Fireball**

The fireball from liquid fuel and gaseous fuel may be different. Theoretical studies of fireball are mainly concentrated on determining the characteristics of fireball such as diameter and duration by developing fundamental models. Bader et al. (1971) developed a model for a fireball of propellant. They assumed fireball to be homogeneous, isothermal and spherical in shape, which radiates heat as a black body with no air enters during the lifecycle of the fireball. Hardee and Lee (1973) give the similar model as Bader et al. (1971) with the additional assumption for growth in a vapour cloud. They considered ignition of the mixture at stoichiometric conditions. Fay & Lewis (1977) model the fireball formed from stationary fuel vapour. In the dimensional analysis, they neglected the volume of fuel compared to that of products. Roper et al. (1991) studied the fireball under buoyancy and momentum regimes. They obtained correlations for burning time for a fireball of both low and high momentum cases. The studies presented by Roberts (1982b) include both development of fundamental model and correlations based on experimental data. This model covers the whole range of features of practical interest and so most widely used. He studied the growth of fireball from bursting vessel that gives the model for hemispherical fireball also. Marshall (1987) modelled fireball diameter and duration based on the correlations. Further, he gives the correlation for the effective surface temperature of the fireball.

### 2.4.1. Mass of fuel involved

Mass of fuel entrained in fireball depends on the fraction of fuel, which is flashed off, and further on the fraction, which forms liquid sprays. Roberts (1982a)deliberated a study on propane for a theoretical adiabatic flash fraction, liquid temperature and vapour pressure. He found that 35% flash fraction occurs at 21°C and 50% fraction at 45°C. Hesegawa and Sato (1977)found that when the theoretical adiabatic flash fraction reaches 35%, virtually all the liquid released burns as a fireball. From this, A. F. Roberts (1982a)derived a relationship:

$$f = \frac{M_{involved}}{M_{released}} = 0 \quad \text{for } \phi = 0$$

$$f = 1 \quad \text{for } \phi \geq 0.35$$
(2.1)

Where,  $f$  is a fraction of fuel, which is entering in the fireball.  $M_{involved}$  is mass of fuel involved in the formation of fireball (kg),  $M_{released}$  is mass of liquid released (kg) and  $\phi$  is a fraction of liquid vaporized. Hence by linear interpolation,

$$f = \frac{\phi}{0.35} \quad \text{for } 0 < \phi \leq 0.35$$
(2.2)

This treatment is commonly used to determine the mass of fuel participating in the formation of the fireball.

### 2.4.2. Fireball Diameter, duration and lifting height

The developed correlations predict the maximum size, duration, lifting height, radiation and a safe distance from hot fireballs. Following correlations for calculating fireball diameter and its duration are proposed by various authors based on their experiments,

$$D_{FB} = k_1 M_{fuel}^{n_1} \quad \text{and} \quad t_{FB} = k_2 M_{fuel}^{n_2}$$
(2.3)

Where,  $M_{fuel}$  is the mass of fuel involved in a fireball. The constants  $k_1$ ,  $k_2$ ,  $n_1$  and  $n_2$  used in the above correlations are summarized in Table 2.3. The average height of the centre of the fireball can be in the range from  $D_{FB}/2$  for high-momentum releases with no buoyancy effects to  $5/6D_{FB}$  for buoyancy-dominated releases. The available expressions for estimating the height of the fireball from the ground are listed in Table 2.4.

**Table 2.3: Constants for correlations of fireball mass (kg), diameter (m) and duration (s).**

Model	Diameter Equations		Lifetime Equations		Parameters
	$k_1$	$n_1$	$k_2$	$n_2$	
Hardee and Lee (1975)	6.24	1/3	1.1	1/6	0.435-435.5 kg of welding gas, 421.8 kg of Propane released to form a fireball
Pietersen (1985)	6.48	1/3	0.85	0.26	385 Tons of LPG in a gas explosion
Marshall (1987)	5.5	1/3	3.8	1/3	$M_{involved} = 2\phi M_{released}$ for Winter $M_{involved} = 3\phi M_{released}$ for Summer
CCPS (1999)	5.8	1/3	0.45	1/3	$M_{involved} = 0.3M_{released}$ for $\phi < 0.3$ $M_{involved} = M_{released}$ for $\phi > 0.3$
TNO (1989)	6.48	1/3	0.85 2	0.32	LPG road and rail tankers in databases for accidents

**Table 2.4: Correlation for estimating the height of fireball centre from the ground**

Model	Height of centre of fireball (m)	Reference
Centre for Chemical Process Safety (CCPS)	$H_{FB} = 4.35M_{fuel}^{0.33}$	CCPS (1999)
The Netherland Organization of applied scientific research (TNO)	$H_{FB} = 6.48M_{fuel}^{0.325}$	TNO (1989)

Figure 2.2 and Figure 2.3 show the comparison of fireball diameters and the duration calculated from various correlations given in Table 2.3. It can be found from Figure 2.2 that the diameters (expansion of fireball) calculated using correlations over predict the diameter measured in the experiments/accidents (Arturson, 1981; Droste et al., 1999; Johnson and Pritchard, 1991; Kodur, 2002; Lees, 2012; Park et al., 2006; Planas-Cuchi et al., 2004). The above correlations are proposed based on the assumption that the ignition occurred when the mixture is in a stoichiometric ratio and all the available fuel burns.

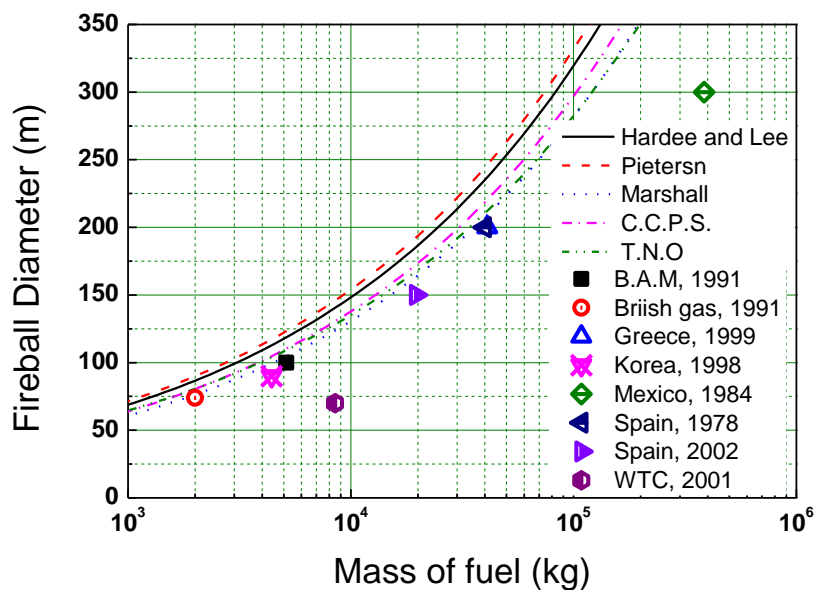


**Figure 2.2: Comparison of maximum fireball diameter obtained from relationships with accident/experimental observations.**

Figure 2.3 depicts the duration of fireball calculated from correlations and compared with the observed values as a function of time of accidents/ experiments. It can be seen that correlation by Hardee and Lee (1975) underpredicts the fireball duration, while TNO overpredicts the fireball duration. The other correlations are in the agreement with the observed duration of the fireball.

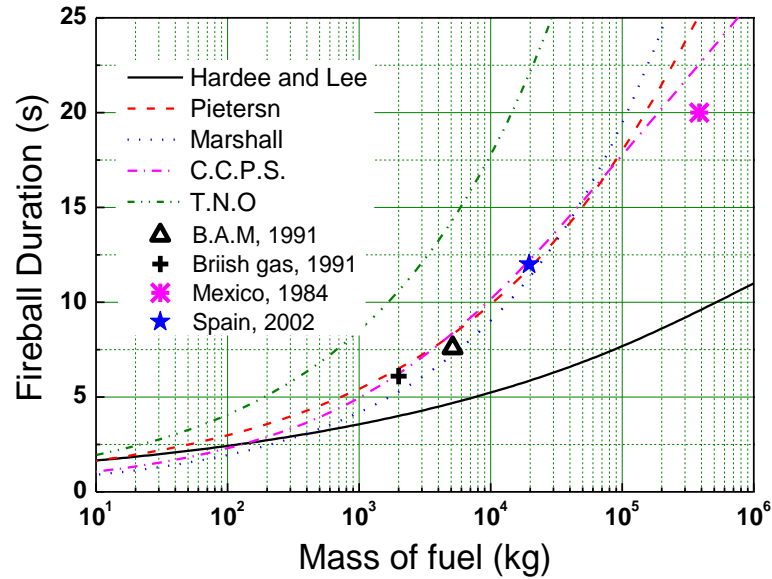


Figure 2.3: Comparison of fireball duration obtained from relationships with accident/experimental observations.

#### 2.4.3. Heat Release Rate (HRR)

The heat release is the critical parameter to study the evolution of fireball. The heat release from a large fireball affects as thermal radiation on the surrounding objects. This can produce fatal injuries or damage to the surrounding building infrastructures or to human life. The heat release can be calculated from the heat of combustion of fuel. The average heat released during the lifecycle of the fireball is,

$$HRR = \frac{\Delta H_c M_{fuel}}{t_{FB}} \quad (2.4)$$

where,  $\Delta H_c$  is the heat of combustion of fuel,  $M_{fuel}$  is mass of fuel involved in fireball and  $t_{FB}$  is the fireball duration. The fireball releases large heat in a short duration due to combustion of fuel into the atmosphere with the availability of oxidizer in the air. This gives the peak value of heat release rate (HRR). The flame at the outer surface of fireball purely “flashes” because

the heat release rate of the establishing flame is insufficient to overcome the rate of heat losses to the surrounding atmosphere. In the initial period, HRR increases with time and this is attributed to the entrainment and mixing of air from the atmosphere, which promotes the rapid combustion. After that, HRR reduces due to unavailability of fuel for combustion. Peak HRR is the highest value of released heat during the lifetime of the fireball.

#### 2.4.4. Radiation effect from the fireball

A Fireball can emit a large amount of radiant energy during its lifetime. Moorhouse & Pritchard (1982) assumed that fireball radiates uniform heat but the radiative emission from a fireball varies over its surface. This causes injuries and damage to an area several times greater than the size of the fireball (Martinsen and Marx, 1999). The incident radiation on the target from the fireball can be estimated by using expressions listed in Table 2.5.

**Table 2.5: Model estimating the incident radiation on the target**

Model	Incident radiation (W/m <sup>2</sup> )	Reference
Solid Flame model	$q_r = \tau \cdot SEP \cdot F$	CCPS (1999), TNO (1989)
Hymes model	$q_r = 2.2\alpha\tau\chi_R \cdot \frac{\Delta H_C M_{fuel}^{0.67}}{4\pi L^2}$	Hymes (1983)
Lees model	$q_r = \alpha\tau\chi_R \frac{HRR}{4\pi L^2}$	Lees (1996)

Here, SEP is Surface Emissive Power,  $\tau$  is the transmissivity of the atmosphere between the fireball and the target,  $\chi_R$  is radiative heat fraction,  $L$  is the distance from the target to the point source location and  $\theta$  is an angle of the target relative to the line of sight connecting the source and target.  $F$  is the configuration factor. The radiative fraction is generally in the range of 0.1-

0.4 depending on the fuel vapour pressure, storage conditions and flame scale (i.e. the optical thickness of fireball).

#### 2.4.5. Thermal dose

The seriousness of injuries and the extent of damage that can be caused by thermal radiation from a fire, depends on the intensity of the incident radiation and the duration of exposure to that level of heat flux. Since, fireballs exist for only a few seconds, the duration of exposure is commonly set equal to the duration of the fireball. The evaluation of the damage caused by the thermal radiation is proportional to the radiation intensity of exposure (Centre for Chemical Process Safety, CCPS 1994),

$$D_{th} = t.q^{4/3} \quad (2.5)$$

Where,  $D_{th}$  is the thermal radiation dose in  $(W/m^2)^{4/3}.s$ ;  $t$  is the duration of exposure in s and  $q$  is the incident radiative flux in  $W/m^2$ .

### 2.5. Fuel dispersion study

The different physical phenomena occur due to leakage of fuel during the impact of aircraft with high velocity. In the initial stage, fuel in the aircraft wings will be dispersed out due to rupture and forms the droplet cloud. Normally, fuel leakage forms liquid chunks for smaller impact velocities and droplet cloud for higher velocities. The fuel spills out from ruptured tanks and disperses to the surrounding. During the dispersion, the primary breakup of liquid occurs due to the destabilizing process of aerodynamic drag and turbulence within the liquid core. The primary breakup phase is followed by secondary breakup phase of flying droplets. Depending on the speed of droplet relative to surrounding gas, the secondary breakup can produce droplets of different sizes. While studying the impact of large mass and dispersion phenomena of liquid,

it is found that Weber number,  $We = \rho V^2 D / \sigma$  associated with these impacts is of the range  $10^5$  to  $10^8$ . Where, V is the velocity of impacting slug and D is the diameter of slug.

A very few publications are available on the study of this phenomenon. Tieszen (1995) described the development of a fuel dispersal model for the Defence Nuclear Agency's (DNA) Fuel Fire Technology based program. They conducted the tests with the scaled model. Twelve tests were conducted over an impact velocity ranging from 12 m/s to 91 m/s and angles of impact from  $22.5^\circ$  to  $67.5^\circ$ . Diagnostics included high-speed cinematography and detailed mass distribution measurements. The test results showed that no liquid pooling occurred for impact velocities greater than 61 m/s. At lower velocities, some pooling occurred, but in no test was the liquid-layer thickness greater than 5.25 mm. Some atomization of the liquid was noted to occur at all velocities. Sandia National Laboratories conducted a water-slug impact test in which a large water volume was ejected and it was dispersed at high speeds (Jepsen et al., 2004). A 1.2 m diameter and 2.4 m long aluminium cylinder (impact slug) was filled with approximately 2830 L of red-dyed water. The slug was rocket propelled down the sled track to a peak velocity of about 105 m/s and ejected water radially at distances up to 40 m. The discharge speed and direction of the liquid core released from the ruptured missile, the propagation speed of the spray front, liquid pooling on the floor, the extent of liquid dispersal away from the target, and the drop size of the liquid spray were measured in experiments.

Xu et al. (2005) investigated the corona splash due to the impact of a liquid drop on a smooth dry substrate with high-speed photography. A dependency of splashing on the pressure of the surrounding gas was observed. The threshold pressure where a splash first occurs was measured as a function of the impact velocity. They stated that the splashes at the expanding rim were not caused by air entrapment near the drop centre on impact.

Silde et al. (2011) studied liquid dispersal phenomena in the IMPACT tests conducted with a fluid-filled missile at the Technical Research Centre of Finland (VTT). Cylindrical missile impact velocities were from 70 to 177 m/s. The liquid front emerging from the ruptured missile was about 2 to 2.5 times the impact velocity of the missile. The propagation speed of the spray front decelerated and decreased rapidly with increased distance from the source. The arithmetic mean droplet sizes of the measurements taken from the oil-coated collection plates on the floor in selected tests were found between 200 and 300  $\mu\text{m}$ .

Hostikka et al. (2015) investigated sprays resulting from the impacts of water-filled metal Aluminium and stainless steel projectiles at speeds of between 96 and 169 m/s on a hard wall. The weights of the projectiles were in the range of 38 to 110 kg, with 8.6 to 68 kg of water. The results indicated that the liquid left the impact position as a thin sheet of spray in a direction perpendicular to the projectile velocity. The Sauter Mean diameters (SMD) were in the 147 to 344  $\mu\text{m}$  range. The data from this experiments can be used to determine the initial boundary conditions for liquid dispersion analysis.

## **2.6. Computational Fluid Dynamics (CFD) Studies**

The advantage of CFD code over engineering formulae is the possibility to simulate the effect of structures deflecting the expansion of fireball and the evaluation of the detailed temperature distribution.

### **2.6.1. CFD Studies on fireball**

Makhviladze et al. (1997) presented a numerical model for the burning of methane cloud released into the atmosphere. Makhviladze et al. (1999) again conducted a numerical study of the combustion of fireballs produced by vertical releases of hydrocarbon fuels i.e. propane into the atmosphere. They analysed the internal structure of fireballs with details and traced the

transformation of the initial burning stream into a spherically shaped fireball. Makhviladze and Yakush (2000) considered fuels ranging from cryogenic pressurized-liquefied propane to medium and low-volatility pentane (and octane) with flashing and non-flashing outflows. They compared radiation characteristics of small (optically thin) and large (optically thick) fireballs. They also showed the behaviour of the two-phase liquid mixture in fireball. Yakush and Makhviladze (2005) carried out the Large Eddy Simulations (LES) of propane fireballs using the Fire Dynamics Simulator (FDS) developed at the National Institute of Standards and Technology (NIST). They presented temperature and reaction rate fields with the transient behaviour of the total heat release rate (HRR) and the fraction of heat radiation. Baum and Rehm (2005) presented an analytical model based on an exact solution of the low Mach number momentum equation for the initial expansion of a fireball. Their solution was used to study the initial expansion of the fireballs generated in the attack on the World Trade Centre (WTC) south tower.

To investigate explosion in fuel vapour cloud, Hu and Trouve (2008) used Large Eddy Simulation (LES) approach with a partially-premixed combustion (PPC) model for simulation of transient combustion of fuel vapour clouds by means of a modified version of FDS code. Luther and Müller (2009) studied experimental data for the BAM fireball using FDS simulation. Shentsov et al. (2016) studied the development of predictive computational fluid dynamics (CFD) model for the assessment of hazard distances from fireball and blast wave resulted from high-pressure hydrogen storage tank rupture in the fire. The simulation of the blast wave and fireball dynamics is performed using the Eddy Dissipation Concept (EDC) model coupled with discrete ordinates (DO) radiation model.

Rajendram et al. (2015) focused on the modelling of fire risk for a range of accident scenario from investigation report of U.S. Chemical Safety Board (CSB 1998). They used two different

fire modelling approaches, the solid flame model and CFD fire based model. In CFD Model Pyrosim and FDS tool are used. They found that lethality from the fireball is very high near the centre of fireball and occurs for short duration. Mishra et al. (2015) performed CFD simulations to predict the fireball characteristics of different fuel. They solved models for turbulence, combustion and radiation in transient runs to account for the essential physics for peroxy-fuel as well as for propane and Jet-A with commercial code Ansys CFX 14.5. Wang et al. (2017) compared theoretical and experimental results with simulated results using the Process Hazard Analysis Software (PHAST). They determined the thermal radiation exposure from the LNG explosive fireball with distance from the explosive point

### **2.6.2. CFD Studies on fireball associated with aircraft crash**

The advantage of CFD code over engineering formulae is the possibility to simulate the effect of structures deflecting the expansion of fireball and the evaluation of the detailed temperature distribution. Baum and Rehm (2003) have presented an analytical model to study the initial expansion of the fireballs generated in the attack on the World Trade Centre (WTC) south tower. They used video images to estimate the expansion rate of the fireball. From this statistics, they estimated the fuel consumed in the fireball by combining the data with the analysis. They calculated the lifting velocity of fireball ( $\sim 20\text{m/s}$ ) and validated with obtained video footage.

Luther and Müller (2009) demonstrated the FDS tool to investigate the effects of fireball caused by the crash of a commercial airliner with Nuclear Power Plant (NPP) structures using 90 ton of kerosene. They studied the initial duration of the fireball before it rises above the NPP and the potential hazard of the flame front on the safety of the NPP. They presented the impact of building structures on fireball evolution and local rise in flame temperature.

### 2.6.3. CFD studies with fuel dispersion

Silde et al. (2011) studied the droplet dispersion using Fire Dynamics Simulator (FDS). They considered the initial speed of water droplets in the range of 100 and 300 m/s and adjusted the artificial source of gas momentum to achieve visually realistic spray patterns. They performed simulations with a combination of log-normal and Rosin-Rammler size distributions with prescribed mean diameters of 100 and 300  $\mu\text{m}$  of water.

Sakai et al. (2014) studied the influence of fuel explosion and consecutive fire which can occur after a postulated aircraft crash using Fire Dynamics Simulator (FDS). They assumed initial droplet velocity and distribution on the basis of observations from the IMPACT water missile experiments performed by Silde et al. (2011). They also analysed the explosion in middle-size commercial aircraft crash to the sidewall of the Boiling Water Reactor (BWR) building using transient fuel droplet dispersion. They found that 60% of total fuel involved in a fireball and residual fuel would attach to the ground close to the wall.

From the above literature survey, it is found that there is limited experimental data available on the fire in the vicinity of a nuclear power plant. In the available accidents and experiments performed on aircraft crash, it is found that the worst-case scenario is the impact of largest aircraft with its maximum cruising speed when it is loaded with its maximum fuel capacity. Experiments were performed using water to study the fuel dispersion phenomena in aircraft crash, but the physical properties of water and fuel are distinct in nature. From the fireball accidents, it is found that fireball is self-sustaining and it can engulf a large area during its evolution. Thermal radiation from the fireball is dangerous and it can cause major hazards to the goods and structures within a very short duration depending upon its intensity. Human fatalities can also happen within short exposure at far distances from the fireball. Experimental

studies were performed on fireball considered unconfined fireballs only. Computational study can be used to study the fireball within the confined environment also.

## **2.7. Gap areas**

Based on the literature survey, it is now known that there exist many unresolved issues for thermal hazards associated with aircraft impact with nuclear containment. Briefly, they are

1. Applying traditional diagnosis for aircraft wing impact and fuel dispersion problem is difficult because of destructive energy associated with high speed. The process of crushing the fuel tank, liquid emerging out and droplet formation with breakup and evaporation is a very complex process to solve by CFD code.
2. In the investigations of spray characteristic, the experiments are conducted for the impact of water-filled metal projectiles on the hard wall. Hydrocarbon fuels typically have lower surface tension than water. The spray characteristics such as droplet size distribution and spreading velocity obtained using water cannot be directly applied to full-scale computations by simply adjusting the mass of fuel.
3. In hydrocarbon fireball, due to the short duration and inherent transient associated with combustion, the accident scenario is difficult to investigate experimentally. Hence, very little information can be inferred from the experiments about the internal structure formation, evolution, combustion and explosion of fireballs resulting from an aircraft crash.
4. In the literature, Models were developed to analyse the fireball behaviour. From these models various correlations were developed to study the maximum diameter, duration and height of fireball. There is need to access various correlations and develop new correlations which can estimate diameter, duration and lifting height in better way.

5. Fireball associated with aircraft crash is caused due to the instantaneous burning of droplet cloud that arises in impact. The raining of fuel larger droplets out of the fireball, which may contribute to the formation of fuel pool and pool fire is not considered in the literature. The traditional correlations for fireballs cannot be directly applied to the case of an aircraft crash. Also, there is lack of study/experiments regarding the engulfment of fireball to building structures due to sticking of droplets to structural surfaces.
6. Safety assessment of NPP integrity for thermal hazard is done only with the effect of elevated temperature on the concrete of outer containment walls. The fuel droplet/ vapour may enter through the openings of containment buildings and could possibly create a hazardous environment inside the building, hence there is need of local prediction of parameters during the aircraft crash.

## **2.8. Scope of the work**

The aircraft impact process is obviously a definite interaction between a very large stationary target and fast moving object. In order to make this problem mathematically tractable, various phenomena associated with liquid dispersion, cloud formation, combustion and heat transfer associated with aircraft crash are required to be investigated.

1. It is necessary to analyse fireball using CFD codes to understand phenomena associated with combustion of fuel and flame structure inside the fireball. A Parametric study is required to comprehend the effect of inlet fuel mass, inlet velocity and inlet opening diameter on the fireball characteristics such as fireball diameter, lifting height, duration of fireball and radiative flux for safety assessment purpose.

2. The radiation energy emitted by the fireball is dangerous for personnel in the vicinity of the fireball. Hence it is important to study incident radiation at different locations from the fireball. The effects on the building structure for the evolution of fireball need to be studied.
3. There is a need to develop a mathematical model for projectiles with the hydrocarbon fuels which can undergo flashing during splashing of liquid with high speed. The theoretical tools which can deliberate the detailed boundary and initial condition for Computational Fluid Dynamics (CFD) to analyse fire hazard associated with aircraft impacts on NPP structures is required.
4. The safety assessment of NPP is required to understand effect of aircraft impact induced fireball on the containment building structures using Computational Fluid Dynamics at the realistic scales of NPP.



## CHAPTER 3: CFD ANALYSIS OF HYDROCARBON

### FIREBALLS

---

#### 3.1. Introduction

There are three main aspects that need attention while analysing a fireball phenomenon, namely, turbulence, combustion and radiation. Fireball formation begins with the ignition of a small amount of fuel. The fuel and air continue to mix and burn in a turbulent manner at or near ambient pressure. The pressure effects are usually small or negligible in the unconfined fireballs (Roberts et al., 2000). While the fireball is burning, there is time for additional turbulent mixing to occur. This can bring most of the fuel in the cloud into the flammable mixture limits.

At the initial stage, the fireball remains in a spherical shape when it is attached to the ground. When most of the fuel is reacted, the radial expansion decreases and buoyant forces begin to act on the hot gases, the fireball starts to lift off from the ground. Once lift-off occurs, a drag and natural convection current approach the fireball, a spherical shape due to Rayleigh-Taylor instability. Most of the thermal energy lost by the fireball is radiated away during the liftoff time.

Due to short duration and inherent transient associated with combustion in fireball, the analysis of accident scenarios is difficult experimentally. Hence, very little information can be inferred from the experiments about the internal structure formation, evolution, combustion and explosion of fireballs. Makhviladze et al. (1999) numerically studied the internal structure of fireballs, sizes, burning times and radioactive fractions. The dynamic shape of fireballs in this study showed quite well agreement with observations by Hasegawa and Sato (1978).

Makhviladze and Yakush (2002) studied the fireball from 2000 kg of butane corresponds to large scale BLEVE experiments reported by Johnson and Pritchard (1991). Makhviladze and Yakush (2002) analysed the consequences of large scale accident using CFD tools which involved release of hydrocarbon fuel in 1989 near Ufa, Russia. Luther and Müller (2009) validated the simulation capabilities of Fire Dynamic Simulator (FDS) tool by comparing experimental data of BLEVE experiment conducted by BAM in Germany.

In this chapter, three Dimensional Computational Fluid Dynamics (CFD) simulations of hydrocarbon fireballs have been performed for their detailed characterization including diameter, lifetime, flame and internal fireball structure. The fireball resulting from the loss of fuel tank containment exposed to fire (an experiment conducted by the German Bundesanstalt für Materialforschung (BAM) in 1999) is considered for the CFD analysis. The incident radiations on the ground are calculated using numerical method along the radial position from the centre of the fireball, to predict the thermal hazards. The new correlations for fireball diameter and duration have been proposed based on the parametric studies using CFD simulations.

### **3.2. Need of Computational Fluid Dynamics (CFD)**

The diameter and duration of the fireball from the available semi-empirical models may only be employed to obtain the maximum diameter and duration of existence of fireballs. To understand the phenomena associated with the combustion of fuel and flame structure inside the fireball, it is necessary to analyse fireball using CFD codes. There are assumptions made by researchers, which also justifies the need of using CFD modelling for fireball detail analysis.

### 3.2.1. Advantages of CFD

CFD has a number of advantages over other evaluation methods, particularly when compared to physical experimentation. These include:

*Reproducibility:* As there are no variables outside the control of the experiment, the model will produce the same results every time when it is run.

*Parameterisation:* Once a model has been set up, it is a trivial task to alter an input parameter and re-run. Many CFD codes have a batch mode to allow many cases to be queued up and run without user intervention. This can be used, for example, to obtain results over a range of fuel inlet velocity for fireball, or to ‘optimise’ the value of certain parameters.

*Economics:* A numerical study requires very little in the way of equipment, space and man-hours. Although the modelling process itself is less than real-time for most flows, the ability to run experiments back to back 24×7, means that the overall time for a study is reduced, typically leading to economic advantages. In a similar way, physical experiments can have a ‘cost’ in terms of environmental impact and health and safety considerations, which would not apply to a numerical simulation.

*Flexibility:* A CFD model allows for independent variation of all model parameters, with very few limitations. Physical experimentation tends to be much more limited. For example, gravitational force and experimental arrangement, however in a CFD model, the gravitational vector can be altered to any direction and magnitude to study its influence.

*Full Scale:* CFD techniques do not require any artificial scaling, which is often a limitation of physical experiments.

*Analysis:* Physical experimentation requires instrumentation (thermocouples, velocity probes,

pressure transducers, infrared (IR) imaging, etc.) in order to produce quantitative data. This instrumentation will always be limited and is often the major constraint on an experimental procedure. By contrast, a CFD model intrinsically contains all the data (and more) that could ever be required. CFD should not, however, it can be considered as a replacement for physical experimentation or for theoretical analysis. Results from a CFD model are meaningless without validation against experimental data.

### **3.3. Mathematical model and numerical method**

The simulations were carried out using FireFOAM module of OpenFOAM developed by Wang et al., (2011). It is an open source CFD software package. The solver has advanced meshing capabilities including adaptive and unstructured mesh with parallel computing capability. The FireFOAM module is embedded with the turbulence model, combustion model, soot model, radiation model and pyrolysis model. The governing conservation equations and models used in FireFOAM are described in the following subsections.

#### **3.3.1. Governing Equations**

The continuity equation is implemented based on the principle of conservation of mass. In order for mass to be conserved, the rate of flow into a volume must be equal to the rate of change of mass within the volume. Newton's second law of motion states that the rate of change in momentum of the fluid in the volume is equal to the sum of forces acting on it. This principle is used in the momentum equation. The energy equation is derived from the first law of thermodynamics. It states that the rate of change of energy of the elemental volume of fluid is equal to the rate of heat added to the fluid plus the rate of work done on the fluid.

Using Favre-filtered quantities (Poinso and Veynante, 2001) and density weighted mean, the

following equations are obtained,

$$\frac{\partial \bar{\rho}}{\partial t} + \frac{\partial}{\partial x_j} (\bar{\rho} \tilde{u}_j) = 0 \quad (3.1)$$

$$\frac{\partial}{\partial t} (\bar{\rho} \tilde{u}_i) + \frac{\partial}{\partial x_j} (\bar{\rho} \tilde{u}_i \tilde{u}_j) = \frac{\partial}{\partial x_j} \left( \bar{\rho} (\nu + \nu_t) \left( \frac{\partial \tilde{u}_i}{\partial x_j} + \frac{\partial \tilde{u}_j}{\partial x_i} + \frac{2}{3} \frac{\partial \tilde{u}_k}{\partial x_k} \delta_{ij} \right) \right) - \frac{\partial p}{\partial x_i} + \bar{\rho} g_i \quad (3.2)$$

$$\frac{\partial}{\partial t} (\bar{\rho} \tilde{Y}_k) + \frac{\partial}{\partial x_j} (\bar{\rho} \tilde{u}_j \tilde{Y}_k) = \frac{\partial}{\partial x_j} \left( \bar{\rho} D_k \frac{\partial \tilde{Y}_k}{\partial x_j} - \overline{\rho Y_k'' u_j''} \right) + \tilde{\omega}_k \quad (3.3)$$

Where,  $k = C_3H_8, CO_2, H_2O, O_2$

$$\frac{\partial}{\partial t} (\bar{\rho} \tilde{h}_s) + \frac{\partial}{\partial x_j} (\bar{\rho} \tilde{u}_j \tilde{h}_s) = \frac{\partial}{\partial x_j} \left( \Gamma_h \frac{\partial \tilde{h}_s}{\partial x_j} \right) + \frac{\partial p}{\partial t} + \overline{S_{rad}} + \overline{S_h} \quad (3.4)$$

$$\text{Where, } \Gamma_h = \left( \frac{\mu}{Pr_h} + \frac{\mu_t}{Pr_{th}} \right)$$

Where  $\rho$ ,  $u$ ,  $p$ ,  $h_s$ ,  $Y$  denote density, velocity, pressure, sensible enthalpy and mass fraction of various gas species respectively.  $\nu$ ,  $\nu_t$ ,  $Pr_{th}$  denote laminar dynamic viscosity, turbulent dynamic viscosity and Prandtl number for enthalpy.  $D_k$  is the mass diffusion coefficient.  $\omega_k$  is source term accounting for production or consumption of species “ $k$ ”. The superscript “-” donates the spatial filter and “ $\sim$ ” donates the Favre filter. In the small Mach number approximation, it is assumed that the pressure derivation of the ambient pressure is small and it can be neglected except for the predictor and corrector step of the momentum equations. This approximation eliminates the stiffness associated with the sound wave propagation.  $S_{rad}$  in the enthalpy equation is the source term accounting for thermal radiation.

### 3.3.2. Turbulence Modeling

In practice, turbulence is both time-dependent and three-dimensional and consists of rotational vortices, or eddies, superimposed over the net flow. These eddies occur over a continuous spectrum of sizes, from very large to very small, and persist for relatively long periods of time. Virtually all-interesting flows are turbulent, and turbulence has a significant impact on the diffusion of energy, mass and momentum in a fluid. Turbulent flows fluctuate on a broad range of time and length scales. This makes the simulation of such flows difficult and it is often necessary to model the turbulence. RANS (Reynolds-average Navier-Stokes) and Large Eddy simulation approaches are used in this work.

#### *Reynolds averaged Navier-Stokes Equation*

In the RANS (Reynolds averaged Navier-Stokes) approach, all of the fluctuation in the flow is averaged out. This solves two extra equations with low computational costs closed set of equations. K-Epsilon model focuses on turbulent kinetic energy and how it is affected by turbulence mechanisms. This model solves two partial differential equations, one for the turbulent kinetic energy,  $k$ , and one for the dissipation rate of turbulent kinetic energy,  $\varepsilon$ . The Reynolds stresses are solved using approximation. Model equations used in OpenFOAM are listed below (Versteeg and Malalasekera, 2005),

Turbulent kinetic energy equation:

$$\frac{\partial \bar{\rho}k}{\partial t} = \nabla \cdot (\bar{\rho}D_k \nabla k) + G_k - \frac{2}{3} \bar{\rho}(\nabla \tilde{u})k - \bar{\rho}\varepsilon + S_k \quad (3.5)$$

Dissipation rate:

$$\frac{\partial \bar{\rho}\varepsilon}{\partial t} = \nabla \cdot (\bar{\rho}D_\varepsilon \nabla \varepsilon) + \frac{C_1 G_k \varepsilon}{k} - \left( \frac{2}{3} C_1 + C_3 \right) \bar{\rho}(\nabla \tilde{u})k - C_2 \bar{\rho} \frac{\varepsilon^2}{k} + S_\varepsilon \quad (3.6)$$

Turbulent Eddy viscosity:

$$\mu_t = C_\mu \bar{\rho} \frac{k^2}{\varepsilon} \quad (3.7)$$

Where,  $D_k$  represents dissipation and  $G_k$  represents generation of turbulent kinetic energy.  $C_1$ ,  $C_2$ ,  $C_3$  and  $C_\mu$  are the model constants. Constants used for turbulent kinetic energy and dissipation rate equations used in the OpenFOAM are (Shih et al., 1995)  $C_\mu = 0.09$ ,  $C_1 = 1.44$ ,  $C_2 = 1.9$ ,  $C_3 = -0.33$ ,  $S_k = 1.0$ ,  $S_\varepsilon = 1.2$ .

### ***Large Eddy Simulations***

In Large Eddy Simulations (LES), large eddies are resolved directly, whilst small eddies are modelled. The rationale behind LES can be summarized as follows:

- Momentum, mass, energy, and other passive scalars are transported mostly by large eddies.
- Large eddies are more problem-dependent. They are dictated by the geometries and boundary conditions of the flow involved.
- Small eddies are less dependent on the geometry, tend to be more isotropic, and are consequently more universal.

In Large Eddy Simulations (LES) a low-pass filtering operation, which relates mainly to spatial grid properties, can be performed. The filter width  $\Delta$  becomes thus a significant parameter and separates the whole flow into larger Grid Scale (GS) and the smaller Sub-Grid Scale (SGS). As its scale is larger than the defined filter width, the GS motion is resolved precisely. For the motion scale smaller than the filter width, SGS can be modelled without direct computation. In order to make the simulation more accurate and efficient in different geometries, flow and boundary conditions, from the available SGS models, one equation model has been

implemented. The turbulent viscosity is calculated based on One Equation Eddy model (Yeoh and Yuen, 2009):

$$\frac{\partial \bar{\rho}k}{\partial t} + \nabla \cdot (\bar{\rho} \tilde{u}k) = \nabla \cdot (\bar{\rho} \nu_k \nabla k) + P - \varepsilon \quad (3.8)$$

Where,

$$P = -\bar{\rho} \cdot (D : B)$$

$$\varepsilon = c_\varepsilon \bar{\rho}^3 \sqrt{k} \Delta^{-1}$$

$$B = \frac{2}{3} kI - 2\nu_{SGS} \cdot \text{div}(D) , D = \text{symm}(\text{grad}(U))$$

Here,  $k$  and  $\varepsilon$  are the turbulent kinetic energy and dissipation rate of subgrid respectively (Yeoh and Yuen, 2009).  $P$  is the double inner product of two tensors  $D$  (Symmetric part of a rank 2 tensor created by the outer product of gradient and velocity vector and  $B$  (Sub grid stress tensor) and  $I$  is unity tensor (Wang et al., 2011). One equation model provides a more accurate timescale, which is independent of the velocity scale definition (Piomelli, 1999). This advantage is glittered by modelling of transitional flows or flows with large-scale unsteadiness.

### 3.3.3. Combustion Model

The rate of combustion is determined by the kinetics of the chemical reaction between the fuel in question and oxygen. This rate is a function of the local temperature, the local concentrations of the reactants, and various constants that relate to the mechanism of the reaction.

The combustion is analysed using the Eddy Dissipation Concept (EDC) (Ertesvåg and Magnussen, 2000). The EDC is a modified version of the eddy dissipation model, which is a good approximation when the chemical kinetics is faster than overall fine structure mixing. This model is based on the infinitely fast chemistry assumption, where fuel burns immediately

when it mixes with air. In aircraft accidents, due to the availability of ignition sources at large, the dispersed fuel ignites within a fraction of time. Therefore, the EDC combustion model can give good predictions. This model is based on the assumption that the rate of reaction is controlled by mixing processes, and that turbulence causes this mixing. The rate is inversely proportional to the large eddy mixing time-scale, which approximates the rate of mixing due to the unresolved turbulence fluctuations within a cell. The mean chemical reaction rate  $\bar{\omega}_k$  is implemented as follows,

$$\bar{\omega}_k = -\frac{\bar{\rho}}{\tau_{mix}} \left( \frac{\chi}{1-\gamma^* \chi} \right) \min \left( \tilde{Y}_{fuel}, \frac{\tilde{Y}_{ox}}{s} \right) \quad (3.9)$$

Where,  $\bar{\omega}_k$  is the reaction rate,  $Y_{fuel}$  and  $Y_{ox}$  are the mass fraction for fuel and oxidizer,  $\bar{\rho}$  is the mean density  $\Delta t$  is the integration time step.  $\tau_{mix}$  is turbulent mixing time,  $\gamma^*$  is mass fraction occupied by a fine structure,  $\chi$  is a fraction of fine structure region which may react.  $Y_{fuel}$  and  $Y_{ox}$  are the mass fraction for fuel and oxidizer. The mixing controlled rate of reaction is expressed in terms of the turbulence mixing time,  $\tau_{mix} = \frac{\tilde{k}}{\tilde{\varepsilon}}$ . In the EDC model, mass fraction occupied by fine structures is defined as  $\gamma^* = 4.6 \left( \frac{\nu \tilde{\varepsilon}}{\tilde{k}^2} \right)^{1/2}$ .  $\chi$  is the fraction of fine structure regions that may react (ratio between the local concentration of reacted fuel and available fuel

for reaction) is given as,  $\chi = \frac{\tilde{Y}_{pr}}{(1+s) \tilde{Y}_{min} + \frac{\tilde{Y}_{pr}}{(1+s)}}$  where  $\tilde{Y}_{pr}$  is the product mass fraction and

$\tilde{Y}_{min} = \min(\tilde{Y}_{fuel}, \frac{\tilde{Y}_{ox}}{s})$ . Here,  $s$  is the stoichiometric mass ratio of oxidiser to the fuel.

The chemical reaction is controlled by turbulent mixing values and it is limited by the species with a lower concentration. This model strongly depends on turbulent resolution and

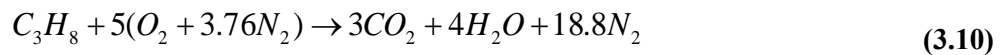
temperature independent. So, this can be used for single or two-step reaction mechanisms. In the turbulent combustion, the global burning rate reasonably depends on the turbulent velocity fluctuation (Haworth, 2005). Therefore, EDC is the best suitable model for such simulations.

The model does have a number of limitations:

- it does not contain a temperature term, and so is only valid where the temperature is high enough for the chemical timescale to be significantly shorter than the mixing timescale
- it's dependence on the turbulent kinetic energy and dissipation rate means it inherits any weaknesses of the turbulence model
- it only works for single- or two-step reaction mechanisms

Because of this fact, the single-phase gas release is considered in the fireball. The fuel used in the calculation is Propane ( $C_3H_8$ ) in case of BAM simulation. The species  $O_2$ ,  $H_2O$ ,  $C_3H_8$ ,  $CO_2$  and  $N_2$  have been used. Individual species transport equations are solved to determine the gas composition.  $N_2$  mass fraction is calculated by the mass fraction of other species. Carlsson, (1999) done the simulation using single step chemical reaction and found good agreement. The single step irreversible infinite reaction for propane can be written as,

Propane Reaction:



The heat of combustion of propane, as described in the equation (8), is  $-2220$  kJ/mol in equation (3.7).

### 3.3.4. Radiation Model

Finite Volume Discrete Ordinates model (fvDOM) is employed to solve the radiative heat transfer equation (RTE). The model applied the conservation method to maintain a heat balance for coarse discretized domains. The accuracy can be increased by using a finer discretization. It is the most comprehensive radiation model as it accounts for scattering, semi-transparent media, specular surfaces and wavelength-dependent transmission using banded-grey option. The equation of the model is,

$$\nabla \cdot (I(\vec{r}, \vec{s})\vec{s}) + (\alpha + \sigma_s)I(\vec{r}, \vec{s}) = \alpha\eta^2 \frac{\sigma T^4}{\pi} + \frac{\sigma_s}{4\pi} \int_0^{4\pi} I(\vec{r}, \vec{s}')\phi(\vec{s}, \vec{s}')d\Omega' \quad (3.11)$$

Where  $\vec{r}$ ,  $\vec{s}$  and  $\vec{s}'$  are the radius vector, direction vector and scattering vector, respectively,  $s$ ,  $\alpha$ ,  $\eta$  and  $\sigma_s$  denote the path length, absorption coefficient, refractive index and scattering coefficient.  $\sigma$  is the Stefan-Boltzmann constant. In addition,  $I$ ,  $\phi$  and  $\Omega'$  are the radiation intensity, scattering phase function and spatial angle respectively.  $CO_2$  and  $H_2O$  are the main contributors to flame radiation. The weighted sum of grey gas model is used to evaluate the absorption, emission coefficient (Smith et al., 1982), (Coppalle and Vervisch, 1983). This model is regarded as a reasonable compromise between the oversimplified grey gas model and narrow-band type models, which take into account particular absorption bands. Soot model and scattering are also incorporated with the radiation model. The work of Mishra and Roy (2007), Modest (2003) and Siegel (1992) are also referred for a full understanding of fvDOM.

#### *Advantages of the fvDOM model:*

- It is a conservative method, which leads to a heat balance for a coarse discretization. The accuracy can be increased by using a finer discretization,

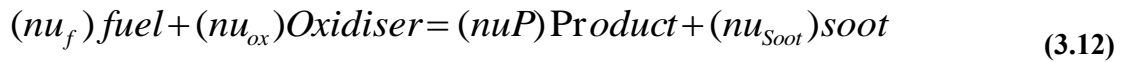
- It is the most comprehensive radiation model: Accounts for scattering, semi-transparent media, specular surfaces, and wavelength-dependent transmission using banded-grey option.

***Limitations of the fvDOM model:***

- Solving a problem with a large number of ordinates is CPU-intensive

### 3.3.5. Soot Model

The soot model used here is based on the mixture fraction. The soot is not considered into the thermodynamics of the system and it is not considered as an extra species in the solver. It calculates the soot mass fraction based on the  $CO_2$  mass fraction at all cells in each time step. The single step chemistry used is read from the combustion. The single step reaction including soot production is,



Where,  $nu_f$ ,  $nu_{ox}$ ,  $nu_P$  and  $nu_{Soot}$  are the number of moles of fuel ( $C_3H_8$ ), oxidizer ( $O_2$ ), the products ( $CO_2$  and  $H_2O$ ) and soot (also known as soot yield). There are two user-defined coefficients for the soot model. The coefficient  $nu_{Soot}$  indicated the number of moles of soot in the combustion reaction.  $nu_{Soot}$  is prescribed by the user as 0.055. The single step reaction for Propane is given as,



The mass fraction of soot is calculated as

$$soot = soot_{Max} \times (Y_{CO_2} / Y_{CO_2_{stoch}})$$

Where,  $soot_{Max}$  is maximum soot fraction and  $Y_{CO_2stoch}$  is  $CO_2$  mass fraction obtained when combustion occurs at the stoichiometric ratio and these are calculated by the solver using equation (3.9).

### 3.3.6. Eulerian-Lagrangian model

The dynamic spray model involves the motion of fuel droplets, mass, momentum and heat exchange between fuel droplet and surrounding gas. To simulate these phenomena Dynamic spray model employs the Eulerian-Lagrangian approach. The fuel droplets are simulated as dispersed phase using a Lagrangian approach, while the gaseous phase phenomena are modelled in Eulerian framework with above mentioned governing equations. Two-way coupling between the gas phase and the dispersed fuel droplet phase is considered in this method. In two-way coupling, each droplet individually interacts with the carrier gas phase. The momentum lost by the fuel droplet is gained by the gas phase and vice versa. Considering that the dominant forces are the droplet drag force and the gravitational force (buoyancy, lift and forces arising from fluid acceleration are neglected as the density of fuel droplet is much higher than the gas phase) (Loth, 2000; Armenio and Fiorotto, 2001), and the droplet momentum equation is written as:

$$m_d \frac{du_p}{dt} = -\frac{\pi d_p^2}{8} C_D \bar{\rho} |u_p - \tilde{u}| (u_p - \tilde{u}) + m_d g \quad (3.13)$$

Where,  $u_p$  and  $d_p$  are the droplet velocity and diameter, respectively. The drag coefficient,  $C_D$ , is defined as a function of the Reynolds number (Kuo, 1996),

$$C_D = \begin{cases} \frac{24}{Re_d} \left( 1 + \frac{1}{6} Re_d^{2/3} \right) & Re_d < 1000 \\ 0.424 & Re_d \geq 1000 \end{cases} \quad (3.14)$$

The droplet Reynolds number is calculated as:

$$\text{Re}_d = \frac{\bar{\rho}|u_d - \tilde{u}|d_d}{\mu} \quad (3.15)$$

Where,  $\rho$ ,  $\tilde{u}$  and  $\mu$  are the gas phase density, velocity and dynamic viscosity, respectively.

The following energy equation accounts for heat transfer between the droplets and the gas phase and for the latent heat due to vaporization of the droplets (Kuo, 1996);

$$m_d C_p \frac{dT_d}{dt} = \dot{m}_d H_v + h A_d (T - T_d) \quad (3.16)$$

Where,  $C_p$ ,  $A_d$  and  $T_d$  are the specific heat, surface area and temperature of the droplets, respectively;  $H_v$  is the latent heat of vaporization,  $h$  is the convective heat transfer coefficient and  $T$  is the gas phase temperature. According to the lumped capacitance assumption, for small droplets temperature within the droplet is considered as uniform. In this simulation, most of the fuel droplets are with the size of a couple of hundred microns, which satisfy the Biot number criteria ( $Bi < 0.1$ ). For  $Bi < 0.1$ , the uniformity of the thermal field is attained instantly. The droplet temperature and radius will be just time-dependent, so this assumption can be implemented. The convective heat transfer coefficient is calculated as;

$$h = \frac{Nu'k}{d_d} \quad (3.17)$$

Where,  $k$  is the conductivity of the gas phase while the Nusselt number, which includes the effect of the relative velocity between the fuel droplet and gas phase is given by

$$Nu' = Nu \frac{\beta}{e^\beta - 1} \quad (3.18)$$

Where,  $Nu$  is determined by Ranz-Marshall correlation (Ranz & Marshall, 1952) as:

$$Nu = 2 + 0.6Re_d^{1/2} Pr^{1/3} \quad (3.19)$$

Prandtl number is calculated as  $Pr = \mu C_p / k$ . Bird's correction (Bird et al., 1960) is applied in the correlation of Nusselt (eq. 3.16) to take into account the effect of Stefan flow (outward flow) on the surface of evaporating droplets causing a reduction of heat transfer due to evaporation. Here,  $\beta$  is the non-dimensional evaporation parameter and this is calculated as:

$$\beta = - \left( \frac{3Pr \tau_d^{st}}{2} \right) \frac{\dot{m}_d}{m_d} \quad \text{where,} \quad \tau_d^{st} = \frac{\rho_d d_d^2}{18\mu} \quad (3.20)$$

Where,  $\dot{m}_d$  is the droplet evaporation rate and  $\tau_d^{st}$  is the ratio of two characteristic times i.e. droplet relaxation time and vortex-life time for Stokes flow. Smaller droplets follow eddies better than the larger ones with their small drag to inertia ratio. The contribution of turbulent to dispersion is important for small droplets with velocity fluctuation.

The mass transfer increases with an increase in relative velocity between the fuel droplet and gas phase. The mass exchange between two phase due to evaporation of liquid from the fuel droplet is taken into the consideration and expressed in terms of Sherwood number as:

$$\frac{dm_d}{dt} = -\pi d_d \rho D Sh \ln(1 + B_M) \quad (3.21)$$

Where,  $D$  and  $Sh$  are the diffusion coefficient and Sherwood number of the gas phase, respectively. The effect of the relative mass fraction on heat transfer across the surface of an evaporating fuel droplet is considered. The Sherwood number, which includes the effect of the relative velocity between the fuel droplets and gas phase, is calculated in the equation below.

The Sherwood number has a value of  $Sh=2$  for no relative velocity is present between the gas-phase and fuel droplet.

$$Sh = 2 + 0.6Re_d^{1/2} Sc^{1/3} \quad \text{where, } Sc = \mu/(\rho D) \quad (3.22)$$

In this,  $B_M$  is the Spalding mass transfer number that relates the liquid-gas interface mass fraction at the fuel droplet surface to the mass fraction in the free stream. For the combustion of most of the liquid fuels burning in the air, the Spalding mass transfer number is found in the range of 1-10. The expression for calculating Spalding mass transfer number is given as,

$$B_M = \frac{X_{v,s} - X_v}{1 - X_{v,s}} \quad (3.23)$$

Where,  $X_v$  is the vapour mole fraction in the gas phase and  $X_{v,s}$ , is the vapour mole fraction at the droplet surface obtained from Raoult's law as:

$$X_{v,s} = X_v \frac{P_{sat}(T_p)}{p} \quad (3.24)$$

Here  $p_{sat}$  is the vapour saturation pressure at droplet temperature and  $p$  the ambient pressure.

### 3.4. Numerical Method

The discretized momentum, species transport and energy equations are solved by the preconditioned bi-conjugated gradient method (PBiCG). Generalized geometric-algebraic multi-grid method (GAMG) is employed to solve the discretized pressure equation originated from the application of momentum interpolation to the continuity equation. This method is also used to solve the discretized turbulent energy and the radiative transfer equations. The second order backward differentiation scheme is employed for temporal discretization. The diffusive

terms and the gradients are discretized using central differencing scheme. Spatial derivatives are estimated on a rectangular grid with all quantities assigned to the cellcentre and velocities linearly interpolated to the cell faces. The *fireFoam* employs a PIMPLE (PISO+SIMPLE) algorithm for pressure-velocity coupling. The PISO algorithm is solved using a Gauss Linear scheme, with an implicit Euler time discretization.

Large Eddy Simulation (LES) is employed to solve the large-scale flow. The effects of the small scales are modelled to estimate a sub-grid turbulent viscosity using One Eddy Equation model (a Sub Grid Scale (SGS) model) with eddy coefficient of 0.07. The transport equation of energy is solved for enthalpy with source terms from combustion and radiation equations. Temperature dependencies of the enthalpies and heat capacities of individual species have been taken into account. The enthalpies of formation of various chemical species are available in NIST-JANAF Thermochemical Tables (Chase, 1998) and are used in the most combustion simulation codes in the form of the standard library. Sixteen solid angles each associated with a vector direction  $\vec{s}$  in a participating media are used for discretization of RTE using finite volume method. RTE is solved using generalized geometric-algebraic multi-grid method (GAMG) and updated after every 10 iterations.

### 3.5. Grid resolution and Time step selection

The grid resolution is an important parameter for CFD simulation. For buoyancy-dominated flows, a useful length scale is characteristic fire diameter. The expression for characteristic fire diameter is given by McGrattan et al. (2013) as,

$$D^* = \left( \frac{\dot{Q}}{\rho_0 C_p T_0 \sqrt{g}} \right)^{2/5} \quad (3.25)$$

The quantity  $\dot{Q}$  is the total heat release rate (HRR) of the fire.  $D^*$  is used to compare the optimum grid resolution with the ratio of characteristic fire diameter and the grid spacing  $(D^*/\delta x)$ . The grid size of  $(D^*/\delta x) > 15$  is found adequate for the wide range of validation cases (McGrattan et al., 2013).

In Large Eddy Simulations, time step needs to obey the Courant–Friedrichs–Lewy (CFL) constraints to resolve eddies of grid size  $(\delta x, \delta y$  and  $\delta z)$ . The well-known CFL constraint is given by the following expression,

$$CFL = \delta t \max \left( \frac{|\bar{u}|}{\delta x}, \frac{|\bar{v}|}{\delta y}, \frac{|\bar{w}|}{\delta z} \right) < 1 \quad (3.26)$$

Where,  $u$ ,  $v$  and  $w$  are velocities in  $x$ ,  $y$  and  $z$ -direction respectively and the grid spacings are  $\delta x, \delta y$  and  $\delta z$ . This equation (3.23) physically states that fluid element should not transverse more than one cell within a time step.

### 3.6. Grid independence and Model Validation

The effect of mesh size on the results has been studied. Simulations were performed using a number of different mesh sizes. The mesh size is reduced until the simulation results are found to be almost the same.

#### 3.6.1. Computational Domain

From the observation of experimental maximum diameter and lifting height achieved by a fireball, the domain  $200 \text{ m} \times 200 \text{ m} \times 300 \text{ m}$  was selected for analysis (see Figure 3.1). By considering the influence of boundaries, the sizes of the computational domain have been chosen large enough so that no significant velocities are developed on the outer boundaries

during the lifetime of the fireball. The sides and top faces of the domain behave as an open atmosphere, in which flow across the boundary of the domain is allowed. At  $y=0$ , the bottom plane of the domain, the no-slip boundary condition is employed. The effect of wind velocity in the simulation of the fireball is not considered in this work. The calculations were set to run for 8 s and data is collected for a time interval of 0.01 s in the simulation. The diameter is calculated for both the cases using the method mentioned in Makhviladze et al., (1997). The acceleration due to gravity ( $9.81 \text{ m/s}^2$ ) has taken in the negative  $Y$  direction. The inlet velocity is directed vertically upward for the calculated time span. The time span of the inlet is dependent on the velocity of the inlet. As soon as the required fuel mass entered the computational domain, the inlet velocity was ramped down to zero.

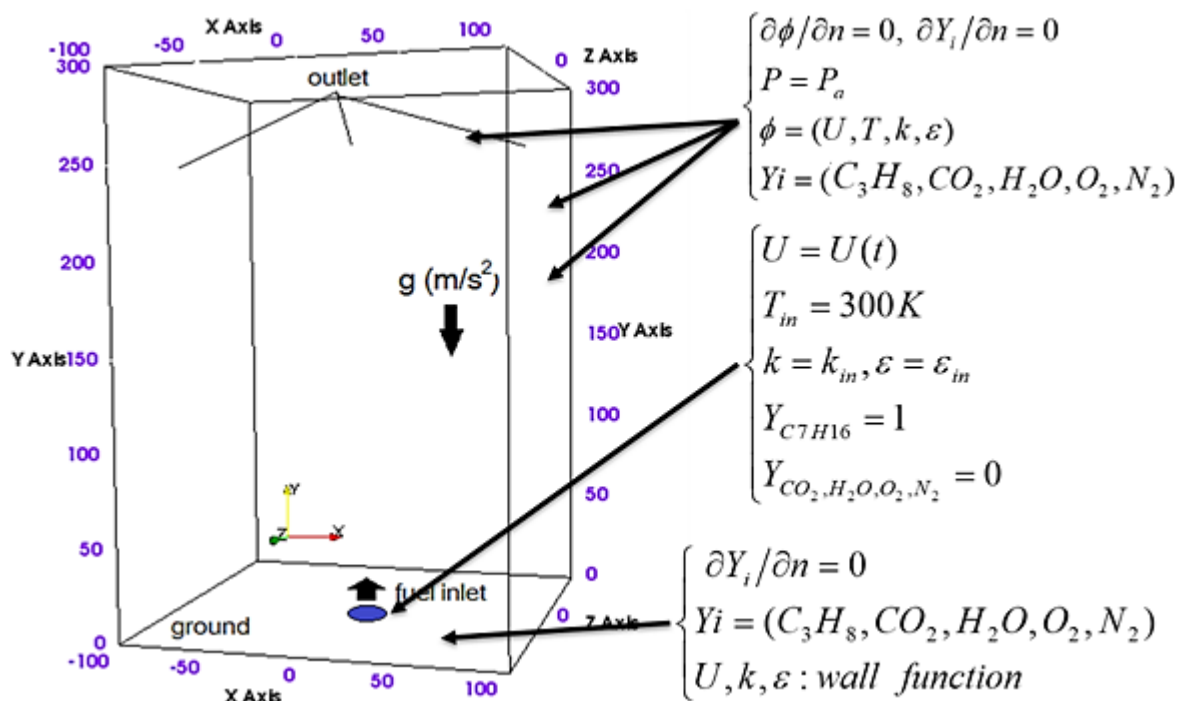


Figure 3.1: Schematic of a computational domain showing the fuel inlet at  $y=0$

### 3.6.2. Initial and Boundary Conditions

The sides and top of the domain behave as an open atmosphere, in which free flow across the boundary of the domain is allowed. At  $y=0$ , the bottom plane (ground) of the domain behaves as the wall where no-slip boundary condition has been employed. The fuel inlet is in circular in shape and located at the centre of the bottom plane (XZ plane,  $y=0$ ). The diameter is calculated for both the cases using the method mentioned in (Makhviladze et al., 1997). The inlet velocity is directed vertically upward for the calculated time span. The time span of inlet depends on the velocity of inlet. As soon as the required fuel mass entered the computational domain, the inlet velocity was ramped down to zero.

Initially, stagnant air at 300 K has been considered as domain fluid. The value of acceleration due to gravity ( $9.81m/s$ ) has taken in the negative  $Y$  direction.

### 3.6.3. Study of grid independency

The effect of mesh size on the results has been studied. Simulations were performed using a number of different mesh sizes. The mesh size is reduced until the simulation results are found to be almost the same. For the calculations grid spacing of 1 m (Coarser mesh: 135070 Cells,  $(D^*/\delta x)=8.95$ ), 0.5 m (Coarse mesh: 540280 Cells,  $(D^*/\delta x)=17.91$ ) and 0.25 m (Fine mesh: 2161120 Cells,  $(D^*/\delta x)=35.81$ ) are used. Figure 3.2 shows the temperature profiles, mixture gas density and radiative flux measured at 50 m elevation at the time instant of 4 s. The profiles obtained from the coarser grid is very similar to the one obtained with the finer grid. The peak in the radiative heat flux differs only slightly in magnitude.

### 3.6.4. Model Validation

The external diameter and the lifting height of the simulated fireball are compared with available experimental data in Figure 3.3. A good agreement between calculated and experimental data of Droste et al. (1999) has been observed for fireball diameter and lifting height.

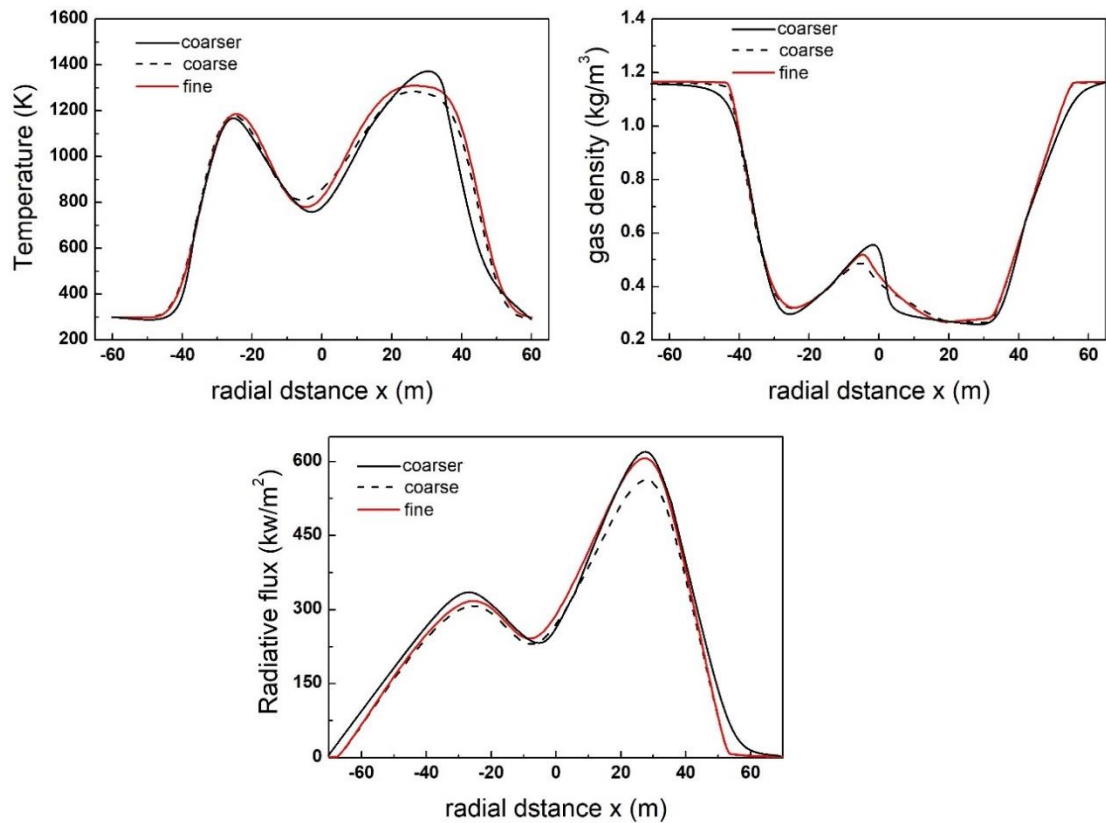


Figure 3.2: Profiles obtained from OpenFOAM with 135070 Cells (black solid line), 540280 Cells (dash line) and 2161120 cells (red solid line)

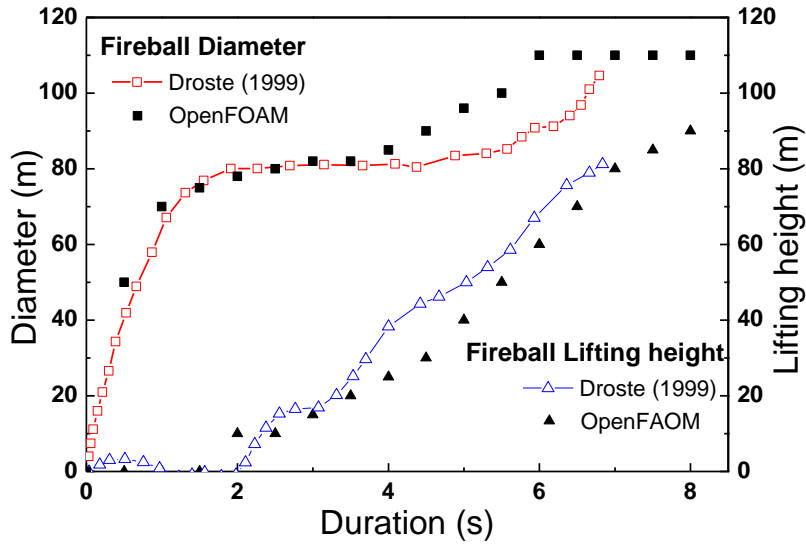


Figure 3.3: Modelling of Diameter and lifting height of fireball from Droste et al. (1999)

### 3.6.5. Lifting velocity of fireball

In the first two seconds, the fireball remains attached to the ground. After two seconds, the uplift starts and the fireball rise within 5.0 s to its maximum height. From Figure 3.3, it can be noted that the fireball diameter changes marginally. Makhviladze and Yakush (2002) have formulated an empirical equation for uplift velocity time scale of the fireball. The equation is given as,

$$U_{lift}^2 = g \left( \frac{M_{fuel} \Delta H_c}{\rho_a C_{p,a} T_a} \right)^{1/3} \quad (3.27)$$

Where  $M_{fuel}$  is the mass of fuel,  $\Delta H_c$  is the heat of combustion of fuel,  $\rho_a$  is the density of ambient air,  $C_{p,a}$  is specific heat capacity of air and  $T_a$  is the temperature of ambient air. From equation (3.27), the calculated upward velocity is 17.57 m/s. In CFD analysis, the fireball rising velocities have been calculated for various inlet velocity cases. Table 3.1 shows the velocity calculated through CFD analysis. The observed rising velocity for fireball is mentioned by

Luther & Müller (2009) in 16.0 m/s and the obtained velocity from CFD calculation is 16.88 m/s. The observed and calculated value of lifting velocity using CFD also compares quite well. In CFD simulation also fireball is attached to the ground initially and starts rising after 2.0 s.

### 3.7. Effect of Turbulence model

Temperature profile obtained with  $k-\varepsilon$  turbulence model is compared with the temperature profile obtained in LES for 100 m/s inlet velocity as depicted in Figure 3.4. Results obtained by LES model for fireball simulation give an idea about instantaneous flame shape in a turbulent cloud while  $k-\varepsilon$  turbulence model predicts smooth fireball shape. Temperature fields calculated by the LES model show the more complicated structure of developed vortex.

**Table 3.1: Average uplifting velocity of fireball**

Parameters		Average Lifting Velocity (m/s)
Observed (Luther and Müller, 2009)		16.0
Calculated from equation (3.24)		17.57
	Vertical Inlet velocity 10 m/s	16.25
CFD-	Vertical Inlet velocity 20 m/s	16.47
Simulations	Vertical Inlet velocity 50 m/s	16.25
	Vertical Inlet velocity 100 m/s	16.88

### 3.8. Effect of Radiation Model

CFD analysis has been performed with and without considering the radiation model. It can be seen from Figure 3.5 that flame outer boundary temperature is higher when the radiation model is not considered in the analysis. The radiative heat loss causes the flame to retreat downstream,

which results in the shrinkage of the flame size. This also causes a decrease in the maximum flame temperature. Thus, the flame configuration is strongly affected by the gas radiation process. As the temperature in the fireball is lower while considering the radiative model, the lifting time is higher (Figure 3.6) due to less buoyancy force.

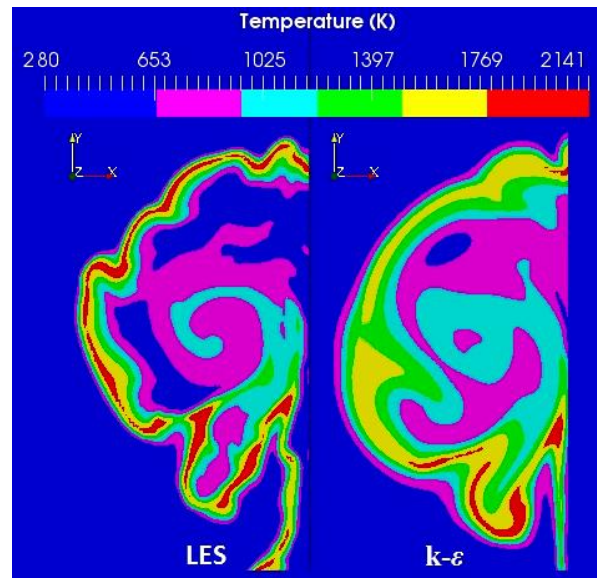


**Figure 3.4:** Temperature profile of gas in a fireball on the plane XY, at  $z=0$  (at  $t=3.0$  s), LES (left) and  $k-\epsilon$  turbulence model (right)

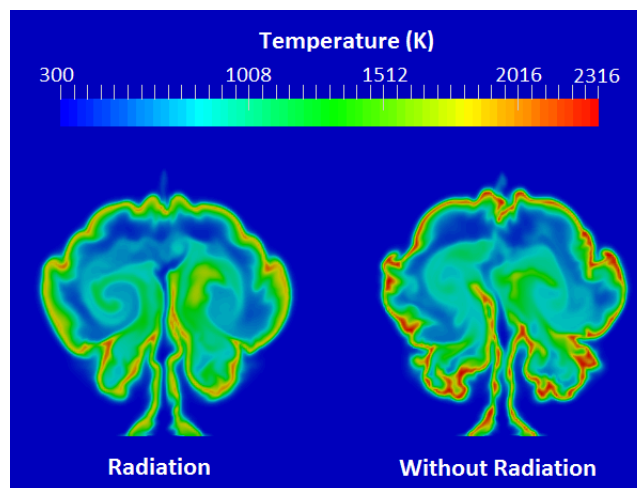


**Figure 3.5:** Effect of Radiation on flame surface temperature, (XY plane at  $z=0$ ) at  $t=3.0$  s

The parametric study was performed to study the effect of solid angles on thermal radiation

The incident radiative flux was calculated at  $x = 30\text{ m}$  (30 m away from the centre) using the solid angles of 4, 8 and 16 for the radiative transfer equations (RTE). Figure 3.7 shows the plot of incident radiative flux duration of the fireball. It is found that the average radiative flux for various solid angles is comparable. Sixteen solid angles covering the hemisphere are used in this study.

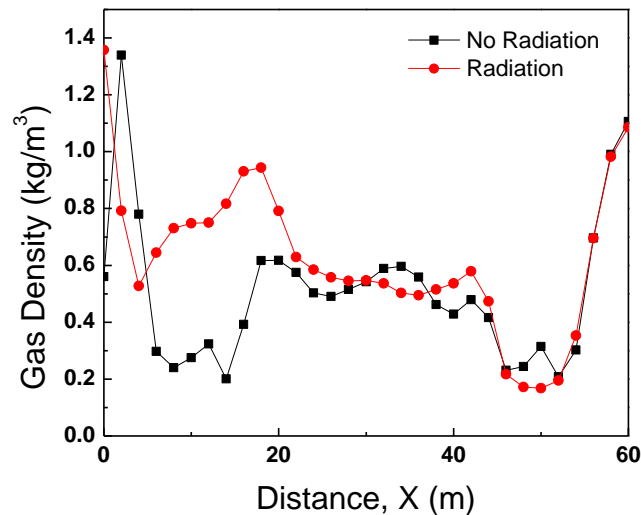


**Figure 3.6: Effect of Radiation on gas density inside the fireball ( in XY plane at the centre of fireball at  $t=3.0\text{ s}$ )**

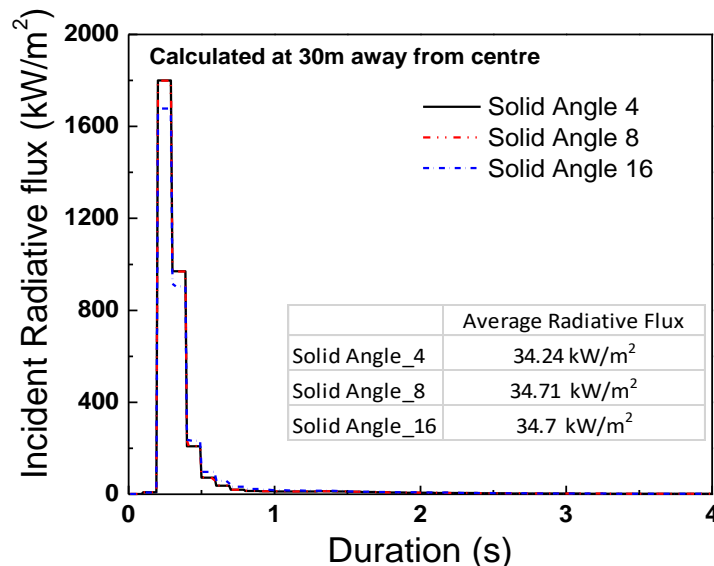


**Figure 3.7: Effect of Radiation on gas density inside the fireball ( in XY plane at the centre of fireball at  $t=3.0\text{ s}$ )**

### 3.9. Internal Structure of fireball

In Figure 3.8, the instantaneous structure of the developing fireball is shown at  $t=2.0\text{ s}$  and  $t=4.0\text{ s}$  after the start of fuel release into the domain. On the right, the mass fraction of  $\text{CO}_2$  is shown, while the temperature of the gas is presented on the left side. It can be seen that the burning cloud is detached from the ground and forms a mushroom-shaped fireball under the influence of vortex. Incandescent gases change a shape due to atmospheric friction.

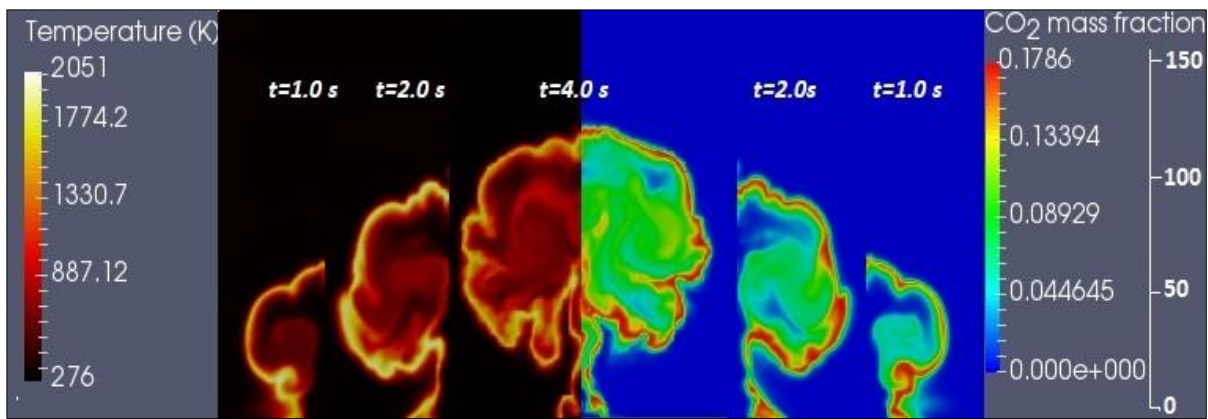


**Figure 3.8: Simulation of BAM fireball:  $\text{CO}_2$  mass fraction, Temperature of gas (K) for vertically inlet velocity of 100 m/s at plane XY,  $z=0$  at different time steps**

From Figure 3.9, it can be seen at  $t=3.0\text{ s}$  that the flow is three-dimensional and the flame is affected by multiple vortices causing its distortion and breakdown in small pockets burning separately. The Rayleigh-Taylor instability occurred at the boundary between the hot fireballs and surrounding air causes turbulence and vortex formation. Entrained air from bottom causes further combustion of fuel inside the cloud and associated heat release. Figure 3.10 shows the mass fraction profile of fuel and combustion products along the X-axis at the centre of the fireball on the XY plane at  $y=50\text{ m}$  and  $z=0\text{ m}$ .

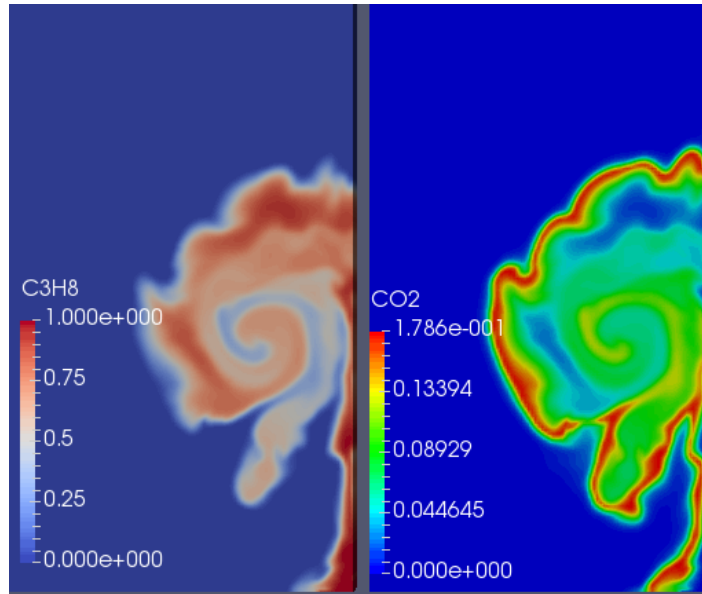


Figure 3.9: Instantaneous frame on cutting plane ( $z=0$ )  $C_3H_8$  (left) and  $CO_2$  (right) at  $t=3.0$  s

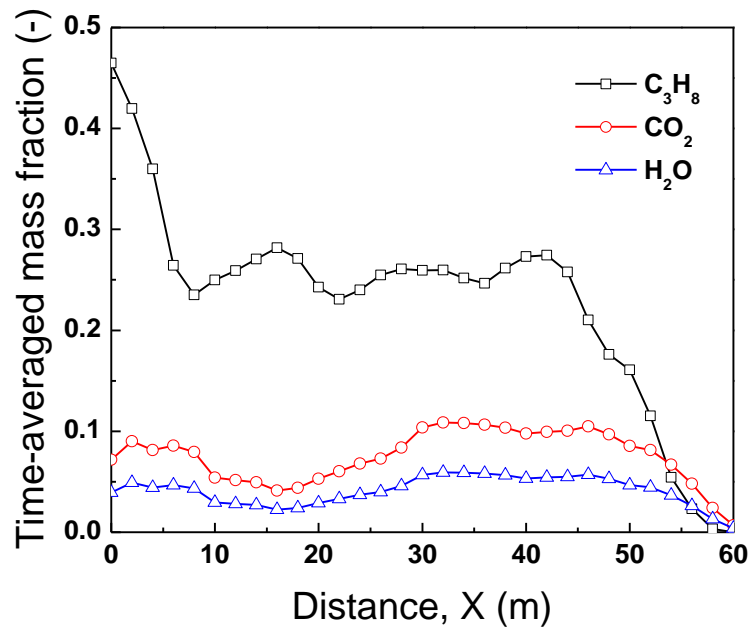
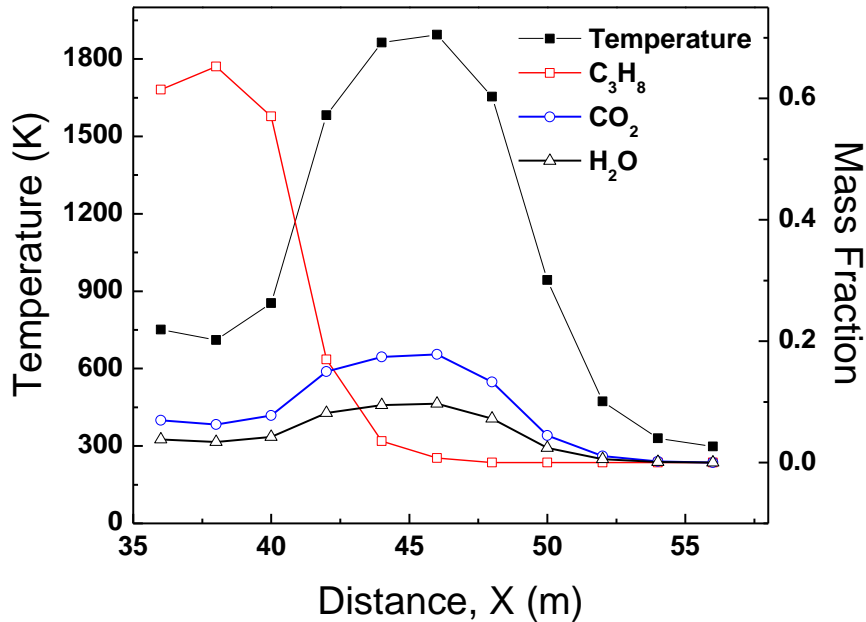


Figure 3.10: Time-averaged profile of concentrations along XY plane at  $y=50$

Figure 3.11 shows the instantaneous mass fraction and temperature profile at the outer surface of the fireball. It can be seen that fuel in the fireball burns mainly at its outer surface as the mass fraction of fuel is low in this region. The complete combustion of fuel is due to the availability of a large amount of oxidant from the surrounding air. The diffusion of heat and

mass increases which, causes a higher product formation rate due to turbulence at the flame boundary. Due to higher combustion at the boundary, the flame temperature is higher. It explains the fire phenomena at fireball surfaces.



**Figure 3.11: Instantaneous Temperature and Species mass fraction at  $t=3.0$  s and  $y=50$  m in XY plane ( $z=0$ )**

In a simulation of a fireball in an open atmosphere, flame propagates as deflagration. The maximum generated overpressure is found to be less than 0.25 MPa. Figure 3.12 shows the pressure wave at various instances. Evaluation of burning cloud for various vertically upward inlet velocities is studied at the *middle XY* plane at  $z=0$  m. Rapid development and turbulisation cause intensive mixing of fuel with the available air, which results in a higher burning rate. It is further found that for higher fuel inlet velocity, higher the amount of combustion of a fuel occurs which causes more products formation.

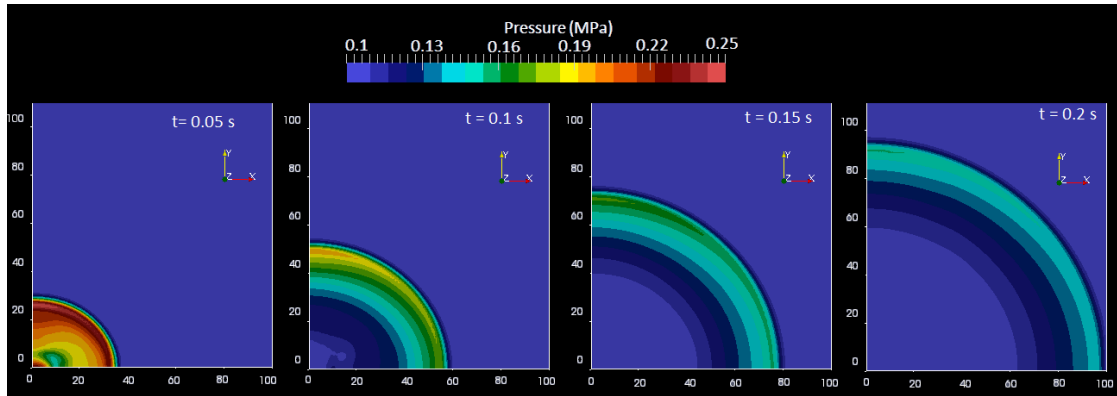


Figure 3.12: Pressure developed during combustion of the fireball on XY plane,  $z=0$

### 3.10. Thermal Hazard from the fireball

Figure 3.13 shows the global heat release rate (HRR) from the BAM fireball. The increase in the HRR with time in the initial period is attributed to the entrainment and mixing of air from the atmosphere, which promotes the rapid combustion. After that, HRR reduces due to unavailability of fuel for combustion. The waviness in the heat-released profile may be due to the use of LES turbulence model.

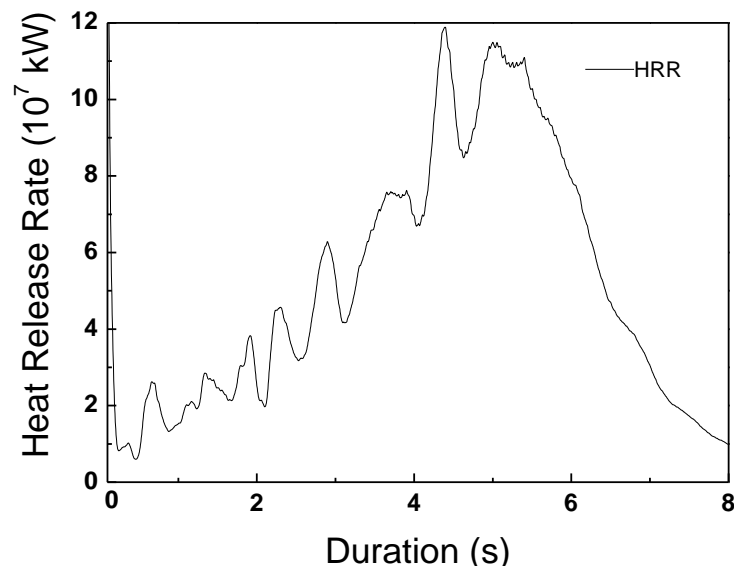


Figure 3.13: Global Heat release rate from BAM fireball

The dynamic behaviour of fireball also affects the temperature rise on the ground due to incident radiation from the fireball. Figure 3.14 shows the temperature on the ground ( $XZ$  plane at  $y=0$ ) obtained from the analysis during the lifetime of a fireball at three locations ( $x=20, 30$  and  $40$  m). The temperature measured at location  $20$  m away from the centre of fireball shows the larger value of temperature for a longer duration. This may be due to engulfment of the fireball. This helps in the study of thermal hazard from the fireball.

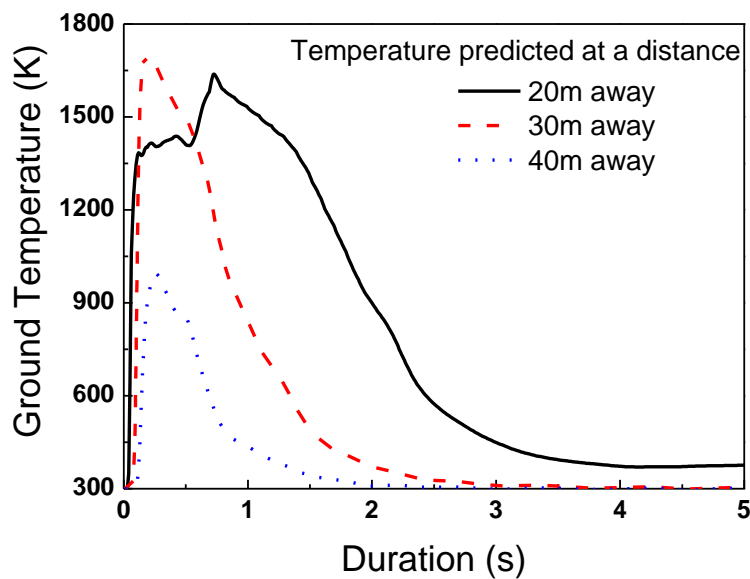


Figure 3.14: Temperature calculated at ground locations

### 3.11. Parametric studies on fireball

In this chapter, the parametric studies have also been performed on formation, combustion and evolution of fireball. In this study, propane is used as fuel in the vapour form and it has gas density of  $2.01 \text{ kg/m}^3$ . The effect of various parameters like inlet velocity, duration, mass of fuel and the diameter of the opening has been studied. The parametric studies are conducted by varying the mass of fuel, inlet velocity and diameter.

### 3.11.1. Effect of fuel mass

In Table 3.2, inputs for the analyses are given for varying fuel mass and the size of inlet openings while the velocity and the duration of injections are kept constant.

**Table 3.2: Inlet velocity of 100 m/s for the release time of 1s with varying inlet mass**

Mass of fuel (kg)	Inlet Diameter (m)	Domain dimensions	
		width & depth (m)	height (m)
10	0.252	25	62.5
100	0.79	50	125
1000	2.52	100	250
10000	7.96	200	500
100000	25.18	400	1000

For the same initial velocity and duration of fuel release, it has been observed in Figure 3.15 (a) that Peak of the Heat Released Rate (HRR) is higher for the higher mass of fuel. Figure 3.15(b) shows that the time required to gain the peak of HRR is smaller for the higher mass of fuels. Based on the analysis performed correlations have been developed for the peak heat release rate and time of achieving peak HRR and are given in Figure 3.15 (a) and (b).

The HRR is limited by the availability of oxidizer from the surroundings of the burning cloud. The larger amount of fuel requires a time to produce peak HRR due to the mixing of fuel with an oxidizer. The HRR value for fuel mass is 100,000 kg shows the approximately the same value as that for fuel mass up to 10,000 kg.

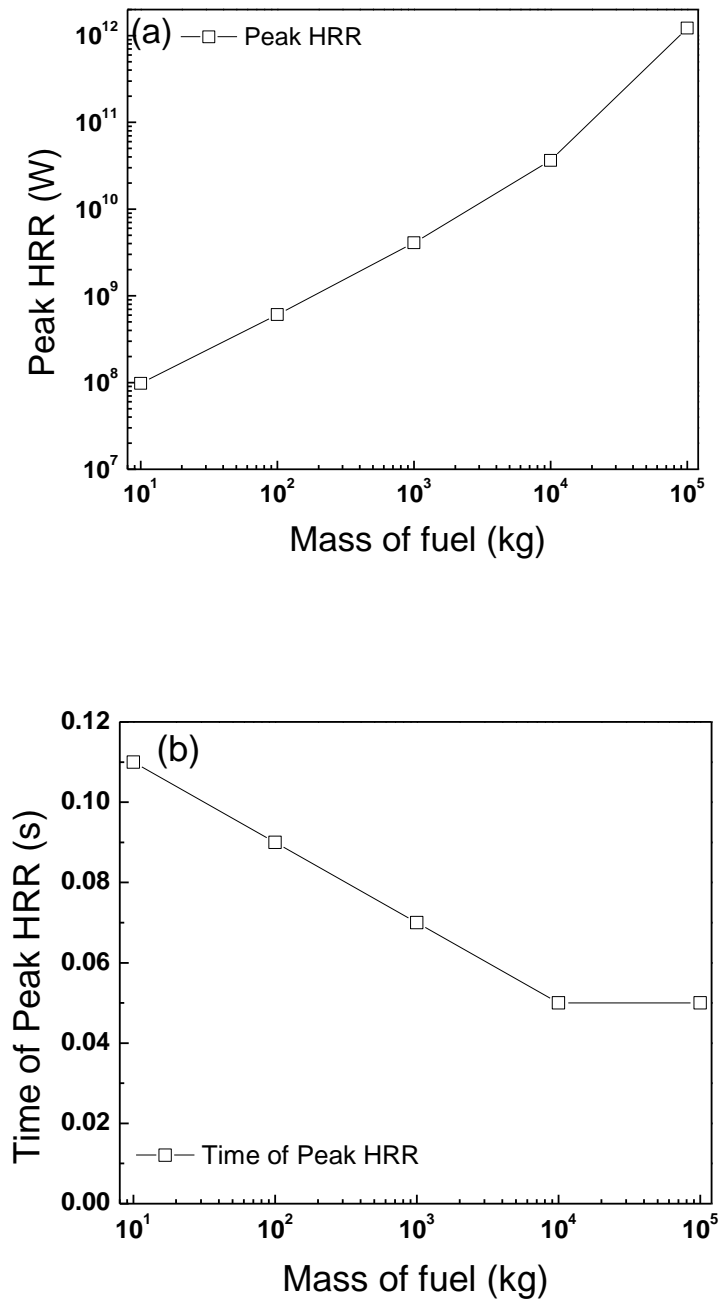


**Figure 3.15: Comparison of fuel mass with (a) peak Heat Release Rate (HRR) and (b) time of peak HRR**

Figure 3.16 shows the fraction of heat released to the total heat ( $Q_{total}$ ) from the fuel combustion for various masses of fuel. It can be seen that a fireball with 10 kg mass releases a higher fraction of heat for a longer duration during its lifecycle. It can be further observed from Figure

3.16, that the fireball with larger mass burns slowly than fireball with smaller mass. This may be due to the mixing of air with fuel.

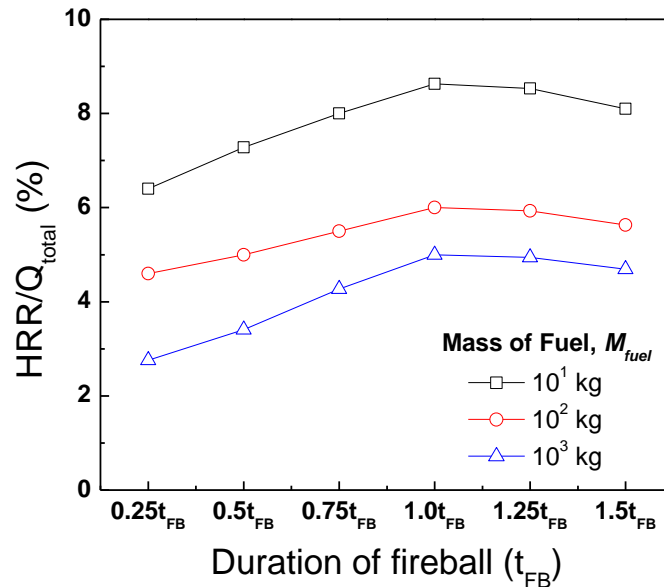


**Figure 3.16: Fraction of heat released during the lifetime of fireball**

Figure 3.17 shows the higher value of HRR peak at an earlier stage for the higher mass of fuel injected. The HRR peak of  $\sim 5 \times 10^5$  (W/m<sup>3</sup>) is found at 0.065s in case of 1000 kg mass, while  $\sim 2 \times 10^5$  (W/m<sup>3</sup>) it is at 0.1s in case of 10 kg mass of propane.

The radiation energy emitted by the fireball is dangerous for personals in the vicinity of the fireball. Hence, it is important to study incident radiation at different locations from a fireball. In CFD analysis, the radiant flux can be calculated both for internal and external points. Figure 3.18 shows the calculated radiation flux received at the location of 50 m away on the ground for  $10^3$ ,  $10^4$  and  $10^5$  kg mass of fuel. It can be seen from Figure 3.18 that radiation received varies with time. This may be due to intermittent burning and mixing of oxygen in the fireball.

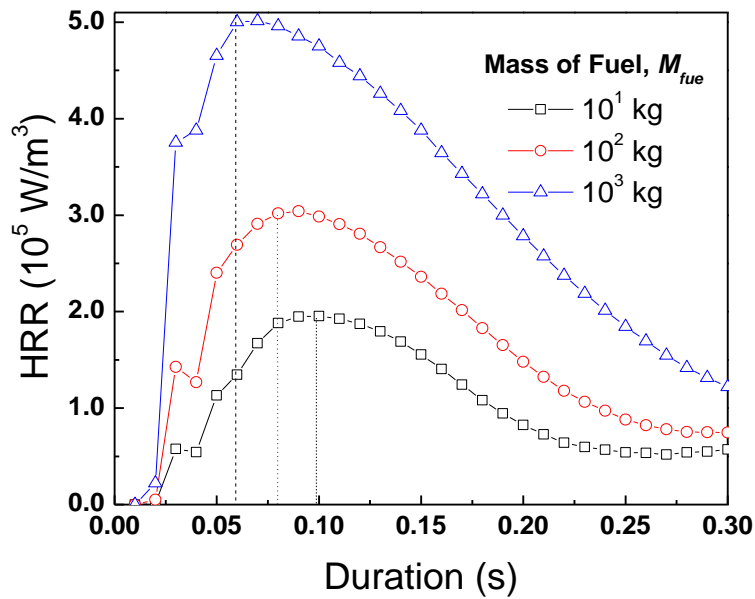


Figure 3.17: HRR per unit volume of fireball

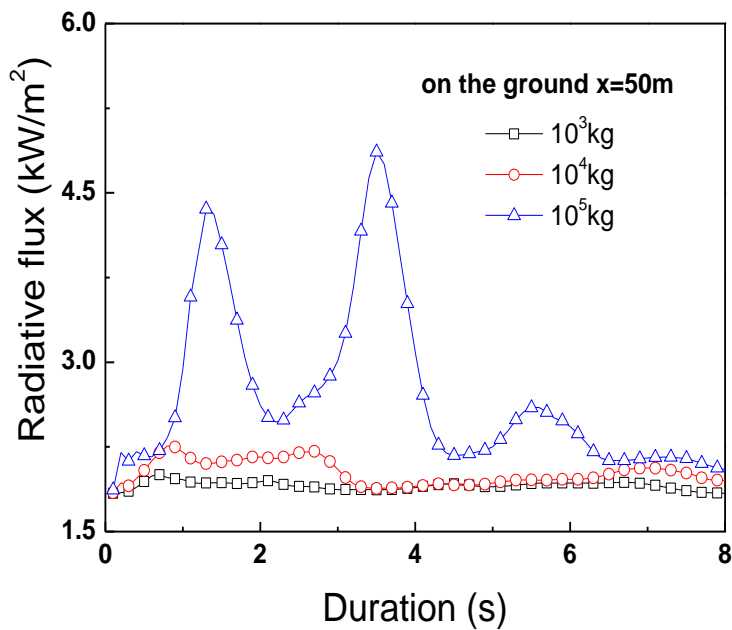
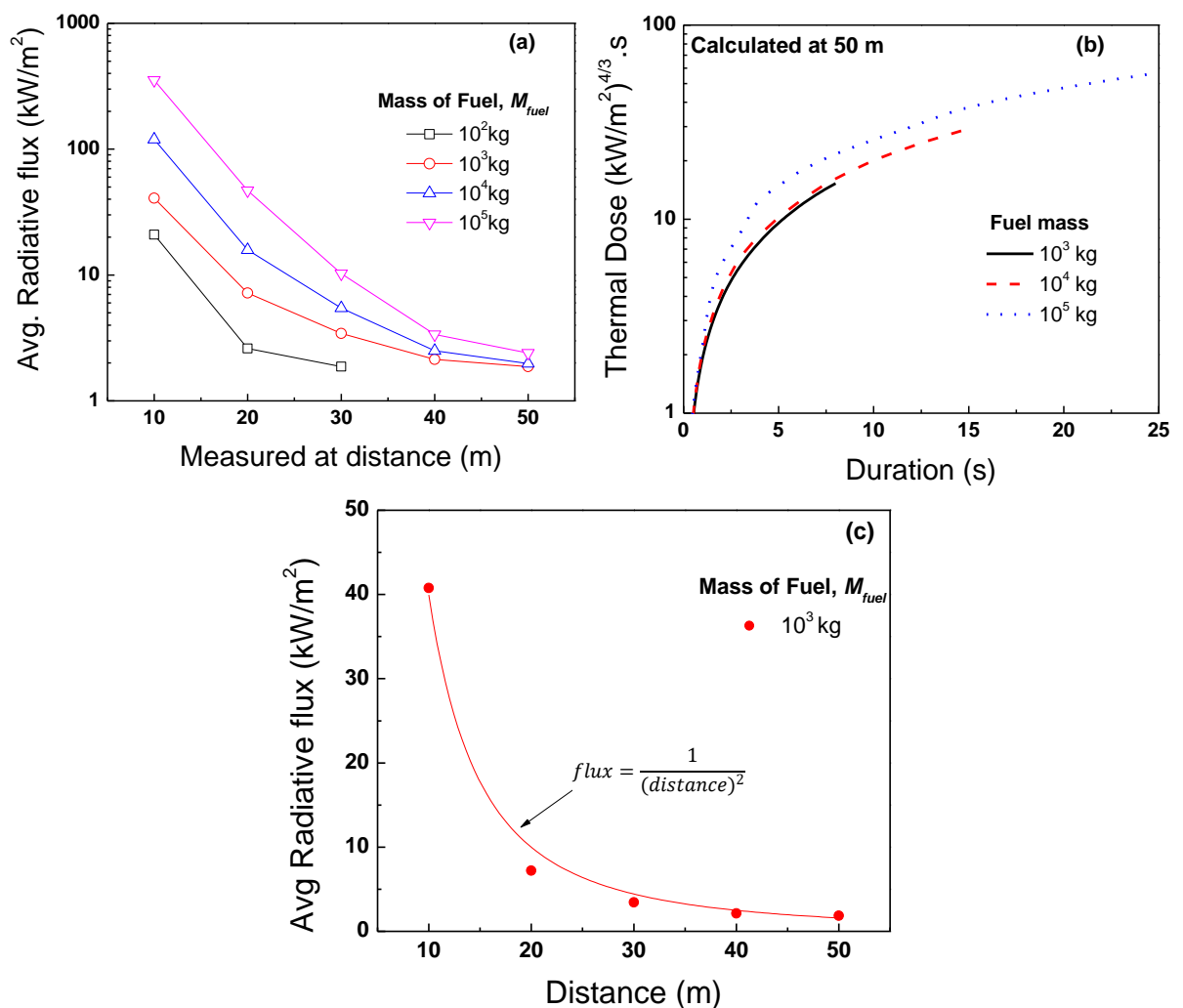


Figure 3.18: Incident radiation flux calculated at 50 m during the fireball

Figure 3.19 (a) shows the average radiative flux received at locations 10, 20, 30, 40 and 50 m away from the centre of the fireball. It can be further noted that the maximum value of the average radiation flux of  $\sim 350 \text{ kW/m}^2$  is obtained for the mass of  $10^5 \text{ kg}$  at 10 m away from

its centre. A drastic reduction in the radiative flux received is observed for larger fuel mass of  $10^5$  kg and  $10^4$ kg, away from the fireball centre (see Figure 3.19 (a)). This shows that larger size fireballs are optically thick in nature. The thermal dose has been compared in Figure 3.19 (b) for different fuel mass. It is found that the calculated thermal dose at a distance of 50 m away from the centre of fireball at the ground follows a similar trend with time. It is further found from Figure 3.19 (c) that the reduction (decay) in the radiation follows almost an inverse-square law.



**Figure 3.19:** (a) Average Incident radiations calculated at the locations on the ground for various masses (b) Thermal dose calculated at 50 m during the fireball (c) Inverse square law fitting for fireball with fuel mass of  $10^3$  kg.

### 3.11.2. Effect of initial velocity

The analysis has been performed by varying the inlet velocity and inlet size. Table 3.3 describes the input data used for analyses. In the analyses, the mass of the fuel and duration of injection are kept constant. The velocities considered are 20, 50, 100 and 200 m/s. For these analyses, fuel mass and the release duration are kept constant. The inlet velocity of fuel is chosen to study buoyancy dominated ( $Fr < 1$ ) and momentum dominated ( $Fr > 1$ ) fireballs. Froude number ( $Fr$ ) gives the parameter that quantifies the relation between momentum and buoyancy force acting on the fireball. Froude Number is ratio of squares of fuel injection velocity in vertical direction  $U_0$  to the Lifting velocity  $U_{lift}$  (Lifting velocity of fireball, explained in section 3.6.5). The relation of Froude number for fireball is given as (Makhvilade and Yakush, 2002);

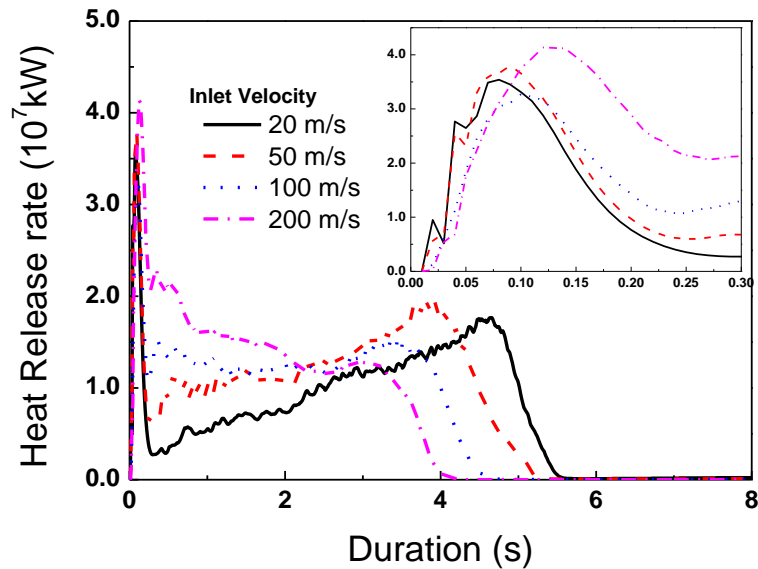
$$Fr = \left( \frac{U_0}{U_{lift}} \right)^2 = \frac{U_0^2}{g \left( \frac{M_{fuel} \Delta H_c}{\rho_{FB} C_{p,a} T_a} \right)^{1/3}}, \text{ where } U_{lift}^2 = g \left( \frac{M_{fuel} \Delta H_c}{\rho_{FB} C_{p,a} T_a} \right)^{1/3} \quad (3.28)$$

Here  $U_0$  is fuel release and  $U_{lift}$  is lifting velocity of the fireball,  $\rho_{FB}$  is the average density of fireball.

Figure 3.20 shows the global heat release rate (HRR) from the fireball at various inlet velocities. For the smaller inlet velocity (20 m/s), the heat release rate is lower as compared to the case with higher inlet velocity. For higher inlet velocities (50 m/s, 100 m/s and 200 m/s), there is no significant change in HRR with time after the initial transient. This may be due to the limited amount of fuel burnt in the fireball.

**Table 3.3: Constant inlet mass of 1000 kg for the release time of 1 s with varying inlet velocity**

Inlet velocity $U_0$ (m/s)	Lifting Velocity $U_{lift}$ (m/s)	Froude Number $Fr=(U_0/U_{lift})^2$	Fireball	Inlet diameter (m)	Domain dimensions ( $w \times d \times h$ ), $m^3$
20	22.18	0.812922	Buoyancy	5.63	100×100×250
50	22.18	5.080761	Momentum	3.56	
100	22.18	20.32305	Momentum	2.52	
200	22.18	81.29218	Momentum	1.78	

**Figure 3.20: Global Heat Release Rate (HRR) from the fireball with different inlet velocities**

The effect of varying velocity of fuel is studied on lifting and expansion of fireball. Figure 3.21 (a) and (b) show the calculated position of the upper edge of a fireball in vertical direction and expansion of fireball in the horizontal direction as a function of time. It can be observed in Figure 3.21 (a) that the fireball with inlet velocity of 50 m/s lifts earlier than the fireball with 100 m/s. This may be due to higher combustion which results in higher buoyancy effect. In case of 200 m/s inlet velocity the initial momentum is dominant over a mixing of fuel and air,

hence it lifts faster than other cases studied. Figure 3.21 (b) shows that a fireball formed from higher inlet velocity achieves its maximum diameter earlier than that formed with lower velocities. This may be due to entrainment of air and higher combustion. The momentum of hot combustion products generates a vortex, which causes a larger expansion of fireball.

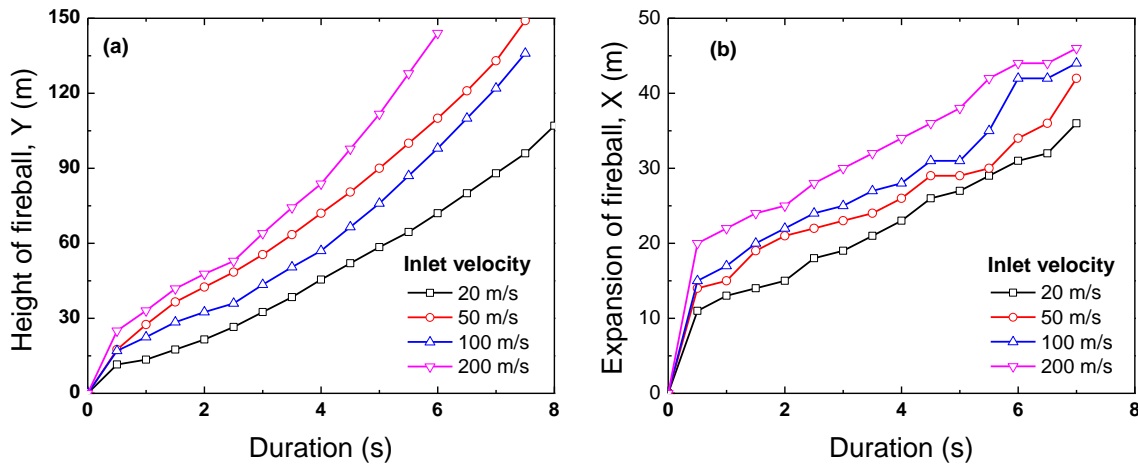


**Figure 3.21: (a) Position of the upper edge of fireball and (b) expansion of fireball in the horizontal direction for different fuel inlet velocities.**

The effect of inlet velocity on the radiative heat flux received at various distances has been studied in Figure 3.22(a). It shows the average radiative flux received at locations of 20, 30, 40 and 50 m away from the centre of the fireball. It can be observed from Figure 3.22 (a) that radiative heat flux at 20 m distance is much higher than the other locations for all inlet velocities. This variation in the incident radiation is due to an inverse-square law of decay (refer to Figure 3.19 (c)).

The 20 m distance from the fireball is nearest than other calculated distances. The average radiative flux for 50 m/s velocity is higher than that of 100 m/s at 20 m and 30 m and this may be due to well mixing of fuel with air, which leads to higher combustion. Nearly the same value of radiative flux has been observed in all inlet velocity cases at distances of 40 m and 50 m

away from the centre. Figure 3.22 (b) shows the time-dependent thermal dose for fireball, calculated at distance 20 m away from the centre. No substantial change in thermal dose is observed for various inlet fuel velocities.

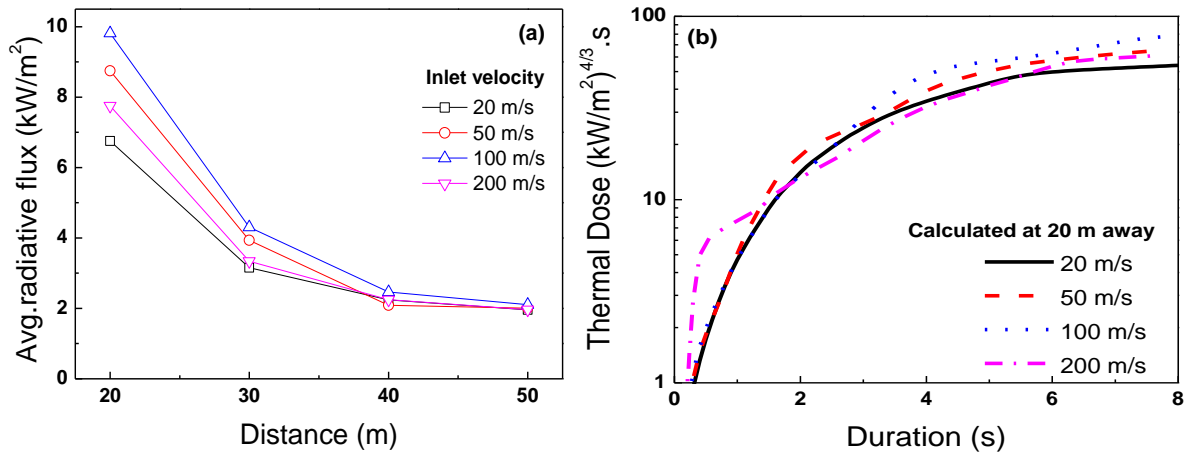


**Figure 3.22: (a) Average Incident radiations calculated at the locations on the ground for various fuel inlet velocity. (b) Thermal dose calculated at 20 m on the ground for various fuel inlet velocity**

### 3.11.3. Effect of inlet diameter

For the analyses described in Table 3.4, the size of the inlet opening and the duration of injection are varied while the mass of fuel and the inlet velocity are kept constant. The analyses have been performed for inlet diameter 1, 2, 4 and 8 m by keeping the inlet velocity and the mass of fuel constant.

Figure 3.23 shows the Heat release rate with time. The HRR is higher for 8 m diameter in the initial period. For higher inlet diameter, the area covered by the fireball is higher. The higher area coverage also causes better mixing of air with fuel.

**Table 3.4: Constant inlet mass of 1000 kg for the release velocity with varying inlet diameters and duration**

mass of fuel (kg)	inlet velocity (m/s)	inlet diameter (m)	Inlet duration (s)	Domain dimensions(m) ( $w \times d \times h$ )
1000	100	1	6.34	100×100×250
		2	1.58	
		4	0.39	
		8	0.01	

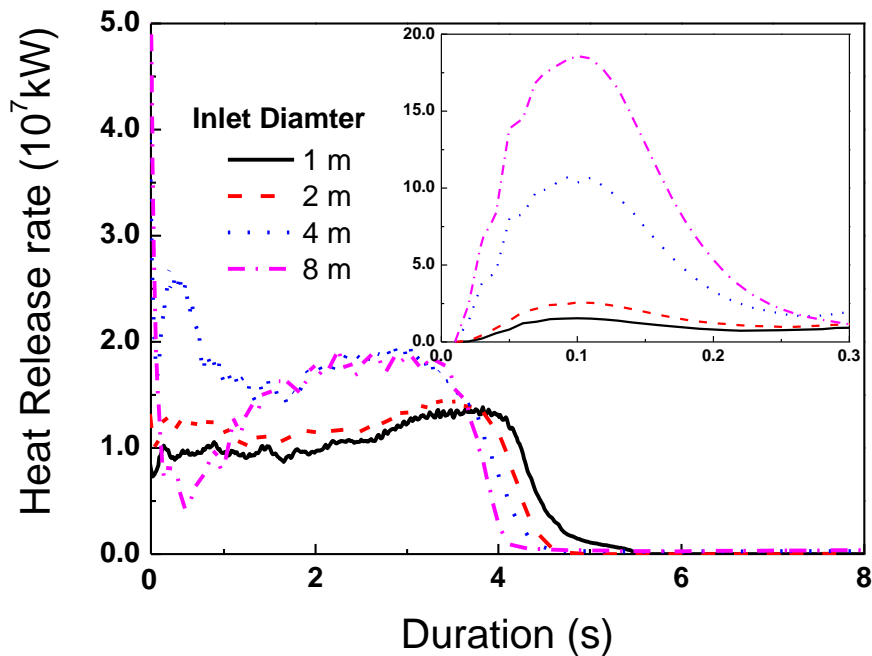


**Figure 3.23: Global heat release rate (HRR) for 1000 kg of propane with different inlet diameters**

Figure 3.24 (a) and (b) show the effect of varying fuel inlet opening diameter on lifting and expansion of fireball. Figure 3.24 (a) shows that the fireball with 8 m diameter loses its momentum due to shorter injection time and lifts slowly. Figure 3.24 (b) further shows the horizontal expansion of fireball as a function of time. It can be observed that the fireball expansion (fireball diameter) with time remains almost same for all the cases.

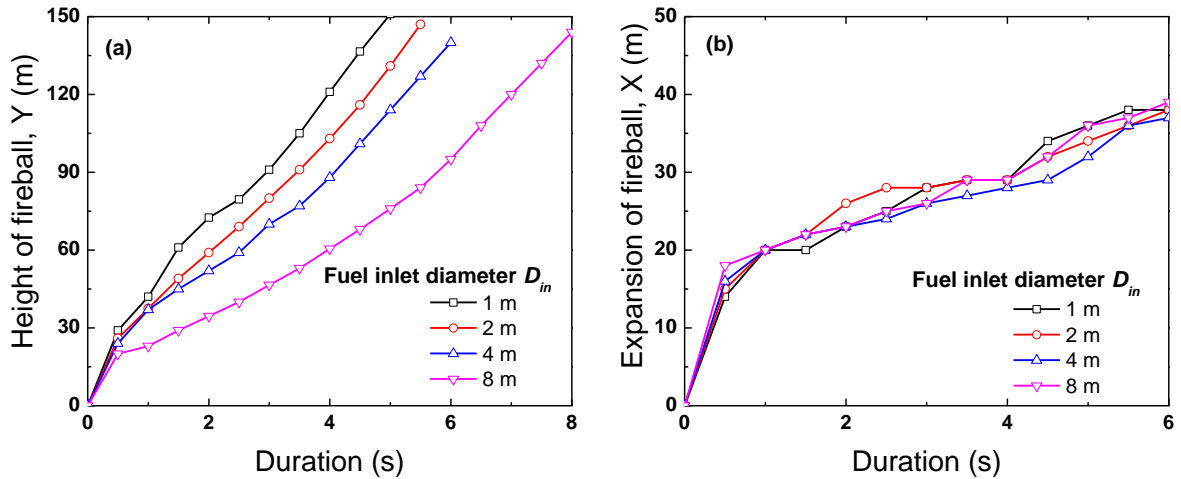


**Figure 3.24: (a) Position of the upper edge of fireball and (b) expansion of fireball in the horizontal direction for the different inlet opening diameters**

Figure 3.25 (a) shows the average radiative flux received at locations of 20, 30, 40 and 50 m away from the centre of the fireball with fuel inlet diameters of 1, 2, 4 and 8 m. It can be observed from Figure 3.25 that radiative heat flux at 20 m distance is much higher than the other locations. This may be due to engulfment of fireball at 20 m distance from the centre. The average radiative flux for fireball from 8 m inlet diameter shows the highest radiative flux at the calculated locations especially up to 30 m distance from the centre. This may be due to the slow lifting of fireball (fireball remains closer to the ground for a longer duration).

The insignificant deviation in the radiative heat flux has been observed at the distances of 30, 40 and 50 m away from the centre for all the inlet diameters. Thermal radiation dose from the fireball, calculated at distance 20 m away from the centre is plotted in Figure 3.25 (b). The higher values of thermal dose are observed in case of fireball with inlet opening diameter of 8 m due to the formation of fireball at a lower height.

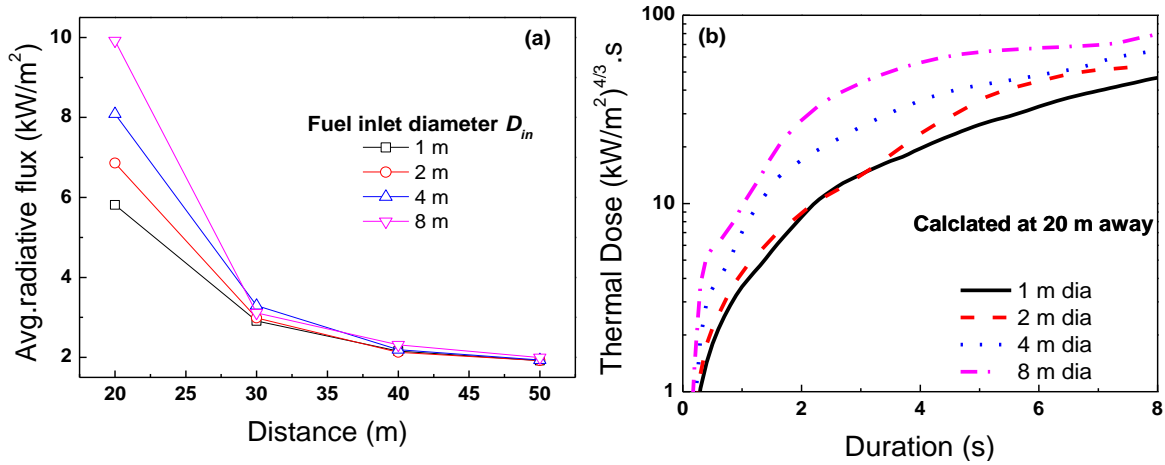


**Figure 3.25: (a) Average Incident radiations calculated at the locations on the ground for various inlet opening diameter. (b) Thermal dose calculated at 20 m at the ground for various inlet diameter**

#### 3.11.4. Correlations based on CFD Simulation Data

A number of cases have been studied in the CFD simulation of the fireball. Correlations for maximum diameter and the duration of fireball have been developed based on the present simulations. Figure 3.26 (a) depicts the fireball diameter as a function of fuel mass. Following is the correlation developed based on the analysis performed.

$$D_{FB} = 5.2M_{fuel}^{1/3} \quad (3.29)$$

Figure 3.26 (b) depicts the comparison between the fireball diameters calculated by the proposed correlation and other correlations given in the literature. It can be seen that the proposed correlation predicts the fireball diameter within 13% of the accident/experimental data. Figure 3.27 (a) shows the fireball duration as a function of fuel mass. Following is the correlation developed based on the analysis performed.

$$t_{FB} = 0.407M_{fuel}^{1/3} \quad (3.30)$$

Figure 3.27 depicts the comparison between the fireball duration calculated by the proposed correlation and other correlations given in the literature. It can be seen that the proposed correlation predicts the fireball duration within 18% of the accident/ experimental data.

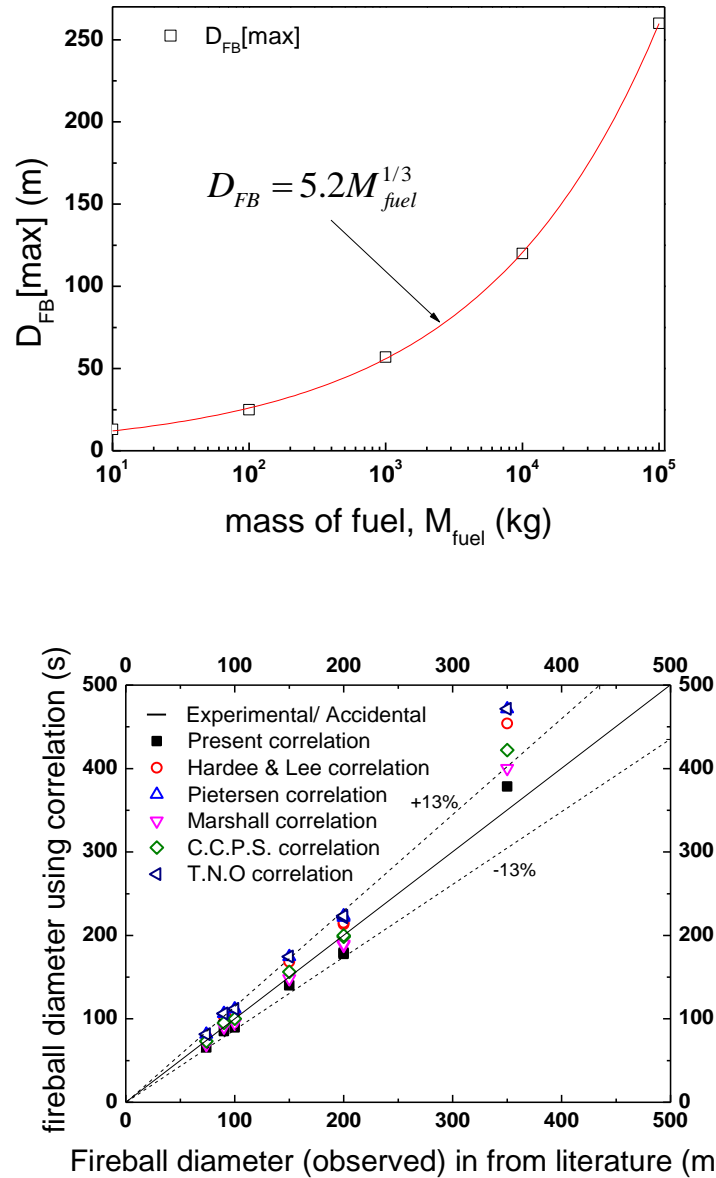


**Figure 3.26: (a) mass based correlation developed for the maximum diameter of fireball using CFD results (b) Comparison of maximum fireball diameter obtained using correlation with accidental/experimental observations**

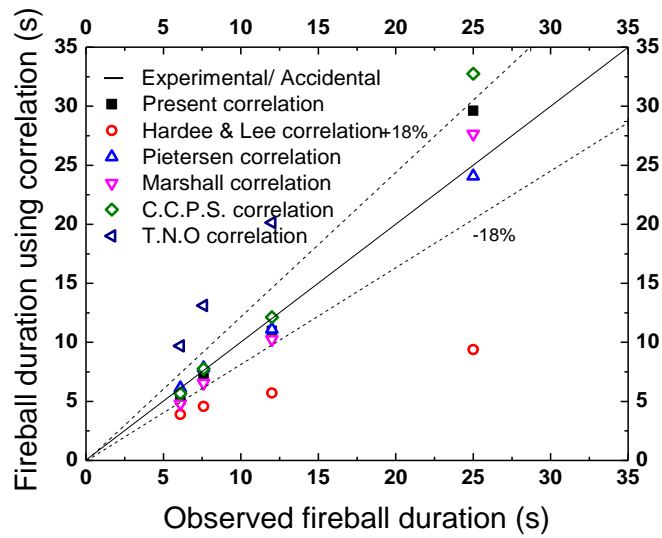
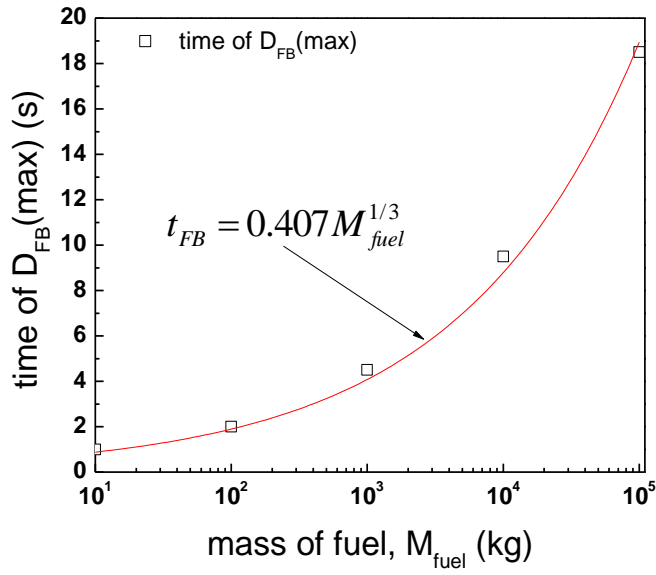


**Figure 3.27: (a) mass based correlation developed for the duration of fireball using CFD results  
(b) Comparison of fireball duration obtained using correlation with accidental/experimental observations**

### 3.12. Closure

The overall agreement between the simulated and the experimental data encouraged the use of FireFOAM CFD Codes for fireball analysis. Following conclusions drawn from the present study in this chapter are,

- The inner zone of fireball does not lose heat through radiation/convection, hence the temperature of inner zone of fireball is close to adiabatic flame temperature in both the cases. The fireball temperature is 1900 K in case of propane fuel.
- For fireball modelling the higher inlet velocity gives accurate results hence, inlet velocity ~ 100 m/s should be considered for such analysis.
- The proposed correlations predict the fireball diameter within 13% and duration of a fireball in 18% of the previously published accidental/ experimental data.



# **CHAPTER 4: IMPACT OF LIQUID CONTAINING PROJECTILE AND FUEL DISPERSION/ MIST FORMATION**

---

## **4.1. Introduction**

During the impact of aircraft with high velocity, the fuel tank can get ruptured which causes fuel leakage. The different physical phenomena occur due to leakage of fuel. In the first stage, fuel in the aircraft wings will be dispersed out due to rupture forming the droplet cloud. Normally, fuel leakage forms liquid chunks for smaller impact velocities and droplet cloud for higher velocities. The second stage is the formation of a large fireball caused by the ignition of the aircraft fuel cloud erupting from the breaking fuel tanks. In the third stage, liquid chunks or droplets with larger diameters may rain out and contribute to pool fire if the whole mass of fuel has not participated in earlier stages. The duration of the pool fire depends on the amount of fuel, which has not been burnt in the initial fireball.

In the first stage, the fuel spills out from ruptured tanks and disperses to the surrounding. During the dispersion, the primary breakup of liquid occurs due to the destabilizing process of aerodynamic drag and turbulence within the liquid core. The primary breakup phase is followed by secondary breakup phase of flying droplets. Depending on the speed of droplet relative to surrounding gas, the secondary breakup can produce droplets of different sizes. While studying the impact of large mass and dispersion phenomena of liquid, it is found that Weber number ( $We$ ) associated with these impacts is of the range  $10^5$  to  $10^8$ . Applying traditional diagnostic of these problems is difficult because of destructive energy associated with high speed. Splashing is often observed during liquid slug impact onto a solid surface with high velocities. The threshold of splashing is known to be related to size, impact velocity, the physical

properties of liquid and the surrounding pressure, but the mechanism that initiates splashing are not understood completely. The final shape of spreading liquid also depends on the above-mentioned parameters. The process of crushing the cylindrical tank, liquid emerging out and droplet formation with breakup and evaporation is a very complex process to solve by CFD code.

In this chapter, a mathematical model is developed for prediction of droplet sizes and distribution associated with the impact of a liquid-containing projectile. This model can predict the transient behaviour of the droplet cloud mathematical model for projectiles with the hydrocarbon fuels which can undergo flashing during splashing of liquid with high speed. The model is validated with experimental data available in the literature. In this chapter, the analysis has been performed using water and hydrocarbon fuel (kerosene). The data obtained from this model can be utilized as a boundary and initial condition for CFD analysis of the fire ball formation and assessment of a typical nuclear power plant building respectively further in **Chapter 5** and **6**.

## **4.2. Mathematical model**

A mathematical model has been proposed to study the droplet size and its distribution during the spreading of liquid from a high velocity impacting cylinder. The impact process is obviously a definite interaction between a very large stationary target and a small but fast moving object. In order to make this problem mathematically tractable, various phenomenon associated with liquid dispersion with impacted projectile have been used. Following are the various phenomena associated, which involve in the determination of parameters.

### **4.2.1. Energy balance in impacting container**

The aircraft wing tanks containing fuel are approximated as a rectangular box by neglecting

the structural integrity with the height  $T$  in the wing. The length of the tank,  $L_{wing}$ , considered as the chord of the wing (length of the fuel tank from leading edge to trailing edge), and  $S$  as the span of the wing (Tieszen, 1995). For simplicity in conducting liquid dispersal experiments and modelling, the fuel tank is assumed as a cylinder by Silde et al., (2011) and (Hostikka et al., 2015). When a soft projectile impacting on a large hard stationary wall, it is assumed that the energy is not absorbed by a wall (Silde et al., 2011) on which the soft projectile is impacting and the soft projectile is getting fully crushed. The soft projectile containing fuel can be of any shape. In this model, fuel containing projectile is considered cylindrical. Imonsén and Wierzbicki (1997) have studied the quasi-static crushing of uniform circular cylinder representing the impacting container (Figure 4.1) and the expression of crushing force is given by

$$F_{crush} = 7.96\sigma_{cyl}t_{cyl}^{1.5}D_{cyl}^{0.5} \quad (4.1)$$

Where  $\sigma_{cyl}$ ,  $t_{cyl}$ , and  $D_{cyl}$  are stress induced in the cylinder, the thickness of cylinder and the inner diameter of the cylinder. Multiplying the crushing force by the total length of cylinder  $L_{cyl}$ , the energy absorbed by the crushing of cylinder is given by the following equation

$$E_{crushing} = F_{crush} \times L_{cyl} \quad (4.2)$$

This energy is absorbed by cylinder material during impact. The total kinetic energy considering the mass of the cylinder and liquid filled is higher for higher impacting velocities. After crushing the remaining energy gets added to the kinetic energy of a liquid slug. The impacting velocity of the slug can be determined from the kinetic energy of a slug. For the lower impacting velocities, the cylinder cannot be crushed totally. The liquid may leak from the container is conservative in nature, hence is not included in the scope of this methodology.

In the aircraft impact case, the hydraulic diameter of cylinder  $D_{cyl}$  is considered based on wing cross-section ( $S \times T$ ) and the length of cylinder  $L_{cyl}$ , is equal to the length of the tank for modelling.

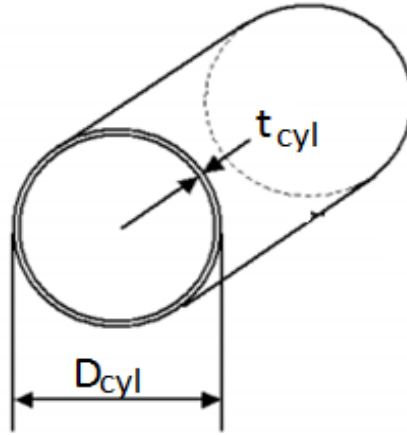


Figure 4.1: Simplified Model of impacting container

#### 4.2.2. Water Hammer Effect

According to previous research of Harlow and Shenon (1967), the pressure inside the bulk mass of liquid is generated during conversion of the momentum of impacting mass into the momentum of flow along the surface of impact. Once the pressure exceeds the surface tension, spreading occurs. Engel (1955) gave a theory that explains how pressure is generated in bulk mass during impact as "water hammer" effect. Pressure due to water hammer effect is given by

$$P = \rho_l \times V_n \times c_t \quad (4.3)$$

Where  $\rho_l$  is the density of the liquid,  $V_n$  is a liquid slug impact velocity and  $c_t$  is the speed of sound in the liquid. In water hammer theory, the liquid on contact area is compressed and the pressure is generated as shock wave that propagates through the liquid with speed of sound. Once the front shock wave reaches the free surface of the liquid, spreading or splashing is initiated. The shock wave travels with the speed of sound and it varies with phase concentration (Gouse et al., 1964)(i.e. the speed of sound varies with the concentration of liquid droplets

formed by fragmentation and further evaporation assisted by surrounding air). The velocity of spreading edge of impacting slug,  $v_s$  at a given time instant can be calculated based on the mass balance between spreading film and impacting slug (see Figure 4.2 b) and it is given by the following equation as,

$$v_s(t) = \frac{V_n D_{cyl}^2}{8 r(t) h(t)} \quad (4.4)$$

Where  $r(t)$  is the instantaneous radius of spreading film and  $h(t)$  is the thickness of the film.

### 4.2.3. Dynamic Spreading Model

Although the liquid slug impact is a dynamic and transient process, we simplified the impact analysis by assuming that slug impact was a pseudo-steady process, which is justified due to very short time scale of ( $\sim 0.05$ s) as shown in Figure 4.2, to illustrate the effect of velocities on pressure varying inside the liquid slug. During the pseudo-steady impact process, Liu et al. (2010) expressed the momentum variation of the mass in contact with the impact surface,

$$\frac{dm\vec{v}_n}{dt} = \vec{F} = P(\pi r^2) \quad (4.5)$$

Where  $\vec{v}_n$  and  $P$  are velocity and pressure of mass normal to the impact surface respectively,  $r$  is the radius of spreading layer. Vander Wal et al. (2006) defined the radius of the spreading layer by the following equation,

$$r(t) = R_{max} \left(1 - e^{-t/t_c}\right) \quad (4.6)$$

In equation 4.6,  $R_{max}$  is the maximum spreading radius, which can be expressed (Pasandideh-Fard et al., 2002) as

$$R_{\max} = \frac{D}{2} \sqrt{\frac{We + 12}{3(\cos \theta) + 4 \left( \frac{We}{\sqrt{Re}} \right)}} \quad (4.7)$$

where,  $D$  is the diameter of impacting slug,  $We = \rho v^2 D / \sigma$ ,  $Re = \rho v D / \mu$  are the Weber Number and Reynolds Number of impacting mass.  $t_c$  is a characteristic spreading time of liquid film the is given by-

$$t_c = L / V_n \quad (4.8)$$

Where  $L$  is the length of impacting slug. Equations 4.6 and 4.7, are used to determine instantaneously and the maximum distance travelled by a spreading film without breaking.

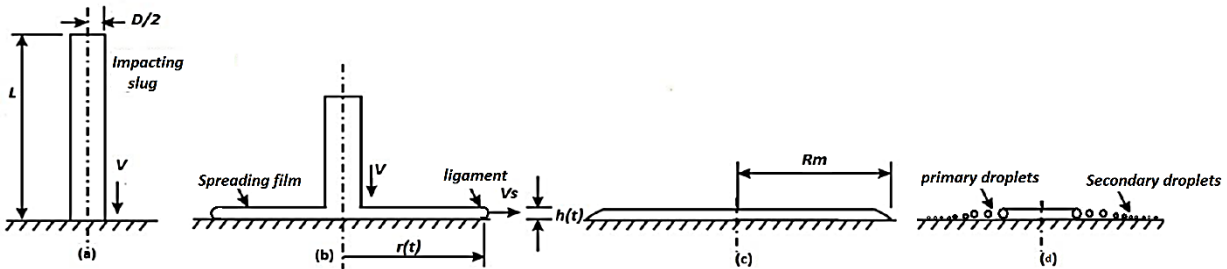


Figure 4.2: Sketch of spreading after slug mass impact onto the rigid surface (a) before impact,  $t=0$  (b) at the intermediate time,  $t$  (c) maximum spreading without breaking,  $t=t_c$  (d) breaking of spreading the film

#### 4.2.4. Breakup of Spreading Film

The slug impact and the dynamics of film spreading depend on Weber number and Reynolds number. As the spreading phase begins other parameters such as the diameter of the impacting slug, velocity, surface tension and viscosity may start affecting the rate at which the lamella spreads. During the later stage of this phase, surface tension effects can play a prominent role in determining the maximum spread of film (Figure 4.2). The surface energy depends on surface tension. When the momentum of the liquid droplet cannot convert into the flow of

momentum along the impact surface during the impact splashing occurs at the location where surface energy is the least (Harlow and Shenon, 1967). When the spreading film has stretched to a maximum diameter, the surface energy is written as,

$$E_s = \pi \xi_{\max}^2 D^2 (1 - \cos \theta) \sigma \quad (4.9)$$

Where  $\xi_{\max}$  is the ratio of maximum film diameter to the initial diameter of a slug,  $\sigma$  is surface tension of the liquid and  $\theta$  is the angle of contact of liquid. By the principle of conservation of energy for the liquid droplet before and after impact, energy equation 4.9 is reduced to,

$$\left( \frac{3(\xi_{\max}^2 - 12)}{We} + \frac{9\xi_{\max}^4}{2Re} \right) = \frac{\Delta\rho}{\rho_l} \quad (4.10)$$

For large differences in density, Gupta and Kumar (2010) reported that the right-hand side of the equation as 1.0. At the instant when the spreading film diameter has reached a maximum, the interplay of the surface and kinetic energies can lead to a possible breakup of this liquid film into smaller daughter droplets. The criterion for predicting the spreading or breakup of an impacting bulk mass as-

- For the situation, when  $\frac{\rho_l}{\Delta\rho} \left( \frac{3(\xi_{\max}^2 - 12)}{We} + \frac{9\xi_{\max}^4}{2Re} \right) > 1$  the spreading film will reach maximum diameter without breaking up into daughter droplets,
- Whereas, when  $\frac{\rho_l}{\Delta\rho} \left( \frac{3(\xi_{\max}^2 - 12)}{We} + \frac{9\xi_{\max}^4}{2Re} \right) < 1$ , the spreading films will break into daughter droplets.

#### 4.2.5. Aerodynamic Breakup/ Splashing

The liquid sheet becomes thinner because of the conservation of mass. Further instabilities are produced due to shear at the interface between two fluids with different physical properties (for example different temperature or different density). Kelvin Helmholtz instabilities are assumed to develop and grow on the film surface and in the formation of the ligament. These ligaments finally break up into droplets. Formation of ligament and droplet from a liquid sheet is explained in Figure 4.3.

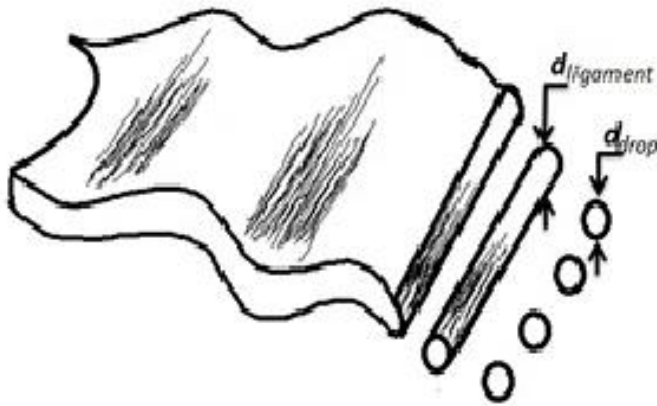


**Figure 4.3: Breakup of the liquid sheet into ligaments and droplets**

The diameter of the primary ligament is obtained from mass balance. It is assumed that every tear in the sheet forms a primary ligament. The resulting diameter is given by

$$d_{lig} = \sqrt{\frac{16h}{K_s}} \quad (4.11)$$

$K_s$  is the wave number of the fastest-growing surface wave. Since the sheet becomes thinner as it departs from the source, the position of the first breakup determines the ligament diameter.

Here  $h$  is film thickness and is given by  $\sqrt{\nu t}$ , where  $\nu$  is the kinematic viscosity of the liquid.

Liu et al. (2010) determined the value of  $K_s$  from the following equation,

$$K_s = \frac{2v_s^2 \rho_g}{3\sigma} \quad (4.12)$$

The subsequent disintegration of ligament into drops is calculated using other stability analysis, which is based on analogy (Weber's results) for the growth of waves on cylindrical liquid columns. The wave number for fastest growing ligament,  $K_{lig}$ , is given by

$$K_{lig} = \frac{1}{d_{lig}} \left[ 0.5 + \frac{3\mu}{2\sqrt{\rho\sigma d_{lig}}} \right]^{-1/2} \quad (4.13)$$

Where,  $d_{lig}$  is the diameter of the ligament. Dombrowski and Johns (1963) assumed that breakup occurs if the amplitude of the wave is equal to the radius of ligament and that one drop is formed per wavelength. A mass balance between the ligament and primary droplet gives the size and number of droplets. The primary drop diameter,  $d_{drop}$  as

$$d_{drop} = 3 \sqrt{\frac{3\pi d_{lig}^2}{K_{lig}}} \quad (4.14)$$

This equation represents the initial droplets formed due to film breakup. These droplet diameters can be used as inputs for the CFD calculations for initial predictions of spray formation.

#### 4.2.6. Drop acceleration

The drop acceleration has contributions due to aerodynamic drag and gravitation, and is given from the expression of droplet velocity the acceleration (deceleration) found to be,

$$\frac{dv}{dt} = \frac{3}{8} C_D \frac{\rho_g}{\rho_D} \frac{|U_{rel}|}{r_{drop}} U_{rel} + g_{component} \quad (4.15)$$

Where,  $C_D$  is the drag coefficient,  $\rho_g$  is the gas density,  $\rho_{drop}$  the droplet density and  $U_{rel}$  the relative velocity between the droplet and surrounding air for  $r_{drop}$  is the radius of the droplet. This relative velocity is determined by using energy conservation (kinetic energies and surface energies) between moving droplet and breaking ligament. Ashgriz (2011) reported the drag coefficient formula as,

$$C_D = \begin{cases} \frac{24}{Re_{drop}} \left( 1 + \frac{Re_D^{2/3}}{6} \right) & \text{if } Re_{drop} \leq 1000 \\ 0.424 & \text{if } Re_{drop} > 1000 \end{cases} \quad (4.16)$$

Here,  $Re_{drop}$  is droplet's Reynolds number, defined by

$$Re_{drop} = \frac{d_{drop} \rho_g U_{rel}}{\mu_g} \quad (4.17)$$

Considering acceleration due to gravity ( $g=9.81m/s^2$ ) at various angles in a two-dimensional symmetry plane shown in Figure 4.4.

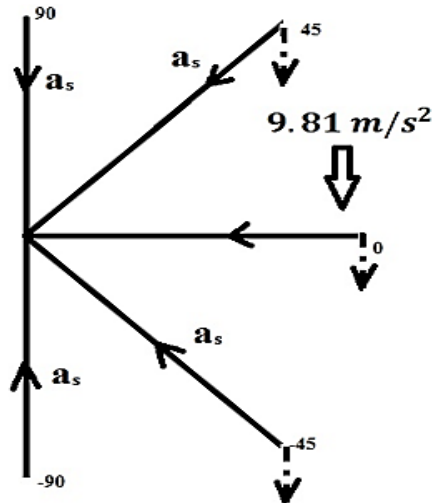


Figure 4.4: Acceleration of droplet and effect of gravity

#### 4.2.7. Secondary breakup

The secondary breakup is the disintegration of already existing droplets into smaller ones due to the aerodynamic forces, which are induced by the relative velocity,  $U_{rel}$  between the droplet and surrounding gas. These forces result in an unstable growing of waves on the droplet surface or of the whole droplet itself and finally lead to its disintegration.

The surface tension force, on the other hand, tries to keep the droplet spherical and counteracts the deformation force. This behaviour is expressed by a non-dimensional number, the gas phase Weber number,  $We_g = \rho_g U_{rel}^2 d_{drop} / \sigma$ , which represents the ratio of aerodynamic and surface tension forces. The smaller the droplet diameter, the bigger the surface tension force and the bigger the critical relative velocity needed for breakup. Depending on the Weber number, different breakup modes and mechanisms of droplets exist. Table 4.1 gives the criteria for the secondary breakup of the droplet. Arcoumanis et al. (1997) distinguished between four different droplet breakup modes, which are all described using semi-empirical relationships for the resulting droplet sizes and breakup times,

$$t_{bu} = \tau_{break} \frac{d_{drop}}{U_{rel}} \sqrt{\frac{\rho_l}{\rho_g}} \quad (4.18)$$

Where,  $\tau_{break}$  is given in Table 4.1. Using the following phenomenological relations, the product droplet sizes are checked from distribution functions and the Sauter mean diameters (SMD) are estimated. According to Arcoumanis et al. (1997), the SMD of the first three modes (vibrational, bag and bag-and-streamer) is

$$SMD_{1,2,3} = \frac{4d_{drop}}{4 + 0.5(1 + 0.19\sqrt{We_g})} \quad (4.19)$$

Prefix 1, 2 and 3 gives the serial numbers in Table 4.1, while for the chaotic breakup mode (serial number 4 in Table 4.1) the following relation is used.

$$SMD_4 = 6.2 \frac{\sigma}{\rho_g U_{rel}^2} \left( \frac{\rho_l}{\rho_g} \right)^{1/4} \left( \frac{\mu l}{\rho_l d_{drop} U_{rel}} \right)^{1/2} \cdot We \quad (4.20)$$

The number of child droplets is determined using mass balance. In the case of stripping breakup, small product droplets are stripped from the parent ones, the size of which decreases continuously and can be predicted by subtracting the mass leaving the parent droplet. The volume mean diameter of small product droplets formed by stripping breakup mode is 0.2 times the initial diameter. Altogether, this phenomenological modelling results in a multitude of different regimes with different correlations for breakup time and product droplet size. Some of them appear within the same range as the Weber number. The product droplet sizes are sampled from distribution functions.

**Table 4.1: Criteria for the secondary breakup of the droplet (Arcoumanis et al., 1997).**

Sr. No.	Weber Number	Breakup mode	Breakup time ( $\tau_{break}$ )
1	$We_g \approx 12$	Vibrational	$\frac{\pi}{4} \left[ \frac{\sigma}{\rho_l d_{drop}^3} - 6.25 \frac{\mu}{\rho d^2} \right]$
2	$12 \leq We_g < 18$	Bag	$6(We_g - 12)^{-0.25}$
3	$18 \leq We_g < 45$	Bag and streamer	$2.45(We_g - 12)^{0.25}$
4	$45 \leq We_g < 100$	Chaotic	$14.1(We_g - 12)^{-0.25}$
5	$100 \leq We_g < 350$	Sheet stripping	$14.1(We_g - 12)^{-0.25}$

#### 4.2.8. Droplet evaporation model

In addition to the breakup of the fuel droplets and the mixing processes of air and fuel droplets, the evaporation of liquid droplets also has a significant influence on ignition and combustion. The evaporation process determines the spatial distribution of the equivalence ratio, and thus strongly affects the timing and location of ignition. The energy for evaporation is transferred from the gas to the colder droplet due to conductive, convective and radiative heat transfer, resulting in diffusive and convective mass transfer of fuel vapour from the boundary layer at the drop surface into the gas, shown in Figure 4.5. This will again affect the temperature, velocity and vapour concentration in the gas phase. Hence, there is a strong linking of evaporation rate and gas conditions and for this reason; there must always be a combined calculation of heat and mass transfer processes. In order to describe the evaporation process mathematically, the following assumptions are made,

- a) The radiative heat transfer is neglected because it is small compared to the convective one
- b) The droplets are assumed to be of spherical shape
- c) Deformation, breakup, collisions, and other interactions of droplets are neglected during the calculation of evaporation
- d) The droplet's interior is assumed to be well mixed
- e) There are no spatial gradients of the relevant quantities like liquid temperature, the concentration of fuel components, boiling temperatures and critical temperatures, the heat of evaporation etc. inside the droplet and only a dependence on time is possible
- f) The solubility of the surrounding gas in the liquid and the effect of surface tension on the vapour pressure are neglected for conservative estimation of the problem of interest.

The effect of an increased mass transfer due to the relative velocity between the droplets and surrounding gas is expressed in terms of Sherwood number by following expression

(Baumgarten, 2006),

$$\dot{m}_{evp} = d_{drop} \pi \rho D_f \ln \left[ \frac{1 - Y_{f,\infty}}{1 - Y_{f,R}} \right] Sh \quad (4.21)$$

Where,  $D_f$  is the diffusivity of vapour in the air (for water  $0.2-0.3 \times 10^{-4}$ ),  $Y_{f,\infty}$  is the vapour mass fraction outside the boundary layer and  $Y_{f,R}$  is the vapour mass fraction at the droplet surface,  $Sh$  is Sherwood number. The properties of the gas phase inside the boundary layer are calculated using the  $1/3^{rd}$  rule. Assuming equilibrium and using Raoult's law (Raoult, 1887), the vapour fraction in the boundary layer is calculated as proposed by Ranz and Marshall (Brennen, 2005)

$$Sh = 2.0 + 0.6 Re^{1/2} Sc^{1/3} \quad (4.22)$$

Where the droplet Schmidt number is defined by  $Sc = \mu / \rho d_{drop}$ . The Sherwood number has a value of  $Sh = 2.0$  if no relative velocity is present.

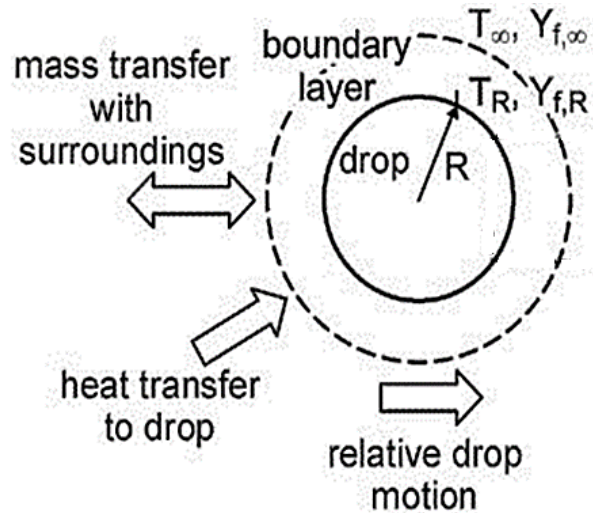


Figure 4.5: Schematic view of drop vaporization

#### 4.2.9. Characteristic Diameters

For spray characterization purpose, Sauter mean diameter  $d_{32}$ , volumetric mean diameter  $d_{43}$  and arithmetic mean  $d_{10}$  are defined as:

$$d_{32} = \frac{\sum_{i=1}^N d_i^3}{\sum_{i=1}^N d_i^2}, \quad d_{43} = \frac{\sum_{i=1}^N d_i^4}{\sum_{i=1}^N d_i^3} \quad \text{and} \quad d_{10} = \frac{\sum_{i=1}^N d_i}{\sum_{i=1}^N 1} \quad (4.23)$$

Sauter mean diameter (SMD) is defined as the diameter of a sphere that has the same volume to surface area ratio. If the volume calculated by using Volumetric mean diameter is multiplied by the total number of droplets, this will give the total volume of the liquid. The arithmetic mean diameter ( $d_{10}$ ) is average of all droplet diameters.

#### 4.2.10. Mass involved in Fireball

Mass of fuel entrained in a fireball is depends on the fraction of fuel, which is flashed off, and further on the fraction that forms liquid sprays. Roberts, (1982) deliberated a study on propane for a theoretical adiabatic flash fraction, liquid temperature and vapour pressure. He found that 35% flash fraction occurs at 21°C and 50% fraction at 45°C. Hesegawa and Sato (1977) found that when the theoretical adiabatic flash fraction reaches 35% virtually all the liquid released burns as a fireball. From this, Roberts (1982b) derives relation:

$$f = \frac{M_{involved}}{M_{released}} = 0 \quad \text{for } \phi = 0$$

$$f = 1 \quad \text{for } \phi \geq 0.35 \quad (4.24)$$

Where,  $f$  is a fraction of fuel released, which is entering in the fireball.  $M_{involved}$  is mass of fuel in a fireball (kg),  $M_{released}$  is mass of liquid released (kg) and  $\phi$  is a fraction of liquid vaporized. Hence by linear interpolation,

$$f = \phi / 0.35 \quad \text{for } 0 < \phi \leq 0.35 \quad (4.25)$$

This treatment is commonly used to determine the mass of fuel in the fireball. The method mentioned above is used by the Centre for Chemical Process Safety to determine the mass of fuel in the fireball (CCPS, 1999).

### 4.3. Solution Methodology

To carry out the study on liquid dispersion, the methodology described earlier has been used in which total energy of impacting cylinder filled with liquid is considered. The projectile cylinder breaks due to impact and internal pressure developed due to *water hammer* effect. The liquid available in the cylinder spills out after crushing of cylinder. This causes spreading and breaking of liquid into droplets. The sequence of solving the above equations is explained using the flowchart given in Figure 4.6.

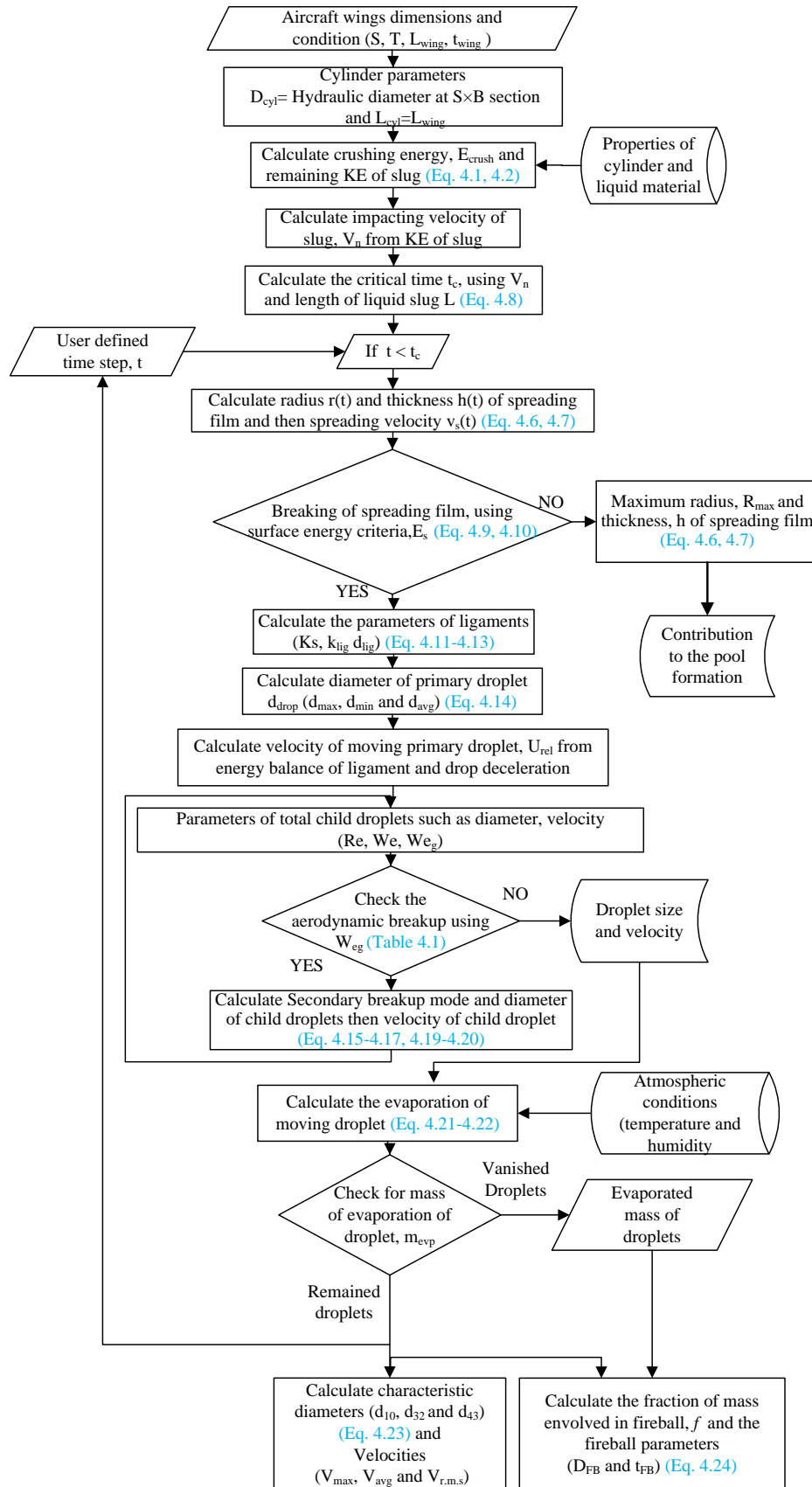
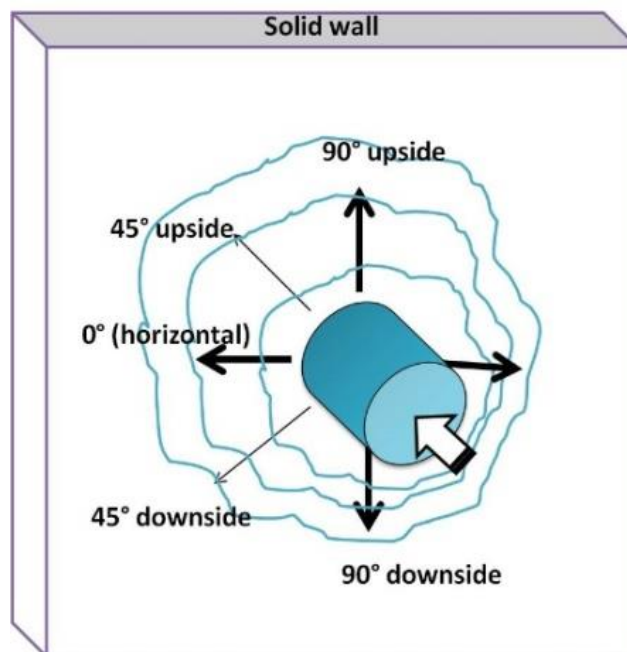


Figure 4.6: Flowchart for calculating the liquid dispersion

#### 4.4. Application of model

The model described earlier helps in determining some important parameters associated with liquid such as splashing, discharge speed and direction of the liquid core released from the impacting ruptured cylinder, propagation speed of the spray front, liquid pooling on the floor, extent of liquid dispersal away from the target, and the drop size and liquid splashed. The following section gives the studies performed using this model



**Figure 4.7: Liquid dispersion pattern**

As discussed earlier, Hostikka et al. (2015) performed experiments on impacting of the water-filled metal projectile on a hard wall. They investigated the spray behaviour using high-speed cameras and droplet size and velocity distribution using ultra-high-speed cameras. They illustrated images of a typical liquid dispersion pattern from a cylindrical projectile at separate moments. Figure 4.7 gives a conceptual representation of the liquid dispersion pattern. The experimental data given by them have been used for validating the above-mentioned

methodology. Table 4.2 gives the specifications of selected tests for the model validation from the study of Hostikka et al. (2015).

**Table 4.2: Specifications of tests (Hostikka et al., 2015)**

<b>Test ID</b>	<b>Wall thickness (m)</b>	<b>Inner diameter (m)</b>	<b>water tank length (m)</b>	<b>mass (kg)</b>	<b>Water Mass (kg)</b>	<b>Impact Velocity (m/s)</b>
<b>SFP 7</b>	0.0015	0.20	1.204	49.75	36.82	103
<b>SFP 8</b>	0.002	0.20	1.204	51.05	37.24	100
<b>SFP 11</b>	0.0015	0.20	1.204	49.9	36.96	126
<b>SFP 12</b>	0.002	0.20	1.204	51.5	37.0	122

The crushing energy of impacting cylinder and energy absorbed by liquid slug is given in Table 4.3. The velocity of the liquid slug is estimated as given in Table 4.4. It can be seen from Table 4.4, that characteristic diameter and velocity calculated by the model match well with the experimental data (Hostikka et al., 2015). The sample calculation for case SFP-7 from the experimental data has been presented in **Appendix A**.

**Table 4.3: Calculations for the energy of crushing cylinder and velocity of slug impact**

<b>Test ID</b>	<b>Impact Velocity (m/s)</b>	<b>Energy of crushing Cylinder (kJ)</b>	<b>Velocity of liquid slug (m/s)</b>
<b>SFP 7</b>	103	62.25	119.71
<b>SFP 8</b>	100	95.84	117.06
<b>SFP 11</b>	126	62.25	146.39
<b>SFP 12</b>	122	95.84	143.92

**Table 4.4: Comparison of experimental data (Hostikka et al., 2015) and calculated characteristic diameters and velocity**

Test ID	Diameter ( $\mu\text{m}$ )		Velocity (m/s)			
	$d_{32}$		$V_{\text{max}}$		$V_{\text{r.m.s.}}$	
Parameters	<i>Exp.</i>	<i>Cal.</i>	<i>Exp.</i>	<i>Cal.</i>	<i>Exp.</i>	<i>Cal.</i>
	<b>SFP 7</b>	344	340.62	116	100.72	19.4
<b>SFP 8</b>	253	291.1	100	113.12	18.4	27.46
<b>SFP 11</b>	316	249.32	130	123.175	27.8	29.92
<b>SFP 12</b>	237	217.21	127	137.63	24	33.42

#### 4.5. Parametric study using water and hydrocarbon fuel

Parametric studies are performed with a cylindrical vessel filled with liquid. The liquid considered for the studies are water and hydrocarbon fuel (Kerosene). The impacted cylinder is of diameter 0.2 m and contains 25 kg of liquid. Weber numbers and Reynolds numbers have been calculated using various impacting velocities.

Figure 4.8(a) and (b) show the variation of Weber number and Reynolds number as a function of impact velocity. From Figure 4.8(a) and (b) the Ohnesorge number,  $Oh = \sqrt{We}/Re$  is more for kerosene. Hence, the size of secondary droplets is less for kerosene.

Figure 4.9 shows the effect of surface tension on droplet formation with the help of predicted smallest droplets. Water with higher surface tension will form some larger droplets than that of kerosene because surface tension increases the amount of energy required to break up into the droplets. Further, studies have been carried for kerosene.

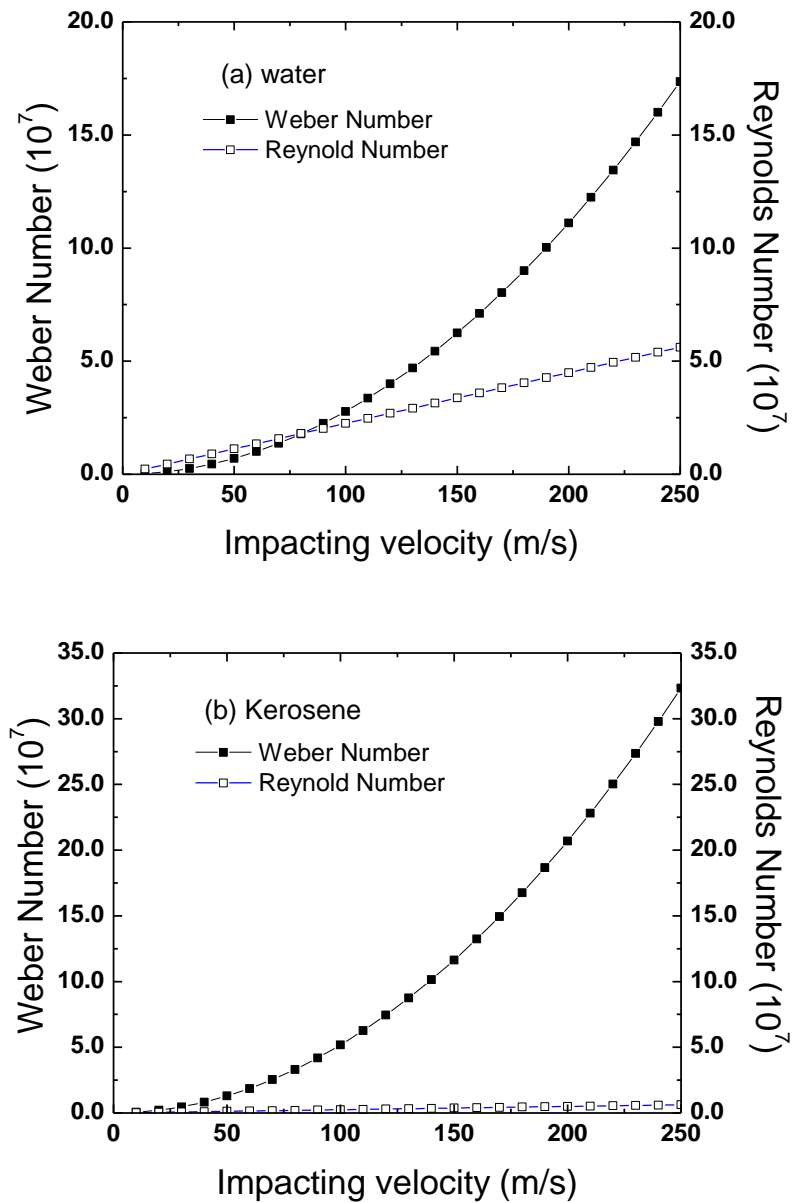


**Figure 4.8: Dimensionless numbers and impacting velocities for water (a) and kerosene (b)**

Figure 4.10(a) and (b) show the maximum, average and (Root Mean Square) r.m.s velocities of primary droplets and their velocity ratios with impacting velocity of the cylinder. It can be found that the maximum velocity of the droplet front is in the range of 2 to 2.5 times the impacting velocity. This agrees well with the initial discharge speed of the liquid front emerging from the ruptured cylinder reported by most of the researchers (Hostikka et al., 2015; Saarenheimo and Tuomala, 2009; Silde et al., 2011).

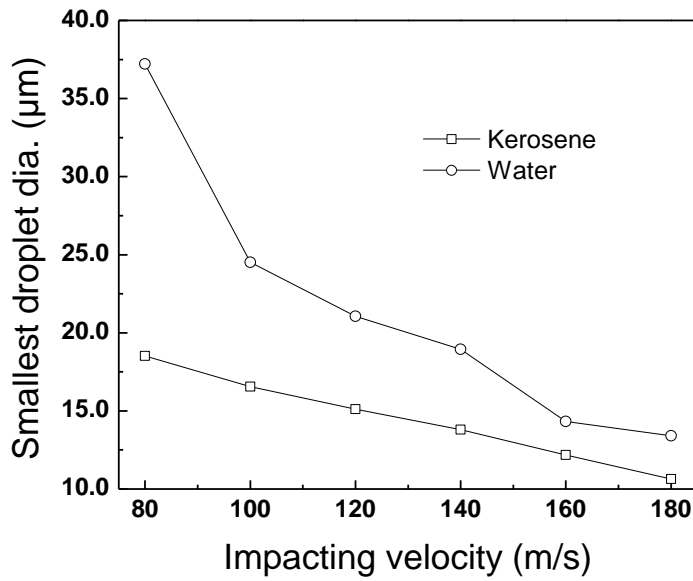


Figure 4.9: Smallest droplet size predicted in a spray

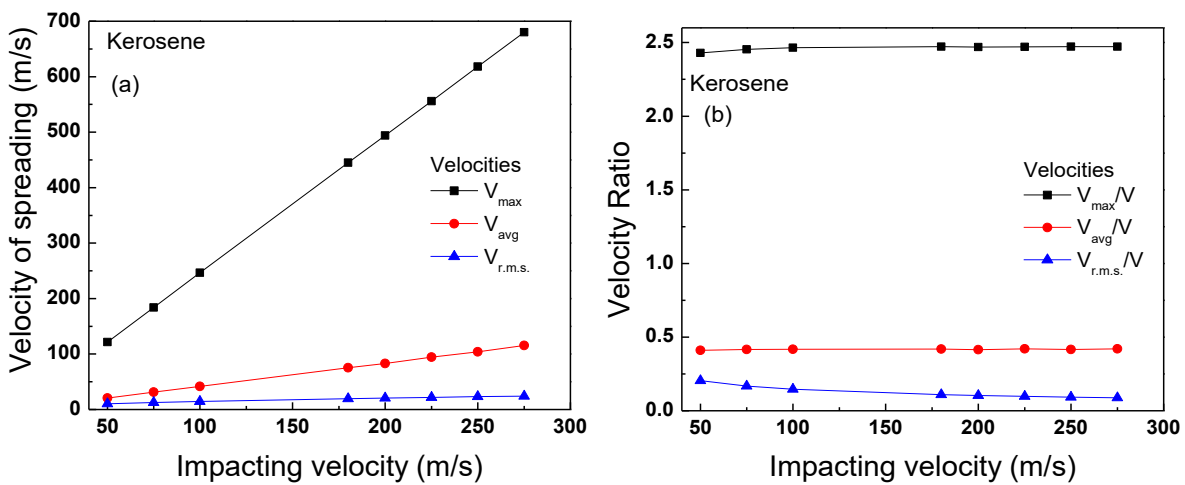
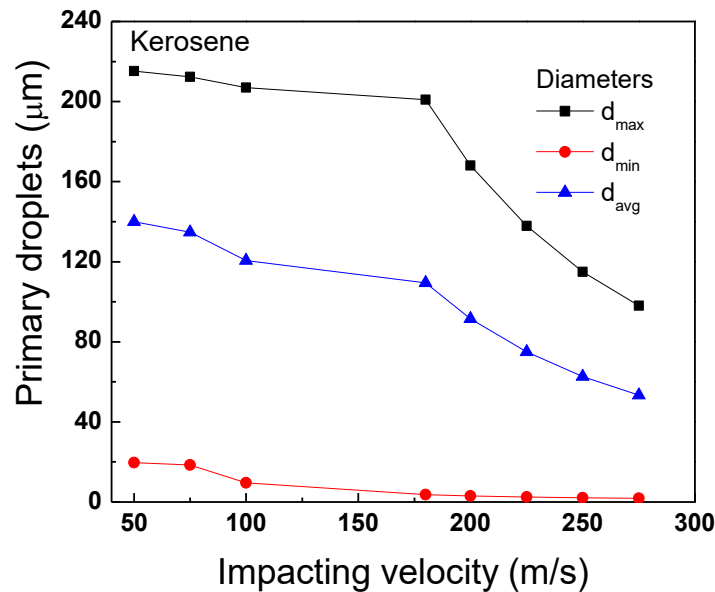


Figure 4.10: Initial spreading velocity (a) variation as a function of impact velocity (b) velocity ratio

Figure 4.11 shows the predicted maximum, minimum and average diameters after the primary breakup for various impacting velocities. The dynamic decrease in the droplet sizes for higher

velocities is due to increase in the aerodynamic force. These initial predicted primary droplets can be used as inputs for the CFD calculation of spray formation.



**Figure 4.11: Prediction of droplet size after the primary breakup**

Figure 4.12 shows the characteristics diameters ( $d_{10}$ ,  $d_{32}$  and  $d_{43}$ ) for the droplets after secondary breakup and evaporation. The larger difference between  $d_{10}$  and  $d_{32}$  shows the wider ranges of droplet sizes. There is significantly more splashing (formation of smaller size droplets) at higher impact velocity as can be seen in Figure 4.12. For the higher impacting velocities (~ above 180 m/s), the all the droplets lie in the narrow range of sizes. Droplet velocity is dependent on droplet size. Smaller drops may have a higher initial velocity, but velocity diminishes quickly. Larger droplets retain velocity for a longer duration, travel further, and may get rained out. Smaller droplets experience a smaller gravitational force and hence a smaller drag force. This is the reason for the formation of droplet cloud in the atmosphere.

Figure 4.13 shows the percentage of evaporation calculated using equation 4.25. It can be seen that the evaporation is more for higher impact velocity. The relative velocity between droplet

and gas determines the convective effects. The liquid evaporates rapidly for the higher velocity, which gives the reason for the flashing of liquids with small quantity.

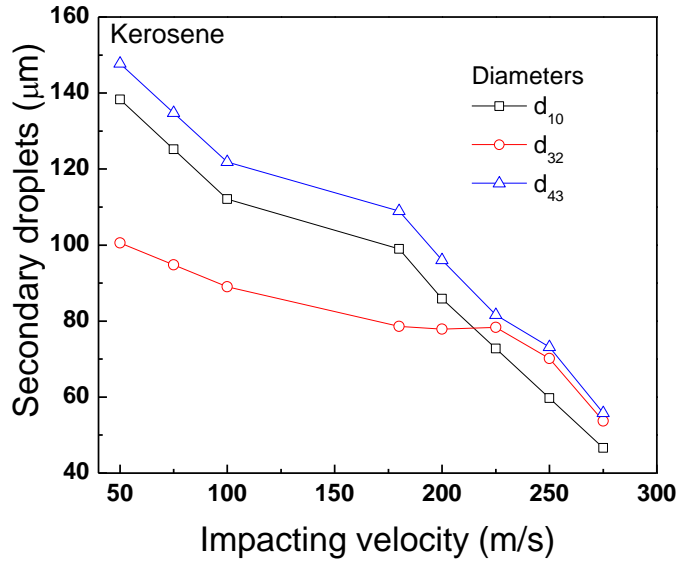


Figure 4.12: Prediction of final droplet size after secondary breakup and evaporation

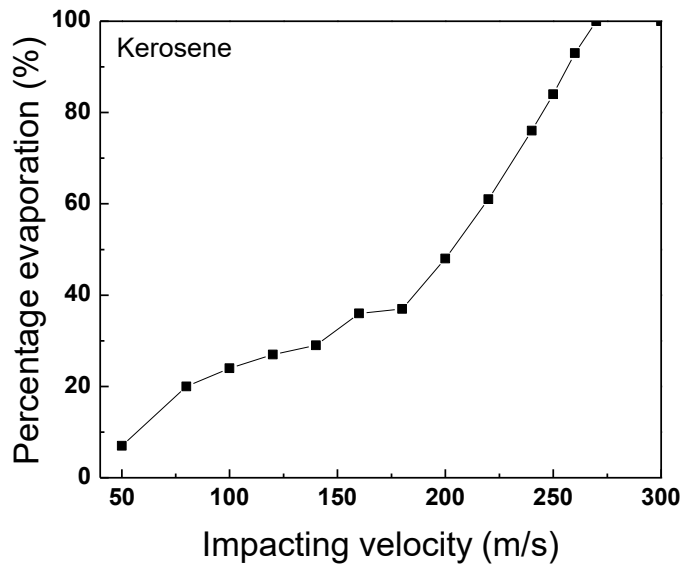
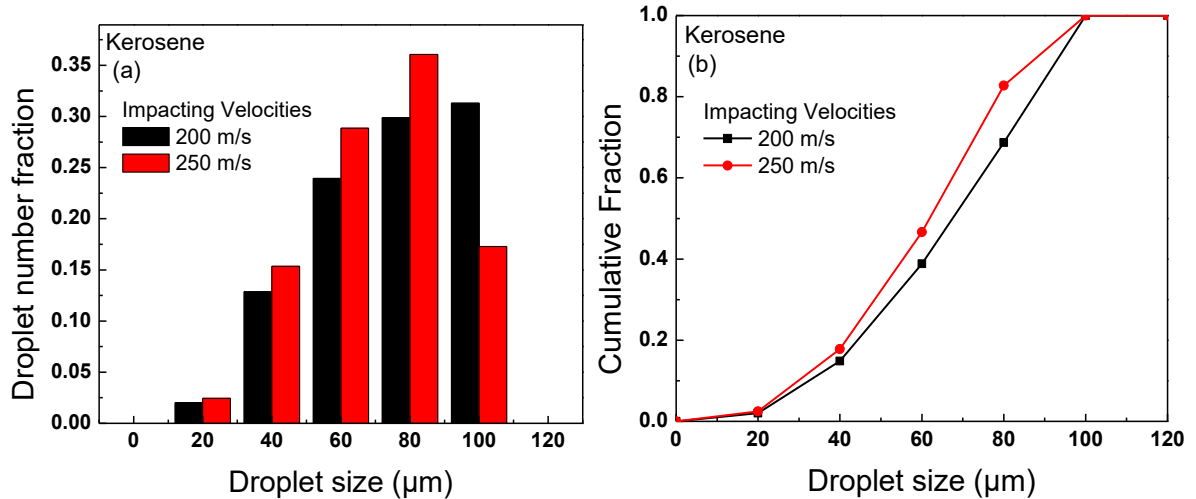


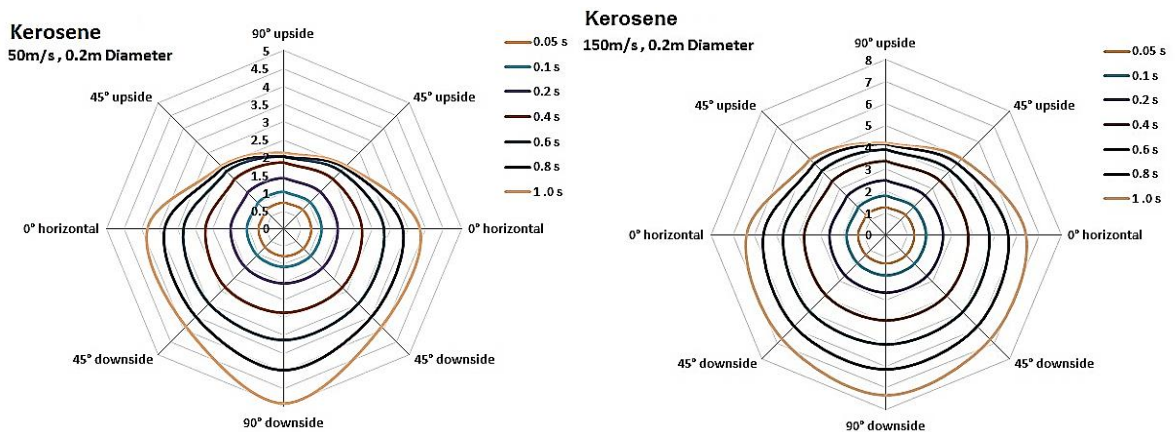
Figure 4.13: Percentage evaporation of kerosene

Figure 4.14 (a) shows the number based droplet size distribution at each diameter intervals. The cumulative fraction of droplets size is depicted in Figure 4.14 (b). Around 80% droplets are below the 80 µm size for impact velocity of 250 m/s while in case of 200 m/s velocity is 65%.



**Figure 4.14: Predicted Droplet distribution (a) droplet number fraction and (b) cumulative fraction**

Figure 4.15 show instantaneous position of spray fronts. The momentum exchange between the liquid and the continuous phase is the influence of the drag force and the gravitational force. Nearly circular pattern is observed for initial time spans, as inertial force is more dominant. The non-circular spray front is observed for both 50m/s and 150 m/s with time due to more effect of gravitational force.



**Figure 4.15: Transient positions of droplet front for impact velocity of 50 and 150 m/s**

## 4.6. Computational Fluid Dynamics (CFD)

The simulations are carried out using interFOAM CFD code based on OpenFOAM software packages. The interFOAM is a transient solver for isothermal and immiscible fluids using an interface capturing technique based a modified Volume of Fluid (VOF) approach first introduced by Hirt and Nichols (1981). Two Dimensional computational domain is selected to trace the dispersion of liquid slug impact on stationary wall.

### 4.6.1. Computational Domain

The geometry considered for analysis is having domain size of 2 m by 2 m with equal mesh spacing of 0.05 m in all the directions (see Figure 4.16). The liquid (water) slug used in model simulation is introduced at the centre of geometry (inlet boundary shown in Figure 4.16). The hydraulic diameter of inlet is taken as 0.2 m, as diameter of impacting-cylinder mentioned in the experiments by Hostikka et al. (2015).

### 4.6.2. Initial and Boundary conditions

The inlet velocity of 30 m/s is set in the horizontal X direction. As soon as slug mass of 10 kg enters the computational domain, velocity is ramped down to zero. All sides of the domain behave as open atmosphere (pressure outlet boundaries), in which flow across the boundary of the domain is allowed. At the wall, no-slip boundary condition is employed. In this analysis, stagnant Air is used as a continuous phase (secondary phase).The standard k- $\epsilon$  turbulent flow models is incorporated. A summary of the boundary conditions used for all simulations are shown in Figure 4.16.

#### ***Relevant Numerical Methods:***

Euler model with the surface tension of water of 0.072 N/m (Pan et al., 2009) is used during

the early time to simulate the continuous fluid flow during impact and to predict ejection velocity time history. To achieve a converged solution, an adjustable time step is used with an initial value of  $10^{-07}$ s in conjunction with a maximum Courant number for mean flow is limited to 0.5 and maximum interface courant number limit is set to 0.1. Standard numerical schemes for interFOAM are used for the velocity component advection term to improve the solution stability. Calculations for pressure-velocity coupling are performed using the PIMPLE (merged PISO-SIMPLE) algorithm with five corrector loops and interface compression is used for the determination of phase fraction to yield a sharp interface.

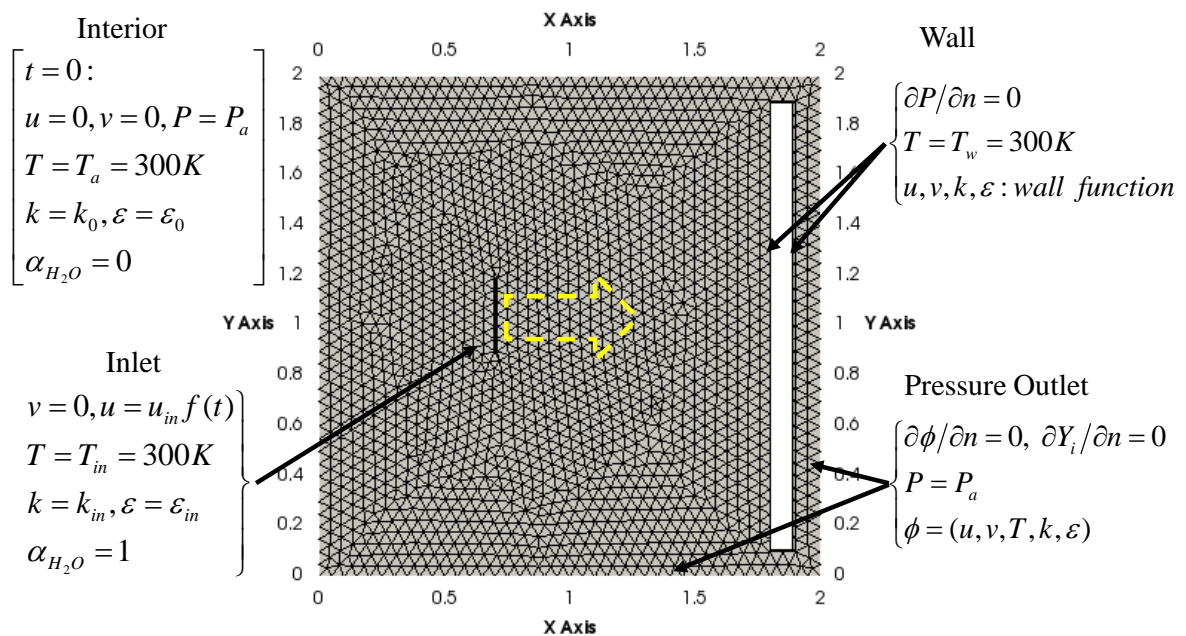


**Figure 4.16: Two Dimensional computational domain used for CFD simulation**

The grid independence study using three different mesh sizes has been performed. Figure 4.17 shows the contours liquid slug velocity at same time instance for different mesh sizes. It can be observed from Figure 4.17, grids finer than 3636 cells (0.05m spacing) did not show significant change in the results. Hence, in both the cases (3636 cells and 14244 cells), the

velocity of spreading front is found to be 33.4 m/s in for 0.002 s at location of 0.066 m in Y direction.

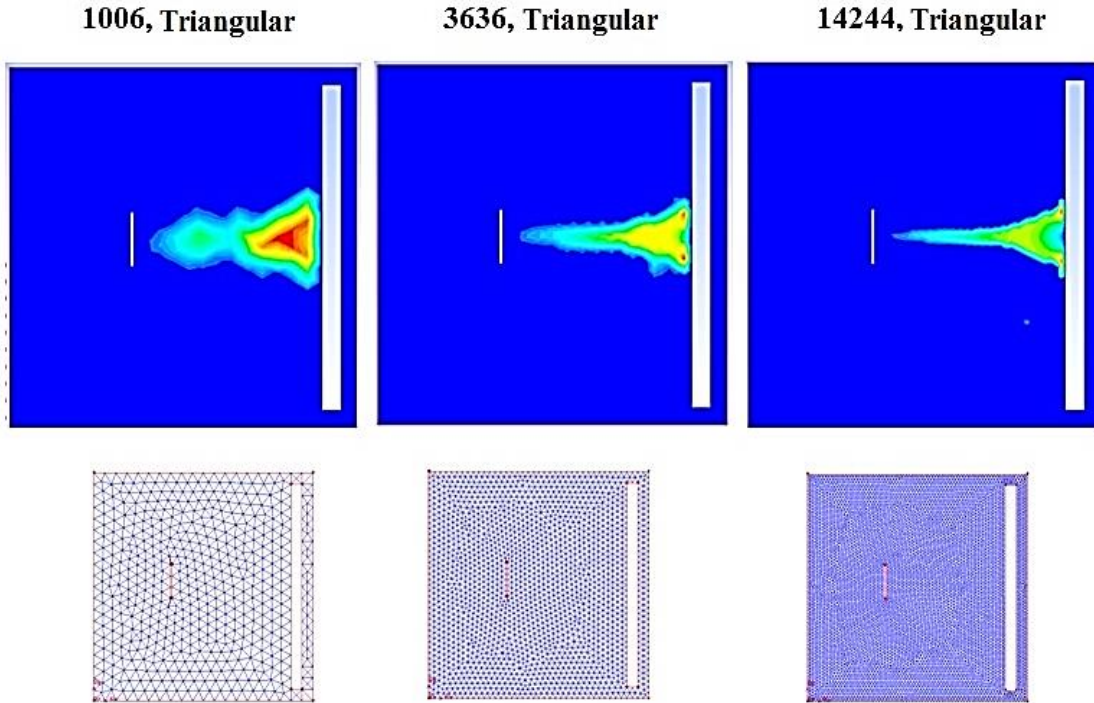


**Figure 4.17: Modeling of slug impact in an unsteady state with unstructured mesh with 1006 triangular, 3636 triangular and 14242 triangular elements**

### 4.6.3. CFD Results

Figure 4.18 shows the selected time frames from the simulation. The time series demonstrate the "pressure built-up" on the wall and speed of wavefront. The modelling effort for the water dispersion dynamics gives the favourable results when they are compared with mathematical model given in section 4.2. Figure 4.19 shows the comparison of the velocity of the wavefront from mathematical model and CFD, for impact of 10 kg mass of water with varying slug impact velocity of 30 m/s for the various time stages after impact. Initial discharge speed of the liquid front emerging from impacted mass is much higher than impact velocity but the propagation speed of wavefront decreases rapidly with increasing time. Also from the Figure 4.19, it is seen

that initial velocity predicted using CFD is quite lower than predicted by the mathematical model because the "wall adhesion" was on during the simulation.

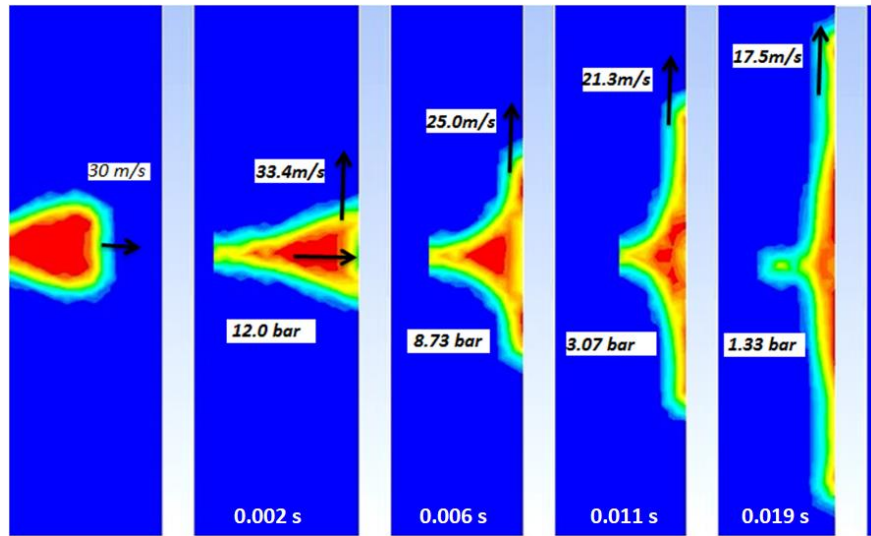


Figure 4.18. Time series of the impact of a slug of water from CFD model

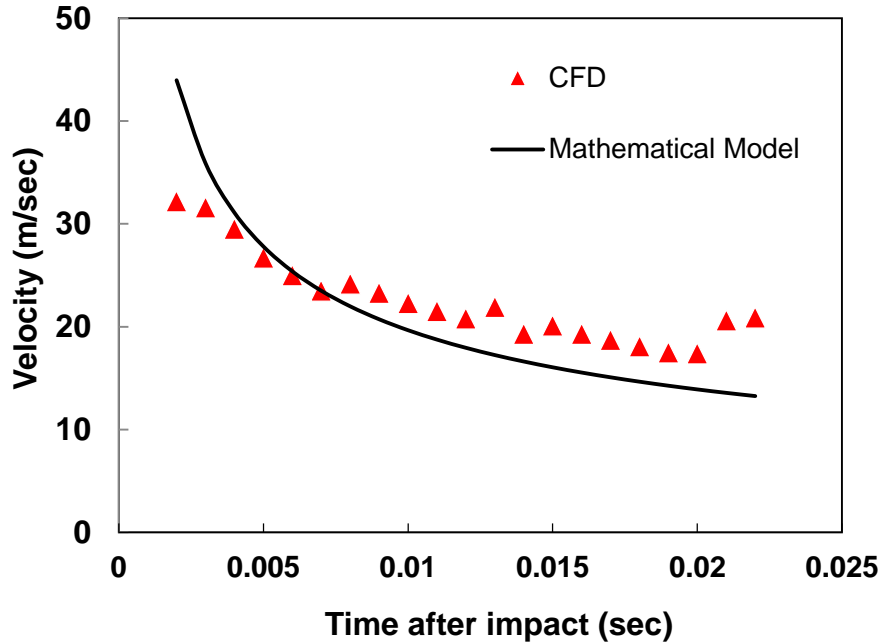


Figure 4.19. The plot of CFD velocity results with a mathematical model

## 4.7. Closure

In this chapter, a mathematical model is developed to investigate the transient behaviour of liquid slug emerging out of the impacting vessel filled with liquid. The model has been validated with experimental data available in the literature (Hostikka et al., 2015). Parametric studies are also performed to examine the effect of impacting velocities on primary droplets, secondary droplets, spreading velocities and evaporation using different fluids. The data of droplet cloud formation (droplet sizes distribution and spreading velocities) obtained in calculation has been used as boundary and initial condition for CFD analysis performed in **Chapters 5** and **6** using dynamic spray method.

# CHAPTER 5: STUDIES ON FIREBALL FORMATION USING FUEL VAPOUR AND DYNAMIC SPRAY AT INLET

---

## 5.1. Introduction

In the aircraft crashes, it is seen that the fuel in the wings is dispersed during the impact. Fuel spills out in a large amount from the broken tanks and gets atomized to form a droplet cloud. The remaining fuel is ejected in the form of liquid chunks or may get leaked from the broken tanks. Due to the availability of heat source either from an electronic circuit (broken) or from hot jet turbine parts, the vaporized portion of dispersed fuel initiates the combustion. A large quantity of the fuel engulfs within the fire in very short duration resulting in a fireball formation.

The CFD codes are used to simulate the expansion of fireball and the evaluation of the detailed temperature distribution. Rehm et al. (2003) presented an analytical model to study the initial expansion of the fireballs generated in the attack on the World Trade Centre (WTC) south tower. Luther and Müller (2009) demonstrated Fire Dynamic Simulator (FDS) tool to simulate the fireball caused by the crash of a commercial airliner upon the Nuclear Power Plant (NPP) structures using 90 ton of kerosene in vapour form.

To deliberate the detailed study of fuel dispersion, combustion of fuel, fireball formation, heat radiation and the thermal hazard from the fireball, the evolution of fireball has been modelled in Computational Fluid Dynamics (CFD) using vapour fuel inlet and dynamic fuel spray methods. The methods are explained in the following subsections,

- Vapour fuel inlet: Fuel is injected into the computational domain in gaseous form through an inlet. Inlet area, velocity and direction of flow are decided based on the case being

simulated. In this method, as fuel is available in a gaseous form directly, combustion occurs based on the availability of oxygen.

- **Dynamic fuel spray:** Fuel is injected into the domain, through an inlet, in the form of droplets with a given size distribution, velocity and direction. These characteristics of droplet spray are determined from the model as mentioned earlier in **Chapter4**. In this method, the evaporation of droplets and consequent combustion (based on the availability of oxygen) are simulated in the domain.

In both the methods described above, the injection of fuel will be stopped as soon as the required mass of fuel (the mass of fuel engulfed into a fireball, determined by the model presented in **Chapter4** and enters the domain.

In this chapter, fireball arising from the aircraft crash has been studied and analysed using two methods. In the first method, the fuel is injected in complete vapour form and in the second method, fuel is injected as a dynamic fuel spray. The input to analyse fireball by dynamic spray model has been obtained from the droplet spray model reported earlier in **Chapter 4**.

## **5.2. Case study: aircraft Boeing 747-400 accident**

To understand aircraft impact and dispersion of fuel, an aircraft accident case has been considered. On 29<sup>th</sup> April 2013, the Boeing 747-400 aircraft of National Airlines N949CA, Afghanistan departed on a cargo flight N8-102 from Bagram to Dubai, UAE with 7 crew and cargo consisting of 5 military vehicles NTSB (2015). The aircraft crashed shortly after take-off from the ground at a high vertical speed, causing an explosion and the resulting fireball erupted into flames. Aircraft stalled due to shifting of vehicles' load. All seven crew-members were killed in this accident. The plane took on 53 tons of fuel at Bagram before taking off for

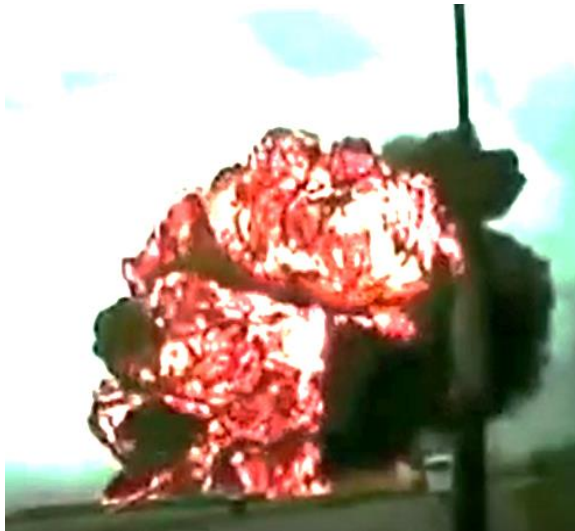
Dubai (The Guardian, 2015). Figure 5.1(a)-(d) show the images captured from video footage. In the initial duration, two separate local flame areas were observed, which further grew as a single fireball.



**(a) Impact of aircraft (Boeing 747) to the ground**



**(b) Fuel spreading with fire**



**(c) Formation of spherical fireball**



**(d) After-burning dispersion of fireball into atmosphere**

**Figure 5.1: Images captured from video footage of Boeing 747-400 crash (Daily Mail, 2013).**

### 5.3. Analysis for calculating fuel dispersion

For determining the mass of fuel engulfed in the fireball and inlet conditions of the fuel, which will be used to size the computational domain and as inputs for CFD model respectively, a fuel dispersion analysis has been performed. In the Boeing 747-400, fuel is stored in several locations, mainly in the wings but also in the hull of aircraft as shown in Figure 5.2. The droplet cloud was formed as a result of fuel tank rupture after the aircraft crash (impact angle was  $39^\circ$  from horizontal). The model mentioned in Chapter-4 has been used to analyse droplet cloud formed because of fuel tank rupture after the impact of a projectile. The inputs used for this model are given in Table 5.1. The fuel tanks have been approximated by an equivalent cylindrical tank with diameter and length calculated based on wing dimensions as given in Table 5.1.

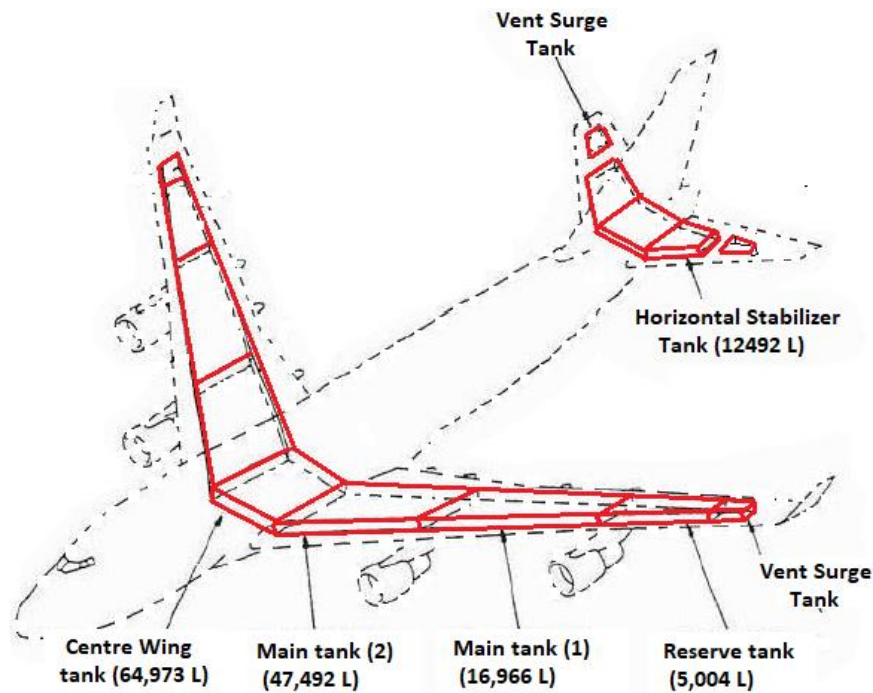


Figure 5.2: location of fuel tanks in Boeing 747-400

**Table 5.1: Inputs to calculate fuel dispersion using model mentioned in Chapter-4.**

<b>Parameter</b>	<b>Symbol</b>	<b>Value</b>	<b>Description</b>
Velocity of impact	$V_n$	87.97 m/s	NTSB (2015)
Mass of fuel	$M$	~53 tons	NTSB (2015)
The diameter of the equivalent cylindrical tank	$D_{H, Cyl}$	5.55 m	4 x frontal cross-section of the wing/perimeter of the wing
Length of equivalent cylindrical tank	$L$	2.74 m	Calculated from 53 ton of kerosene, which was available at the time of aircraft crash.
Energy absorbed by the wing during crushing	$E_{crushing}$	20 MJ	Energy absorbed by wing tank during crushing (Wierzbicki & Hendry-brogan, 2002)

### 5.3.1. Vapor fuel inlet method

The inlet velocity and direction of fuel vapour have been determined from the model explained in **Chapter 4**, as 130 m/s and 129° (from horizontal) respectively. Mass of fuel entrained in fireball depends on the fraction of fuel evaporated. The mass fraction of fuel evaporated in fireball has been estimated as 0.22 using the model expressed in **Chapter-4**. The fraction of mass engulfed in fireball has been estimated as 63% of total fuel available (i.e.  $0.22/0.35=0.63$  of available mass, i.e.  $0.63 \times 53 \text{ ton} = 33.06 \text{ ton}$ ).

### 5.3.2. Dynamic spray method

To determine the characteristics of droplet spray like size distribution and velocity of injection, the model explained in **Chapter 4** has been employed for the case under study. The results of the analysis are summarized in Table 5.2. The maximum velocity of droplet spray emerging out has been calculated and found to be 130 m/s (which is approximately 1.5 times the impact velocity of aircraft). The predicted sizes of the droplets in the droplet cloud are in the range of 30-225  $\mu\text{m}$  with Sauter Mean Diameter ( $D_{32}$ ) of 168  $\mu\text{m}$ . The maximum numbers of the droplet

are smaller than 250  $\mu\text{m}$ . Figure 5.3 shows the number based droplet distribution at each diameter interval. The direction of injection is taken perpendicular to the angle of impact of crashing aircraft.

**Table 5.2: Results of fuel dispersion modelling (for Dynamic spray method)**

Sr. No.	Parameters	Symbol	Value
1	Characteristic diameter	$D_{32}$	168.62 $\mu\text{m}$
		$D_{max}$	222.67 $\mu\text{m}$
		$D_{min}$	31.41 $\mu\text{m}$
2	Characteristic velocity	$V_{max}$	129.45 m/s
		$V_{r.m.s.}$	10.57 m/s
		$V_{avg}$	21.83 m/s

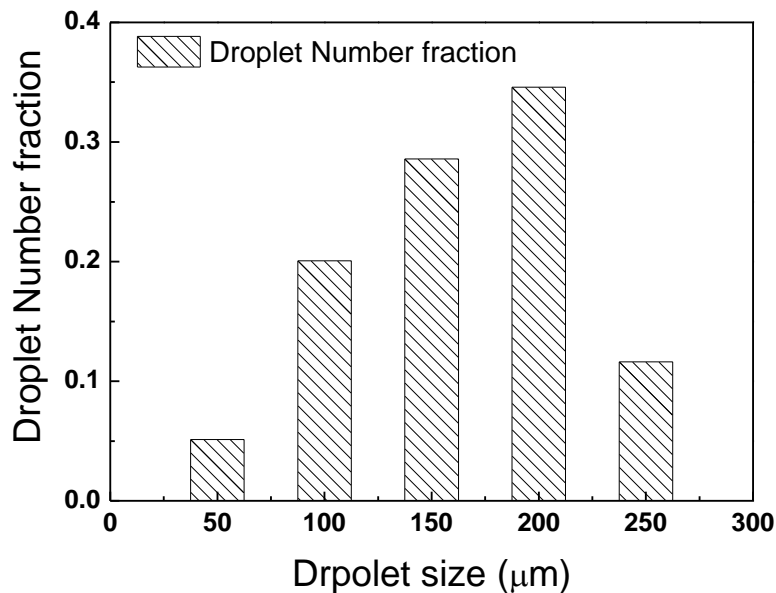


**Figure 5.3: Predicted droplet distribution**

### 5.4. Computational domain

Figure 5.4 shows the three-dimensional rectangular domain selected to analyse the fireball using both approaches of dynamic spray and vapour inlet. The sizes of the domain have been selected as 200m×200m×300m based on preliminary calculations of maximum diameter and the lifting height of fireball (as shown in Table 5.3).The influence of boundaries on the evolution of fireball is checked so that no significant velocities are formed at the boundaries. The maximum fireball diameter and the duration are calculated using equation (2.3) mentioned in **Chapter 2**. The constants for most commonly used correlations available in the literature (Abbasi and Abbasi, 2007) are considered.

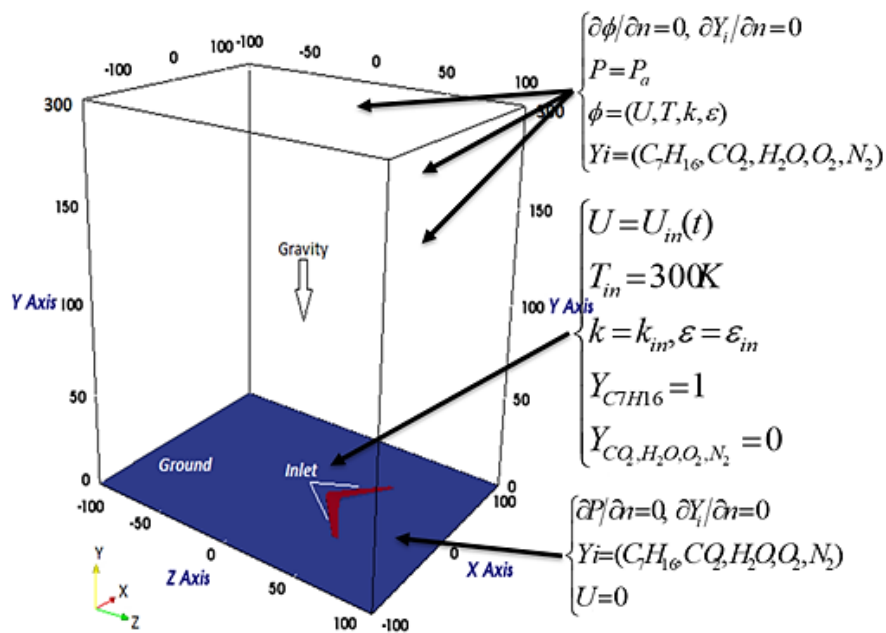


**Figure 5.4: Schematic of the computational domain showing the fuel inlet at y=0**

Table 5.3 shows the estimated maximum diameter, duration and lifting height of fireball centre. It also shows the observed values of maximum diameter and lifting height obtained from the video footage of the accident NTSB (2015). Fuel inlet is calculated using actual dimensions of

the wing and located at the centre of the bottom plane (i.e. ground,  $XZ$  plane,  $y=0$ ). The inlet face area is taken as wing area.

**Table 5.3: Correlations (Abbasi and Abbasi, 2007) for fireball with ~33 tons of kerosene**

Parameter	Correlation	Calculated	Observed
Fuel mass	$M_{fuel}$	33063 kg	-
Maximum diameter	$D_{max} = 5.8M_{fuel}^{1/3}$	186.15 m	175 m
lifting height	$h = 0.75D_{max}$	140.62 m	145 m at 10 s
Duration of fireball	$t_{max} = 2.6M_{fuel}^{1/6}$	14.7s	-

#### 5.4.1. Initial and Boundary Conditions

The sides and top of the domain behave as an open atmosphere, in which free flow across the boundary of the domain is allowed. At  $y=0$ , the bottom plane (ground) of the domain behaves as the wall where the no-slip boundary condition has been employed. For the inlet boundary, the conditions determined in sections 5.1.1 (for vapour fuel inlet method) and 5.1.2 (for dynamic fuel spray method) have been used. Initially, stagnant air at 300 K has been considered as domain fluid. Figure 5.4 show the details of the boundary conditions applied to the computation domain.

#### 5.4.2. Numerical Method

The discretized momentum, species transport and energy equations are solved by the preconditioned bi-conjugated gradient method (PBiCG). Generalized geometric-algebraic multi-grid method (GAMG) is employed to solve the discretized pressure equation originated from the application of momentum interpolation to the continuity equation. This method is also

used to solve the discretized turbulent energy and the radiative transfer equations. The second order backward differentiation scheme is employed for temporal discretization. The diffusive terms and the gradients are discretized using central differencing scheme. Spatial derivatives are estimated on a rectangular grid with all quantities assigned to the cell centre and velocities linearly interpolated to the cell faces. The FireFOAM employs a PIMPLE (PISO+SIMPLE) algorithm for pressure-velocity coupling.

Large Eddy Simulation (LES) is solved in form of one equation with eddy coefficient of 0.07. The energy equation is solved for sensible enthalpy. Temperature dependencies of the enthalpies and heat capacities of individual species have been taken into account. The enthalpies of formation of various chemical species are available in NIST-JANAF Thermochemical Tables (Chase, 1998) and can be used in the most combustion simulation codes in the form of the standard library.

## **5.5. Simulation Results**

A grid size of 1 m has been used to simulate the fireball associated with aircraft impact. This states that eddies of size above 1 m have been resolved during the simulations. The simulations are set to have an adjustable time step such that the CFL number would fluctuate around 0.5. Analyses have been performed up to a physical time of 10 s for both methods and data have been collected for every 0.01 s during the CFD simulation.

### **5.5.1. Vapor inlet method**

The fireball formation starts as kerosene fuel enters into the domain. Figure 5.5 shows the evolution of fireball at 2, 4, 6 and 8 s. It can be observed from Figure 5.5 that fuel burns at a local area, which is similar to that observed from video footage (see Figure 5.1(b)). This may be attributed to the separation of the flame due vortex created by fuel flow. In the fireball

evolution, it can also be observed that the local area, which is separated from the main fireball burnt earlier due to limited availability of fuel. The local flame cooled faster and dispersed in the atmosphere (as seen for 4, 6 and 8 s in Figure 5.5).

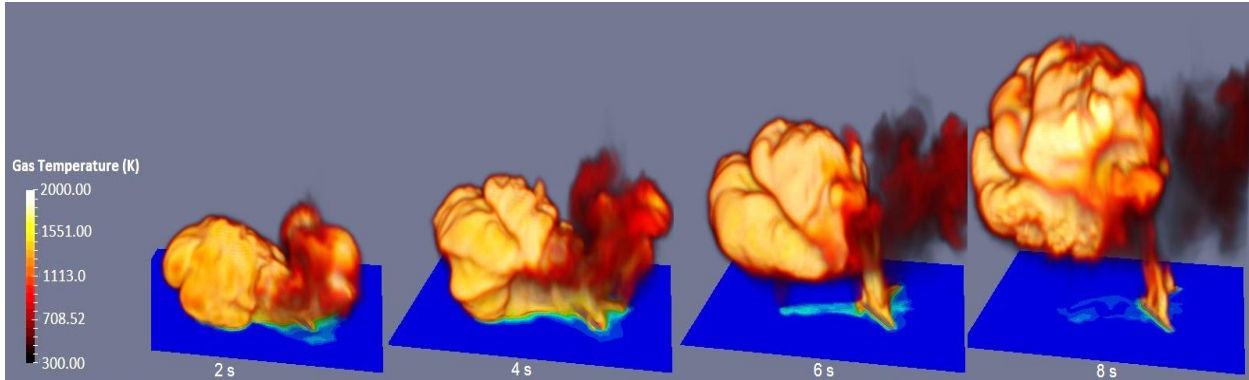


**Figure 5.5: Fireball evolution during 2, 4, 6 and 8 s in vapour inlet approach**

### 5.5.2. Dynamic spray method

The combustion starts as the fuel droplets enter and evaporate in the computational domain. Figure 5.6 shows a sequence of spatial distribution of evaporating droplet diameters of fuel in the dynamic spray.

Figure 5.7 shows the evolution of fireball formed from dynamic spray model. It can be observed from Figure 5.7 that once the fireball starts forming; the droplets in the surrounding evaporate by receiving energy from hot gas nearby. The fireball shows the similarities in behaviour with that of the accident. The outer surface of the fireball is dominated by Taylor instabilities, which greatly enhance the burning at the surface. This can be the reason of self-sustaining turbulent combustion. It can be seen from Figure 5.7 that temperature of fireball at the outer surface decreases rapidly. This may be due to heat loss from the fireball to the surroundings.

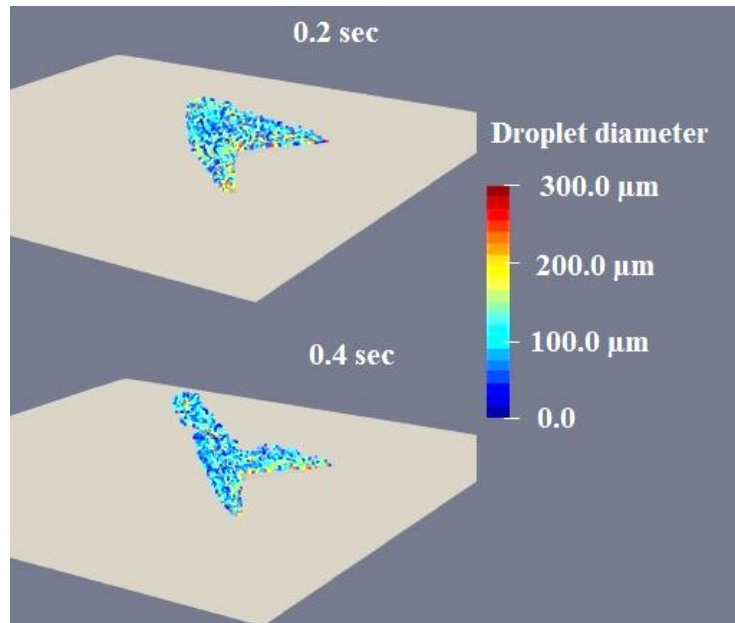


**Figure 5.6: Droplet spray from aircraft wings**

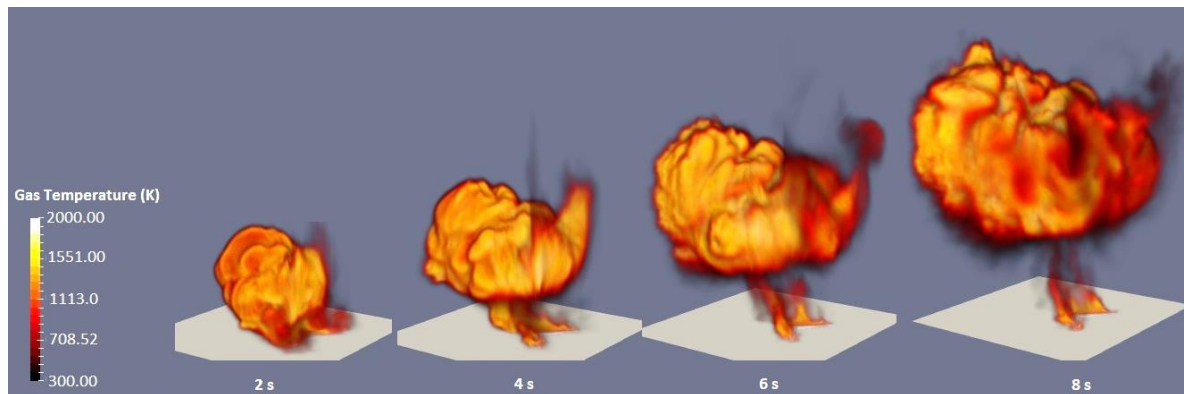


**Figure 5.7: Evolution of fireball during 2, 4, 6 and 8 s occasioned from dynamic spray**

### **5.5.3. Comparison of models:**

Figure 5.8 shows the comparison of flame fronts obtained from CFD simulations with those observed from the accident. The fireball modelled with dynamic spray shows the smaller diameter in the initial period. The fireball with dynamic spray contains liquid fuel droplets, which take time to evaporate and participate in the combustion. Hence, on the timescale, this

shows a lesser expansion. Once all the fuel in liquid form evaporates, the fireball from both simulations shows nearly the same diameter.

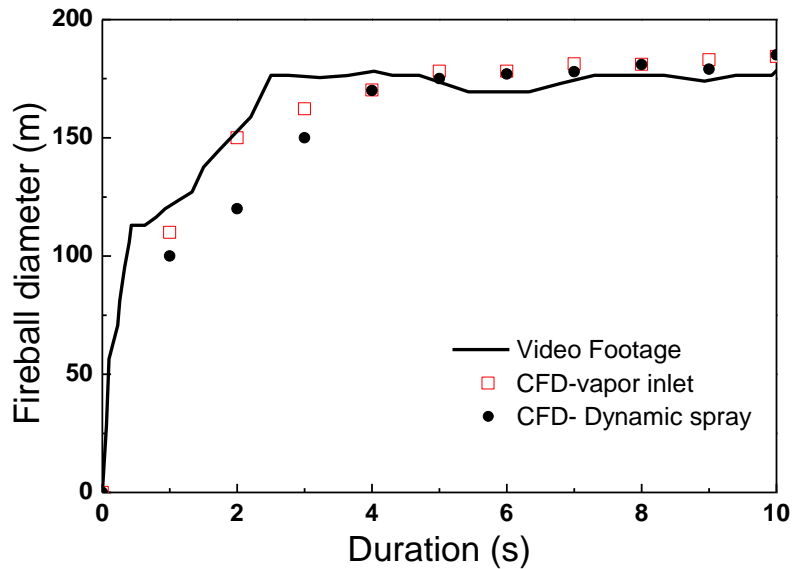


**Figure 5.8 : Comparison of fireball diameter from video footage and CFD simulations**

Figure 5.9 shows the comparison of CFD predictions with an accidental data, for the lifting of fireball centre from the ground. In the initial duration, the fireballs from CFD models lift earlier, because of initial momentum. The fireball associated with dynamic spray model lifts slower as compared to that formed from injecting vapour at the inlet. This is due to the initial momentum of fuel and buoyancy effect during the lifting of the fireball. Both the fireball models show similar behaviour when all the droplet fuel evaporates. The behaviour of a fireball in terms of shape, size and lifting in the CFD simulations are found to be in good agreement with that observed in video footage.

The fireball characteristic is measured using global Heat Released Rate (HRR) from the fireball. Figure 5.10 shows the HRR profiles from the fireball obtained from dynamic spray and vapour inlet models. The increase in HRR with time in both cases is attributed to entrainment and mixing of air from the surrounding. After that, HRR reduces due to unavailability of fuel

for sustaining combustion. The extended view in Figure 5.10 shows HRR profile in the initial small period. The peak value of HRR is higher for vapour inlet case as can be observed in Figure 5.10. This signifies more “flashing” of fireball with vapour inlet method.

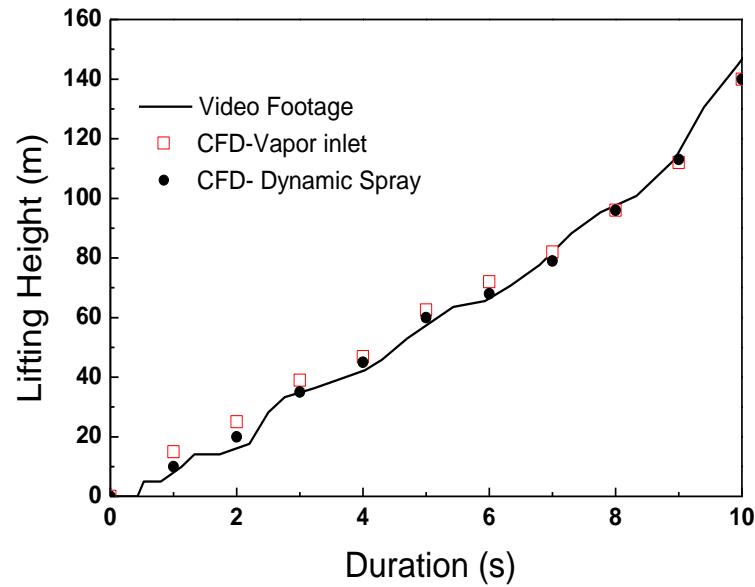


**Figure 5.9: Comparison of lifting height of fireball centre using video footage and CFD simulation**

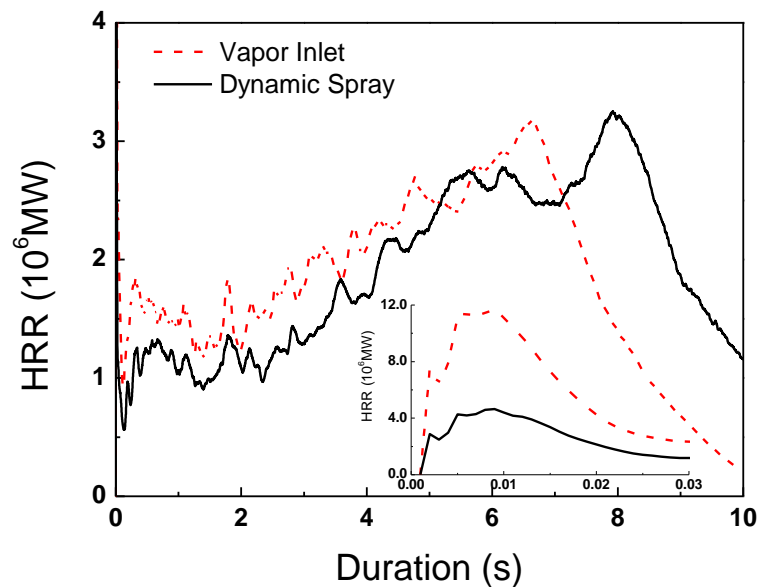


**Figure 5.10: comparison of heat release rate (HRR) during the evolution of fireball obtained from dynamic spray and vapour inlet methods**

#### 5.5.4. Local Parameter measurements

To analyse the evaluation of fireball and thermal hazard due to radiation and fireball engulfment, the various parameters have been calculated at different locations on the ground (XZ plane at  $y=0$ ). The locations at 0, 10, 20, 30 and 40 m away from the centre of wings (inlet in the computational domain) in the Z directions have been considered. Figure 5.11 shows the locations selected for analysis.

Figure 5.12 and 5.13 show the time-varying mass fraction of fuel and  $CO_2$  at ground locations. In Figure 5.12, fireball with dynamic spray model shows the higher fuel mass fraction on the ground for a longer duration. Due to the higher density of droplet, the fuel remains on the ground for a longer duration until it evaporates and takes part in combustion.

Figure 5.13 shows the higher value of  $CO_2$  mass fraction for the initial duration in case of fireball with vapour inlet. This may be due to good mixing and combustion. This can also be attributed to the existence of the stem of the fireball for a longer duration.

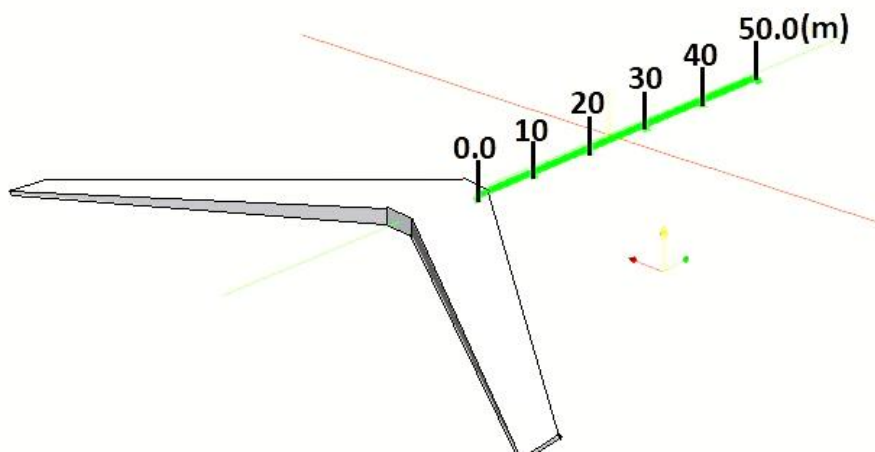


**Figure 5.11: The location of probes for calculation of various properties**

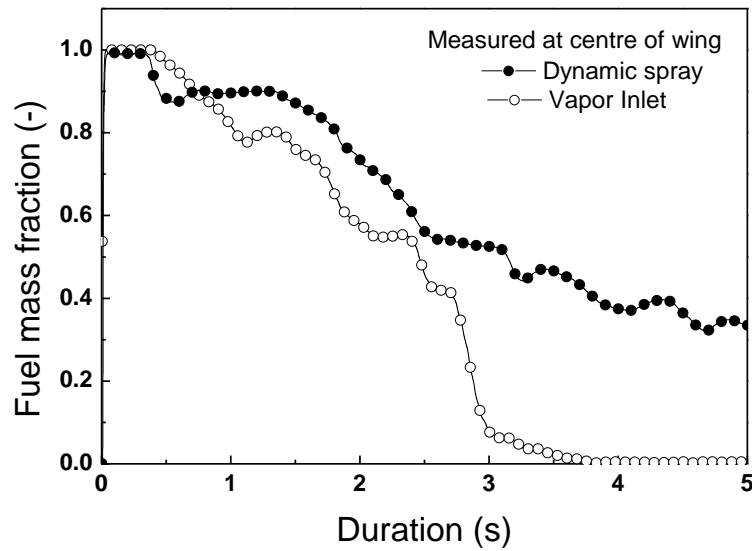


Figure 5.12: Fuel mass fraction plotted along the Z axis (centre of wings, 0 m away)

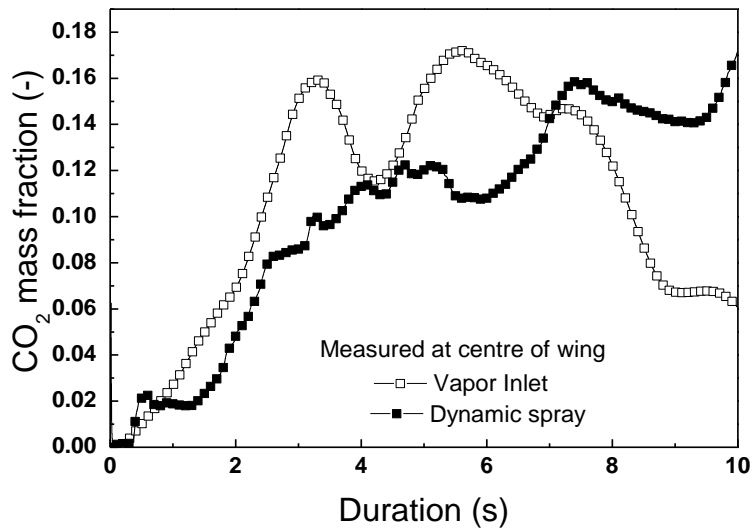
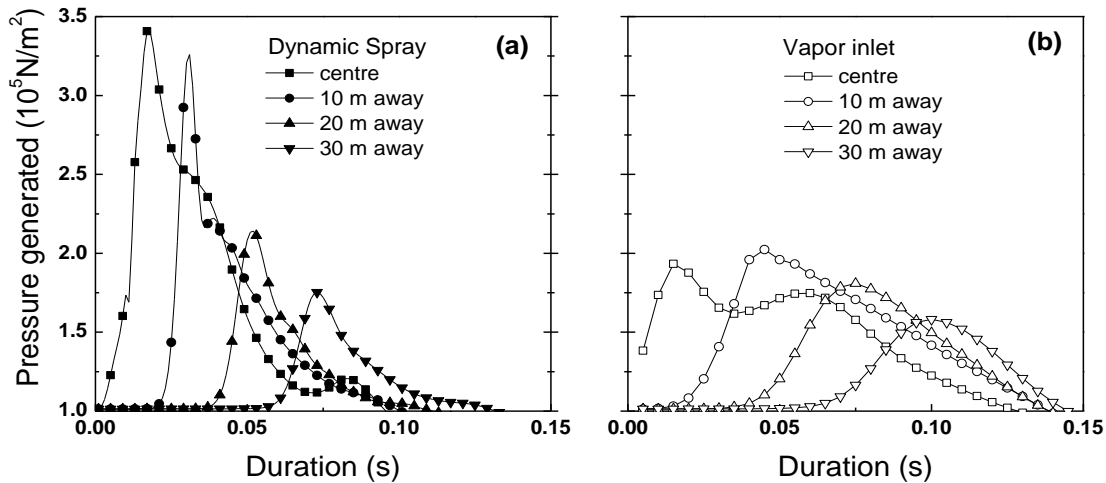


Figure 5.13  $CO_2$  mass fraction calculated at the centre of wings

Figure 5.14 demonstrates the pressure calculated at the locations, 0 (centre), 10, 20 and 30 m away from the wings. The pressure is generated due to the expansion of product gases. Higher values have been observed in case of fireball with the dynamic spray method. This is due to the evaporation of spray droplets, which lead to volume expansion and exert more pressure in the gaseous cloud.



**Figure 5.14: Pressure Calculated at locations 0 (centre), 10, 20 and 30 m for (a) dynamic spray and (b) vapour inlet methods**

Figure 5.15 shows the velocity traced at the probe locations of 0 m (centre) and 20 m away from the wings during fireball evolution. The increase in velocity is due to sudden combustion and expansion of product gases. The reduction in the velocity at locations away from the centre is due to the loss of momentum of flame fronts in expanding fireball due to atmospheric friction while the gases are expanding in a fireball. The velocity observed at the centre of wings in case of dynamic spray is smaller compared to vapour inlet case during the initial period of the fireball formation.

To analyse thermal hazard from fireball radiation, the time-averaged radiative flux is calculated at the locations 0, 10, 20, 30, 40 and 50 m away from the centre of wings. Figure 5.16 shows the higher values of radiative flux at all locations in case of the fireball from the vapour inlet method. The spreading and evaporating droplets may absorb the heat from the fireball during its evolution.

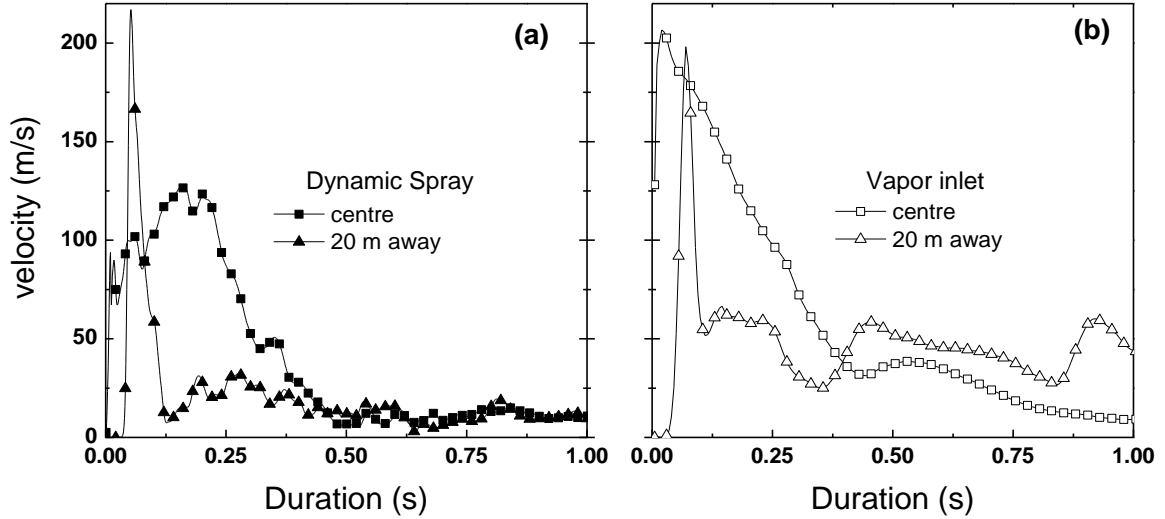


Figure 5.15: Velocity calculated at the locations 0 (centre) and 20 m for (a) dynamic spray, (b) vapour inlet approach

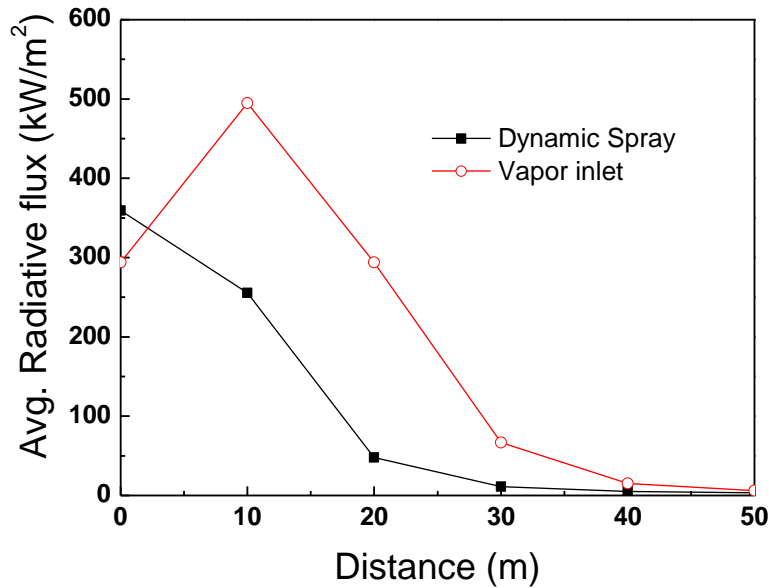


Figure 5.16: Average radiative flux calculated at the locations on the ground

The effect of thermal radiation and engulfment has been analysed using time-averaged temperature calculated at the locations 0, 10, 20, 30, 40 and 50 m away from the centre of wings. It can be observed from Figure 5.17 that at locations close to the source, the lower temperature has been predicted in case of dynamic spray model. This may be due to the

consumption of energy by the droplets for evaporation. Droplet spray may spread to these locations during the fireball evolution. The locations up to 20 m away from the centre may be critical (in terms of damage to structures and human fatality), as the time-averaged temperature is above 400 K during the fireball duration as obtained from both methods.

It has been found that both methods give similar predictions for fireball diameter and lifting height though other parameters like pressure developed, radioactive heat flux and time-averaged temperature are predicted differently. Experimental data for the above parameters would be required to derive a conclusion on both the methods.

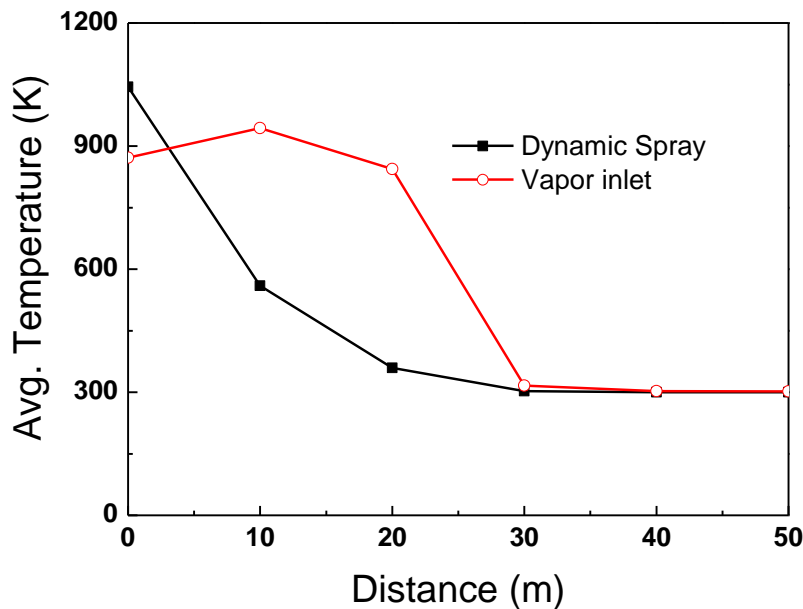


Figure 5.17: Time-averaged temperature of ground locations

## 5.6. Further studies with vapour inlet and dynamic spray methods

To study the effect of modelling approach on the prediction of the evolution of fireballs and corresponding heat release rate, further simulations have been performed using both Dynamic spray method and Vapour inlet method. Two cases with fuel mass of 20 ton and 80 ton have been considered to compare the results obtained from these methods. In both the cases, the

mass is released in the vertical direction with an inlet velocity of 100 m/s. The sizes of the domains for respective cases have been selected based on the maximum diameter of fireball and lifting height (calculated using **equation (2.3)** mentioned in **Chapter 2**). The diameter of the inlet is calculated for both the cases using the method mentioned by Makhviladze et al. (1997). Figure 5.18 shows the global heat release rate for fireballs with a fuel mass of 20 tons and 80 tons. It has been observed from the Figure 5.18 (a) and (b) that, fireballs with dynamic spray release heat slowly as droplet evaporation takes time.

Figure 5.19 shows the fireball diameters predicted using dynamic spray and vapour inlet method for the cases of 20 ton and 80 ton of fuel mass. The fireball modelled with dynamic spray shows a smaller diameter in the initial period of evolution. The fireball with dynamic spray contains liquid fuel droplets, which take time to evaporate and participate in the combustion. Hence, on the timescale, this shows a lesser expansion. Once all the fuel in liquid form evaporates, the fireball from both simulations shows nearly the same diameter.

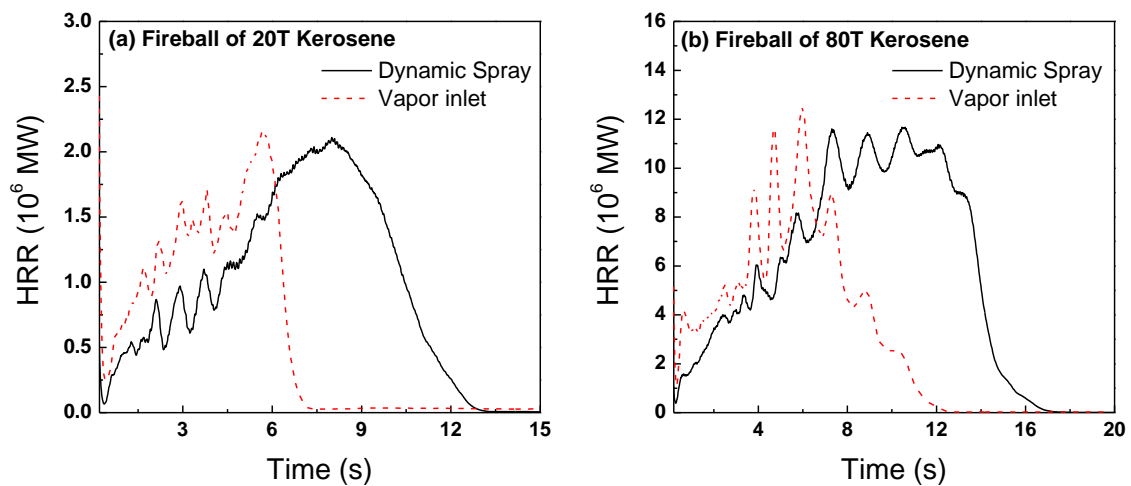


**Figure 5.18: Global Heat Release Rate (HRR) for fireballs with fuel mass of a) 20 ton and b) 80 ton**

Figure 5.20 depicts the average radiative heat flux calculated at various locations away from the centre, for both fireballs formed from the fuel mass of 20 tons and 80 tons. There is no significant change has been observed (Figure 5.20(a)) in average radiative flux values calculated by both the methods for the fireball with fuel mass of 20 tons. However, it can be observed (Figure 5.20(b)), for the fireball with fuel mass of 80 tons, that dynamic spray method predicts a lower average radiative flux. This may be due to consumption of heat by evaporating droplets.

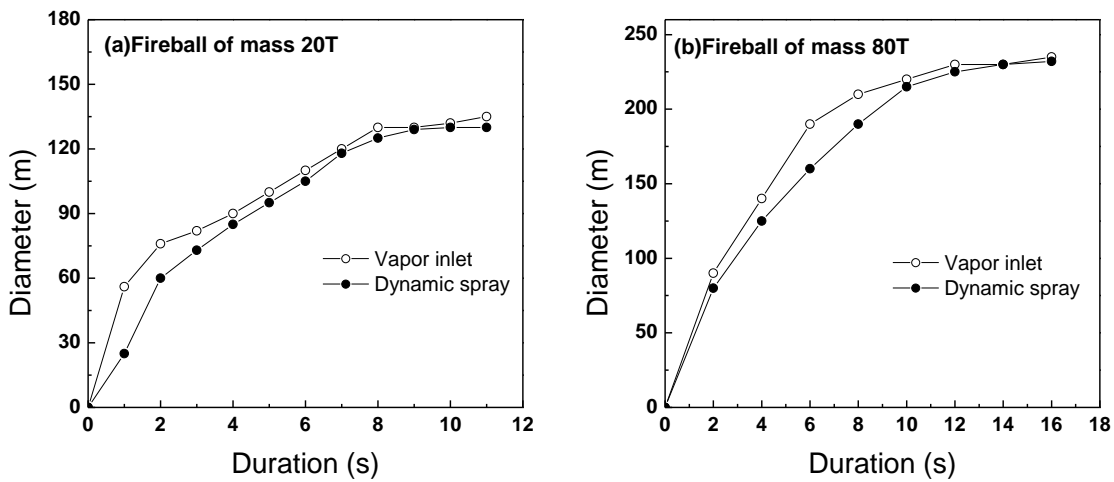


Figure 5.19: Fireball Diameters predicted using dynamic spray and vapour inlet method for fireball with fuel mass of (a) 20 ton and (b) 80 ton.

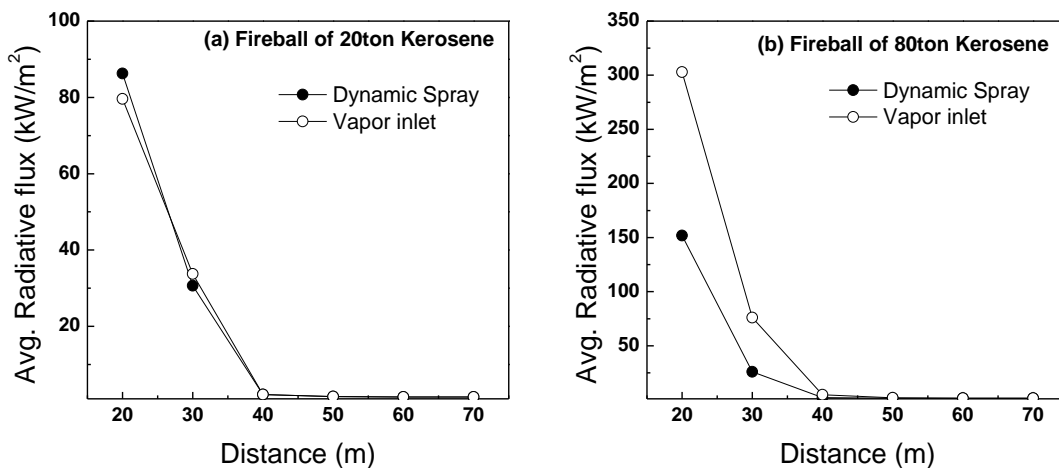


Figure 5.20: Average radiative flux calculated at the locations on ground calculated for fireballs with fuel mass of a) 20 ton and b) 80 ton

## 5.7. Closure

In this chapter, CFD analyses have been carried using CFD software, OpenFOAM in the three-dimensional domain to study the evolution of fireball formed from dispersed fuel in an accident case of Boeing 747-400. Two different methods have been used to analyse the fireball, vapour inlet and dynamic spray. The behaviour of a fireball in terms of shape, size and lifting has been studied. Effect of droplet evaporation and engulfment has been studied. The time-averaged temperature predicted around the area engulfed by fireball up to a distance of 20 m from the centre of wings has been observed to be greater than 400 K, which is high enough for causing human fatalities as well as spalling of concrete structures. With the verification of developed CFD models further studies on the effects of Nuclear Power Plant (NPP) structures on the evolution of fireball and the thermal hazard on the surface of building structure have been studied in **Chapter-6** as per the identified objectives of this study.



## CHAPTER 6: SAFETY ASSESSMENT OF NPP STRUCTURE

---

### 6.1. Introduction

An aircraft crash can potentially affect the integrity of the Nuclear Power Plant (NPP) through mechanical destructions and thermal damage. In the safety assessment of NPP, the direct impact of aircraft upon a primary nuclear containment or related service buildings could potentially lead to serious radiological consequences around the site unless the appropriate mitigation measures are in place. Aftermath the impact, the fire-resistant structural elements (columns, slabs) may suffer loss of fire protection covers and/or coatings. This may damage the equipment and major structures. The cracks in the containment shell may result in a more severe thermal environment beyond the estimates as obtained through the conventional fire rating.

In the aircraft crashes, it is seen that the fuel in the wings is dispersed while crashing. The wings (hosting the fuel tanks underneath) of modern commercial aircraft consist of open section beams, ribs and a skin reinforced by stringers and made of Aluminium body (Forasassi and Lofrano, 2010). The fuel is expelled out in a large amount from the broken tanks and gets atomized to form a droplet cloud. The remaining fuel is ejected in the form of liquid chunks or may get leaked from the broken tanks. This leaked fuel possibly will lead to the formation of a liquid pool. Depending on the availability of heat source either from the electronic circuit (broken) or from hot jet turbine parts, the vaporized portion of dispersed fuel initiates the combustion. The large quantity of the fuel engulfed within fire in very short duration results into a fireball. The portion of fuel that does not involve in the fireball formation, spills around and leads to a local pool fire formation. This would further supplement with unburnt liquid fuel rain.

Earlier in **Chapter 1**, Figure 1.1 in showed a typical Nuclear power plant. It is difficult to analyse the thermal hazard associated with the aircraft crash by accomplishing the experiments due to its complexity and distinct nature. In the view of this, there is a need of three-dimensional Computational Fluid Dynamics (CFD) tools to deliberate the detailed study of fuel dispersion, combustion of fuel, fireball formation, heat radiation and the thermal hazard from the fireball.

In this chapter, the evolution of fireball associated with hypothetical accident of large commercial aircraft has been studied using CFD simulations to study the combustion, evolution and heat radiation from the fireball. Parametric studies have been performed for different locations of aircraft impact. The inputs to the fireball analysis needs the droplet size and distribution from the impact of aircraft have been predicted using model developed in **Chapter 4** to analyse the fuel spreading and formation of fireball using OpenFOAM CFD code. The local values of fuel mass fraction, gas velocity and temperature are plotted to study effect of engulfment from developing fireball.

## **6.2. Safety Assessment of NPP for aircraft crash-induced fireball loads**

In the safety-relevant issues, the data must be analysed and following key points need to be considered during the aircraft crash. These issues have to be defined before the start of the assessment process in order to make conservative choices in the process to demonstrate the capability of the NPP to cope with the fireball loads. (IAEA Safety Guides)

- Aircraft type, fuel capacity and speed of impact
- location and direction of impact (height from the ground)
- type of building structure (size and shape of the building)
- the amount of fuel involved in the fireball and in the fuel spill fire
- the damage done to the exterior of the buildings

- the vents, where the fireball or smoke may enter, and the hazards inside the buildings

In the case of fireball, the safety objectives are “safe shut-down” and “no substantial radioactive release to the environment” and the initiating events to be investigated are “entry of fuel or fire in the air intake vents or air exhaust vents of the reactor building and the auxiliary reactor building and the diesel buildings”. In case of a large spill-fire, the effect of the smoke and the entry of fuel into cable duct and piping systems or sewage systems has to be investigated after the fireball analysis. In this study, spillage of fuel and fireball formation after ignition of spilt fuel (or droplet cloud) is considered for safety analysis. The debris from aircraft crash and secondary local fires due to auxiliary materials that may arise in this sequence are not within the scope of this research work.

### **6.3. Primary analysis**

Commercial aircrafts consume around 4 ton of fuel to take off and 10 ton/hr fuel in cruise. For a worst-case scenario, the flight from nearer airport needs to be considered for safety analysis. The size of the aircraft structure is larger than the containment building. Obviously, two wings will smash at two different locations. This may leads to a single fireball and/or pool fire formation. Lipton and Glanz(2002) summarised the impact velocities at the time of WTC events. They reported velocity of aircraft impact for North Tower was 191.94 m/s while for South Towers, it was 225 m/s. In the case of the Pentagon, the impact velocity of aircraft was found to be 156 m/s(Powell, 2001). It is noted from these events that the maximum velocity of aircraft close to the ground surface is limited by stagnation pressure. The impact velocity of aircraft is considered for simulation in this research work is 200 m/s with the loadings of 90 ton of fuel. Using these inputs for aircraft crash and the model for droplet spray, the output for fuel dispersion and distribution has been calculated for fireball analyses. Following Table 6.1 gives the input used for the dispersion of fuel.

**Table 6.1: Inputs to calculate fuel dispersion using model mentioned in chapter 4 using jet fuel.**

Parameter	Symbol	Value	Description
Velocity of impact	$V_n$	200 m/s	Velocity of impact
Mass of fuel	$M$	90 tons	-
Energy absorbed	$E_{crushing}$	20 MJ	Energy absorbed by wing tank during crushing (Wierzbicki & Hendry-brogan, 2002)

The droplet cloud is formed as a result of fuel tank rupture after the aircraft crash. The method developed in **Chapter 4** has been used to find dynamic properties of droplet cloud erupting from ruptured tanks. This involves the velocity of droplets, droplet sizes distribution and mass of fuel evaporated during this transaction. The distortion of the fuel tank is considered in the model and the debris scatter after aircraft crash is excluded. These results of droplet spray and cloud are used to generate the model inputs for the CFD simulation of fire developed during an aircraft crash.

#### 6.4. Results of fuel dispersion analysis

Analysis has been performed to get fuel distribution in the vicinity of the building using the model developed in **Chapter 4**. Table 6.2 gives the results of primary analysis for the fuel dispersion. Figure 6.1 shows the number of droplet distribution for each diameter interval. The maximum numbers of droplets are found smaller than 150  $\mu\text{m}$ .

**Table 6.2: Results of fuel dispersion modelling**

Sr. No.	Parameters	Symbol	Value
1	Characteristic diameter	$D_{32}$	120.86 $\mu m$
		$D_{max}$	353.02 $\mu m$
		$D_{min}$	11.86 $\mu m$
2	Characteristic velocity	$V_{max}$	232.5 m/s
		$V_{r.m.s.}$	14.18 m/s
		$V_{avg}$	39.38 m/s

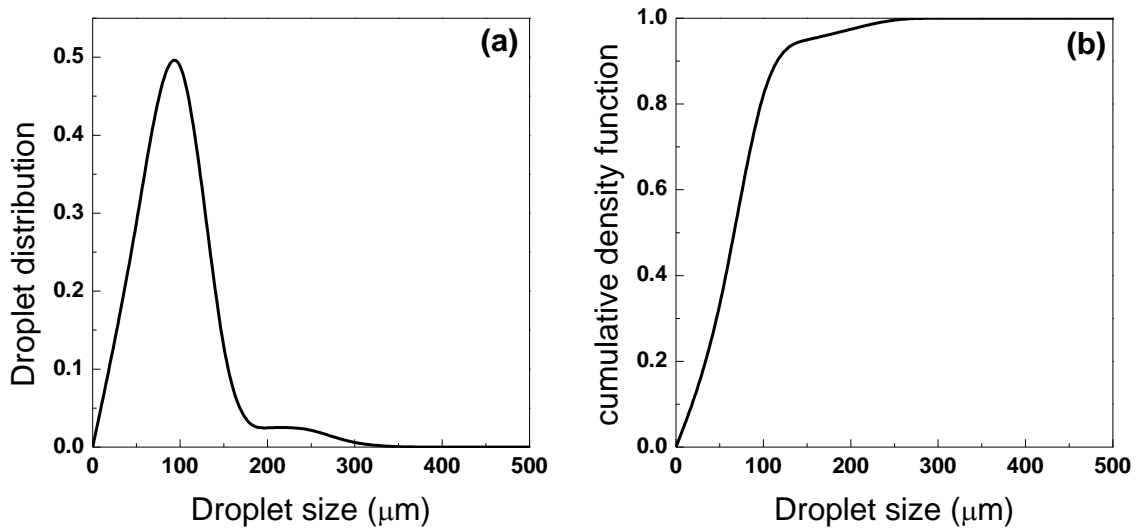


**Figure 6.1: (a) Predicted droplet sizes distribution and (b) cumulative density function of droplet spray using the model developed in Chapter 4.**

## 6.5. Initial and Boundary Conditions

An unstructured Cartesian computational mesh is used in the simulations. Figure 6.2 (a) shows a three-dimensional rectangular domain selected to analyse the fireball using dynamic fuel spray. The sizes of the domain have been selected as 300 m x 250 m x 150 m based on

preliminary calculations of maximum diameter and the lifting height of fireball using **equation (2.3), Chapter 2**. The initial fuel dispersion and evolution of fireball is the main interest of this study. So, computational domain is considered based on the region of interest.

An open boundary condition is employed at the sides and top. In open boundaries flow across the boundary to the outer external atmosphere are allowed along with the backflow from the external atmosphere to the computational domain. In this boundary type, eddies are lost and hence there will not get a realist feedback. At  $y=0$ , the bottom plane (ground) of the domain behaves as the wall where the no-slip boundary condition has been employed. At the building exterior surfaces also, wall boundary condition is applied for sub-grid-scale viscosity and the no-slip boundary condition for velocity is used. At the wall zero temperature gradient is applied along the wall normal. The acceleration due to gravity ( $9.81m/s$ ) is accounted in the negative  $Y$  direction. Initially, stagnant air at 300 K has been considered as domain fluid. Fuel inlet is calculated using actual dimensions of the wing. Figure 6.2 (b) shows the inlet face area which is taken as wing area. The direction of injection is taken the angle of impact of crashing aircraft. The spray introduces air drag in the domain due to its own momentum. The droplet cloud decelerates immediately after removing air drag due to aircraft impact.

The fuel spray is injected into the computational domain via a Lagrangian particle injection model. Aircraft wing is used as inlet area for fuel injection (see Figure 6.2(b)). The direction of injection is taken the angle on the impact of crashing aircraft (depending on the cases considered). The injection velocity was set 232 m/s (Table 6.2). Once all the 90 ton fuel entered into the computational domain, injection velocity ramped down to zero. The spray introduces air drag in the domain due to its own momentum. All the simulations for this study are carried out with  $2 \times 10^6$  parcels per second. The distribution for the droplet initial size distribution is

used based on the fuel dispersion analysis mention in section 6.4. The various cases of aircraft impact locations considered are explained further in the section 6.7.

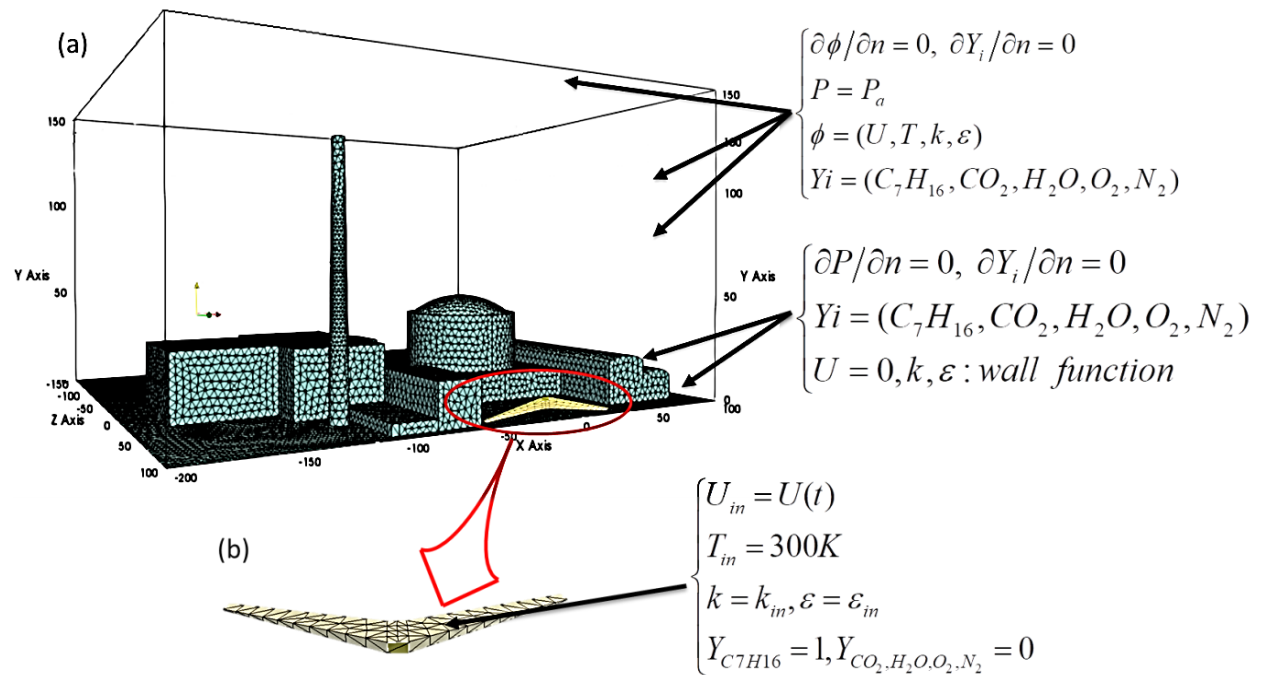


Figure 6.2: (a) Schematic of a computational domain showing the fuel inlet (b) aircraft wing (fuel inlet)

## 6.6. Numerical Method

In this system, the fuel is introduced in the form of droplet spray. Dynamic spray method is the most refined and promising approach in which combustion of fuel spray is considered (Luther and Müller, 2009). The aircraft fuel emerging out of the broken fuel tanks is simulated dynamically in the form of fuel spray. The spray model is explained in section 6.4 in details. The simulation is carried out using combustion module of OpenFOAM developed by Wang et al. (2011).

A grid size of 1 m has been used to simulate the fireball associated with aircraft impact. This mean that eddies of size above 1 m have been resolved and turbulence at the scales below 1 m

is assumed to be isotropic and homogeneous. As the fireball occurs most in the open space, the turbulence has negligible effect on its evolution near the wall. The fuel spreading, combustion and expansion of fireball are atmospheric flows. The main effect of turbulence is on the sub-grid scale, which affects the combustion reaction. In this study, Eddy Dissipation concept (EDC) combustion model is used which assumes the infinitely fast chemistry (fuel burns immediately on the availability of oxygen). Further, the convective heat transfer inside the turbulent boundary layer and heat penetration through the walls of building structure is neglected. Therefore, mesh refinement near wall is not considered in the computational domain.

The discretized momentum, species transport and energy equations are solved by the preconditioned bi-conjugated gradient method (PBiCG). Generalized geometric-algebraic multi-grid method (GAMG) is employed to solve the discretized pressure equation originated from the application of momentum interpolation to the continuity equation. This method is also used to solve the discretized turbulent energy and the radiative transfer equations. The second order backward differentiation scheme is employed for temporal discretization. The diffusive terms and the gradients are discretized using central differencing scheme. Spatial derivatives are estimated on a rectangular grid with all quantities assigned to the cell centre and velocities linearly interpolated to the cell faces. The FireFOAM employs a PIMPLE (PISO+SIMPLE) algorithm for pressure-velocity coupling. The PISO algorithm is solved using a Gauss Linear scheme, with an implicit Euler time discretization.

Large Eddy Simulation (LES) is employed to solve large scale flow. The effect of small scaled eddies are modelled to estimate a sub-grid turbulent viscosity using One Equation Eddy model (a Sub Grid Scale (SGS) model) with eddy coefficient of 0.07. The transport equation of energy is solved for enthalpy with source terms from combustion and radiation equations. Temperature

dependency of the enthalpy and heat capacity of individual species has been taken into account. The enthalpies of formation of various chemical species are available in NIST-JANAF Thermochemical Tables (Chase, 1998) and are used in the most combustion simulation codes in the form of a standard library. Sixteen solid angles each associated with a vector direction in a participating media are used for discretization of RTE using finite volume method. RTE is solved using generalized Geometric-Algebraic Multi-Grid method (GAMG) and updated after every 10 iterations.

### **6.7. Results of Impact analysis**

This work focused on the first few seconds of fireball evolution before it rises above the NPP and potential hazard of the spreading flame on the safety of the NPP. The other miscellaneous effects such as secondary missiles and heat radiation leading to damage of structural integrity are not accounted in this research work. The secondary or domino effects are also not considered here. Following impact-conditions have been used for safety assessment. Analyses have been performed up to a physical time of 10 s and data have been collected for every 0.01 s during the CFD simulation. Figure 6.3 presents the various conditions considered for simulations.

- Case 1: Aircraft strikes horizontally on auxiliary building from the backside at the ground
- Case 2: Aircraft strikes horizontally on containment building from the generator building side
- Case 3: Aircraft strikes horizontally on containment building from the opening side of the auxiliary building.

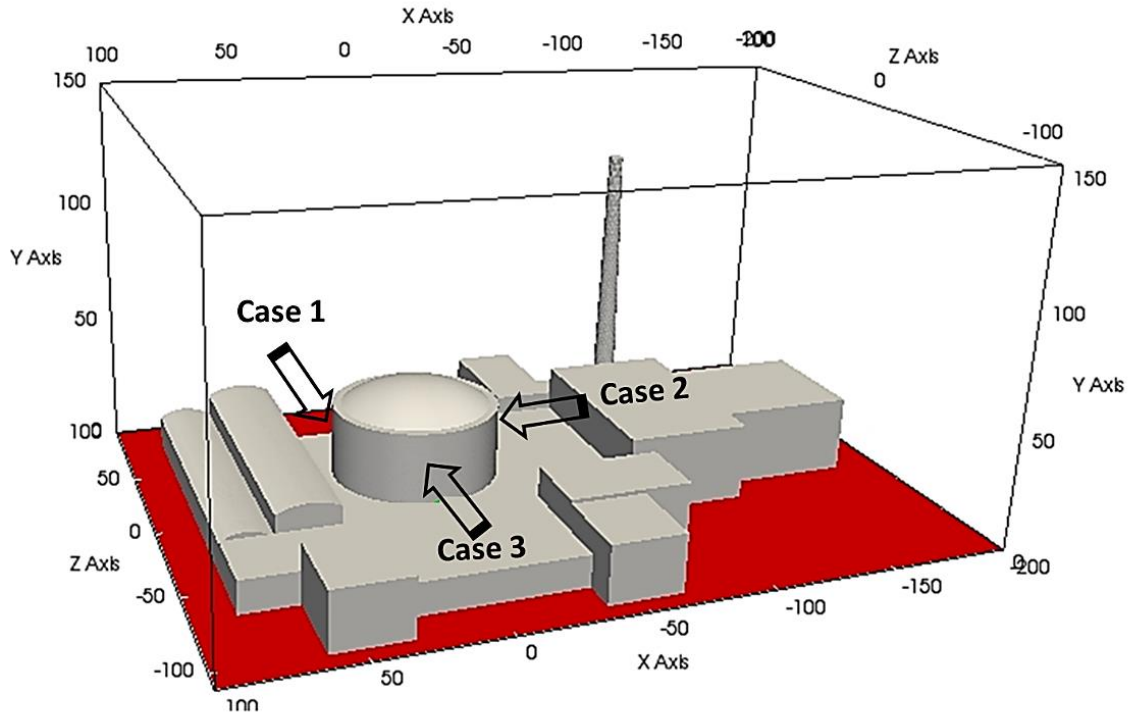


**Figure 6.3: Impact conditions considered for safety assessment**

In the simulations, the fireball starts as the fuel droplets enter and evaporate in the computational domain. Further, the mixing of surrounding air with a fuel mixture leads to self-sustaining fireball. Figure 6.4 shows the dispersion of fuel in the form of droplet spray for case 1. The droplets get evaporated due to radiative heat from developing fireball and engulfed in fireball.

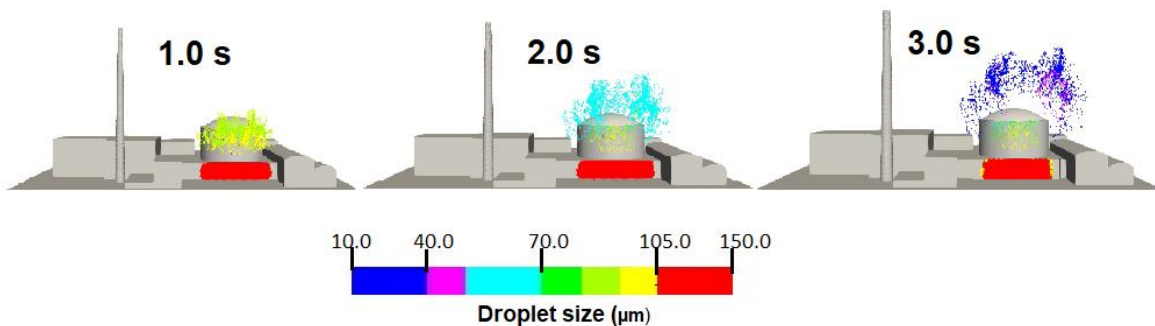


**Figure 6.4: Dispersion of fuel droplet spray at 1, 2 and 3 s for case 1**

The global evolution of fireball in case 1 is shown in Figure 6.5 at for different intervals. The expansion phase of the fireball is close to ground at 2 s. The fireball forms its spherical shape during the time of 4 to 6 s. It can also be seen that fireball is not very hot during the first few seconds. The outer surface of the fireball is dominated by Taylor instabilities, which greatly enlarge the burning at the surface. Due to turbulent dissipation, the transient development of fireball shows the typical self-sustained expansion of hot gas from turbulent combustion. The combustion is mixing controlled and it is limited by lack of oxygen supply from the atmosphere. The fireball size can be approximated by a hemisphere, which is growing with time. The fireball evolution is near to ground in this case and fireball flame front does not contribute potential hazard to NPP structures.

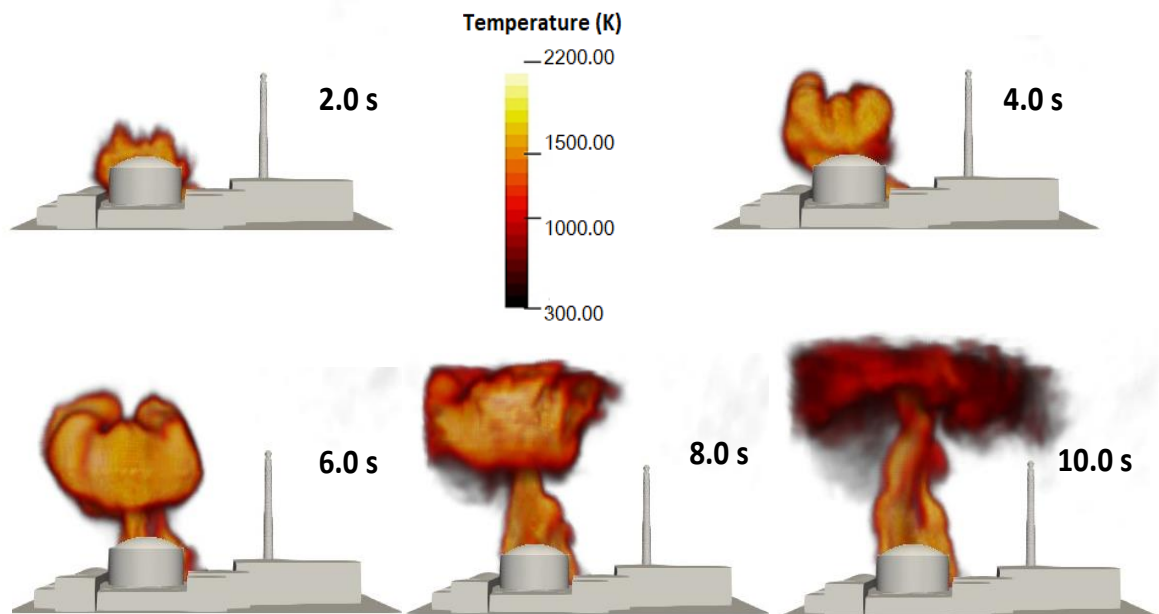


**Figure 6.5: Evolution of fireball for case 1**

Figure 6.6 shows the dispersion of liquid fuel at 1.5, 2.5 and 3.5 s after aircraft impact for case 2. Due to atmospheric friction, the droplet spray disperses in the atmosphere. The final size of

the droplet cloud diameter is observed to be 50–70 m. The temperature and concentration conditions lead to evaporation of dispersed droplets, as these take heat from fireball.

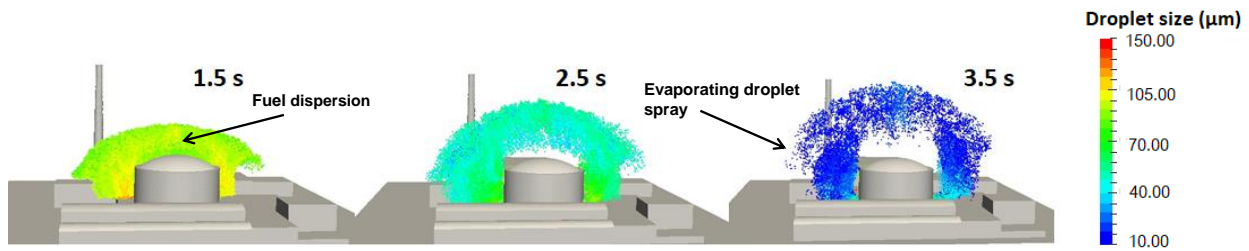


**Figure 6.6: dispersion of fuel droplet spray at 1.5, 2.5 and 3.5 s for impact condition 2.**

Figure 6.7 depicts the evolution of a fireball during 1.5, 2.5 and 3.5 s. This is attributed to quasi-hemispherical expansion in the fireball. Further, presence of structure causes turbulence and hence, the combustion increases. During this time, fireball front expands over NPP structures. The temperature of the fireball is low as only a small part of the fuel is evaporated and burnt.

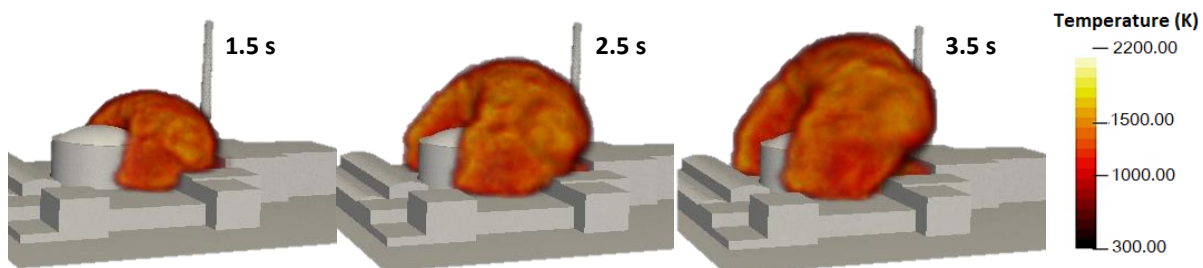


**Figure 6.7: Burning of dispersed droplets and fireball evolution at the duration of 1.5, 2.5 and 3.5s for impact condition 2**

The released heat is used in the evaporation of fuel droplets. It can be observed from Figure 6.8 that fireball starts lifting at 5 s. It moves upward and away from the NPP structure. The fireball burns away from the NPP structures. During the lifting phase, only radiation contributes to the thermal hazard. The fireball starts leaving computational domain at 10 s (see Figure 6.8).

The results after this duration are inadequate in consideration of thermal hazards. Figure 6.9 shows the droplet spreading around the containment building above the auxiliary building for case 3 for two different times. The droplets remain in the domain until they evaporate and take part in the combustion.

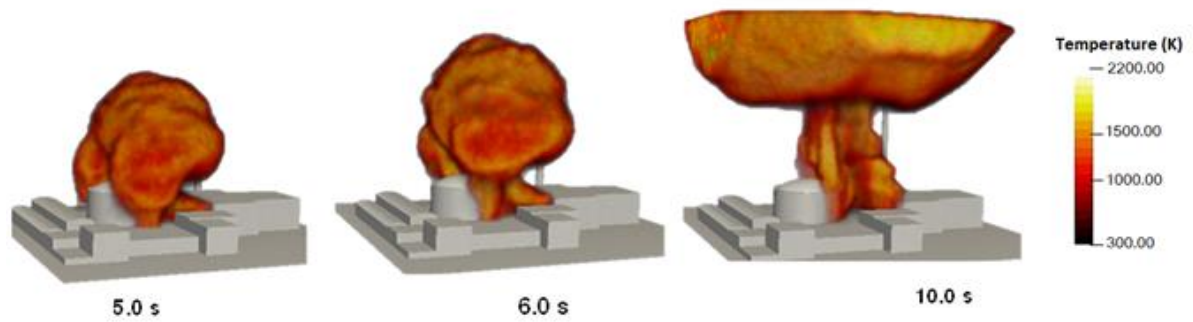


**Figure 6.8: the evolution and lifting-up of fireball at time durations of 5, 6 and 10 s in impact condition 2**

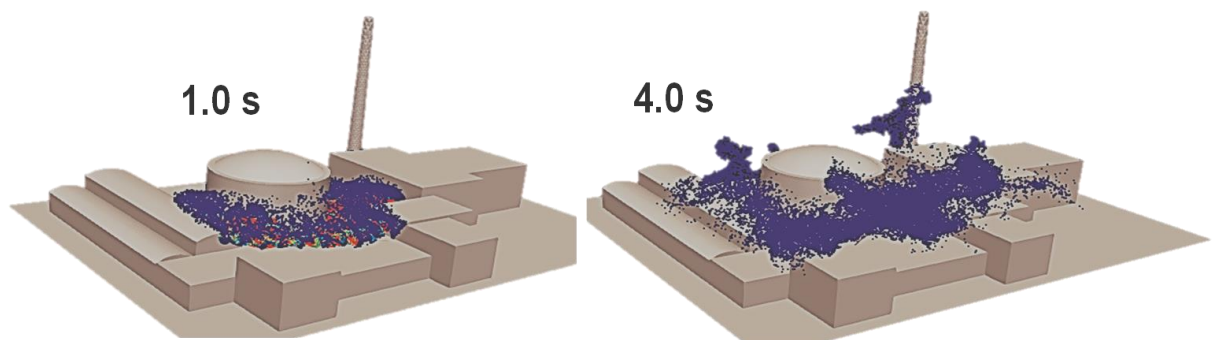


**Figure 6.9: dispersion of fuel droplet spray at 1.0 and 4.0 s for impact condition 3.**

Figure 6.10 depicts the evolution of fireball associated with aircraft impact for case 3. The fireball is in close contact with the NPP buildings. Due to non-symmetry of NPP buildings, the expansion of the hemisphere is not symmetric. The fresh air from the sides of the buildings gets entrained and causes vortex formation to the auxiliary building. The fireball remains attached to the building for the larger duration to the NPP structure compared to other impact conditions.

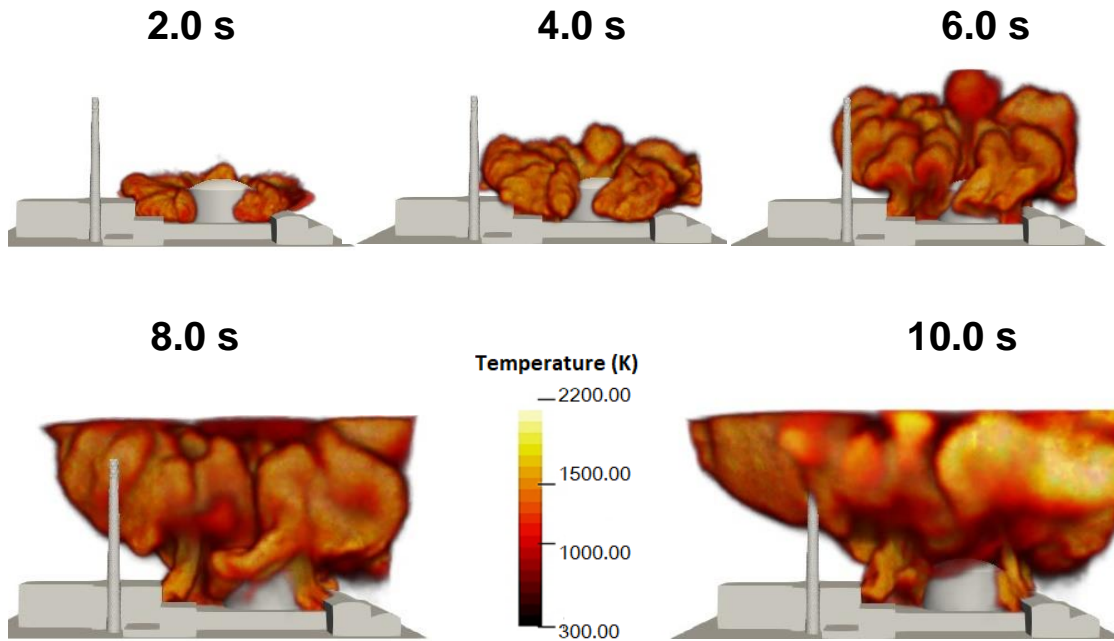


**Figure 6.10: the evolution and lifting-up of fireball for impact condition 3.**

Figure 6.11 depicts evolution and lifting of fireball on buildings. From Figure 6.11, it can be seen that though fireball is lifted up from the NPP structure, the wall of structure experiences the radiative heat flux from the fireball as the fireball lifting is not fast enough with time. The average containment building wall temperature during the fireball duration is 1200 K. Local hot spots created due to turbulence in spreading flame can also be observed (above 1600 K) in Figure 6.11.

For safety assessment, the key parameters related to safety are calculated at the opening 30 m away from the containment building (Figure 1.1, **Chapter 1**). Figure 6.12 depicts the local values of fuel mass fraction,  $CO_2$  mass fraction, gas velocity and temperature of gas as a function of time. The turbulence in the flow is observed during the evolution of fireball. (blow of 50 m/s at initial 0.5 and 2s and blow of 40m/s in the duration of 4-8 s).The fuel mass fraction also drops down from 0.65 to zero in the initial transient (Figure 6.12 a). Then this gas is lean in fuel. After the initial heavy blow of the, temperature of the gas flow reaches to a maximum

of  $\sim 2000$  K as shown in Figure 6.12 (b). The presence elevated temperature (Figure 6.12 b) and high fraction of  $CO_2$  (Figure 6.12 d) ensures the occurrence of flame at considered location. This data can be used to study fire hazard in the vicinity of structure and amount of fuel burning during the evolution of fireball.

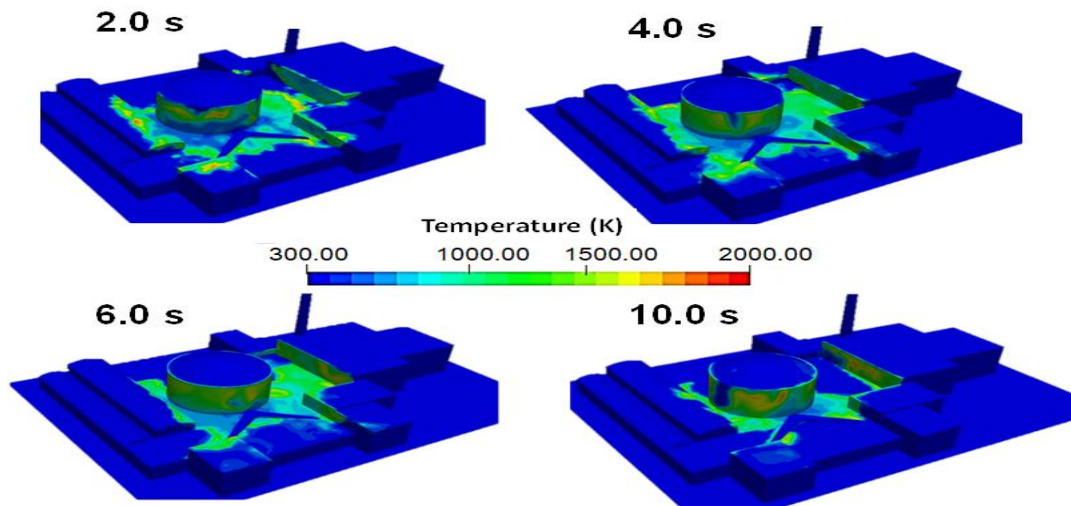


Figure 6.11: Profile of temperature predicted for impact condition 3

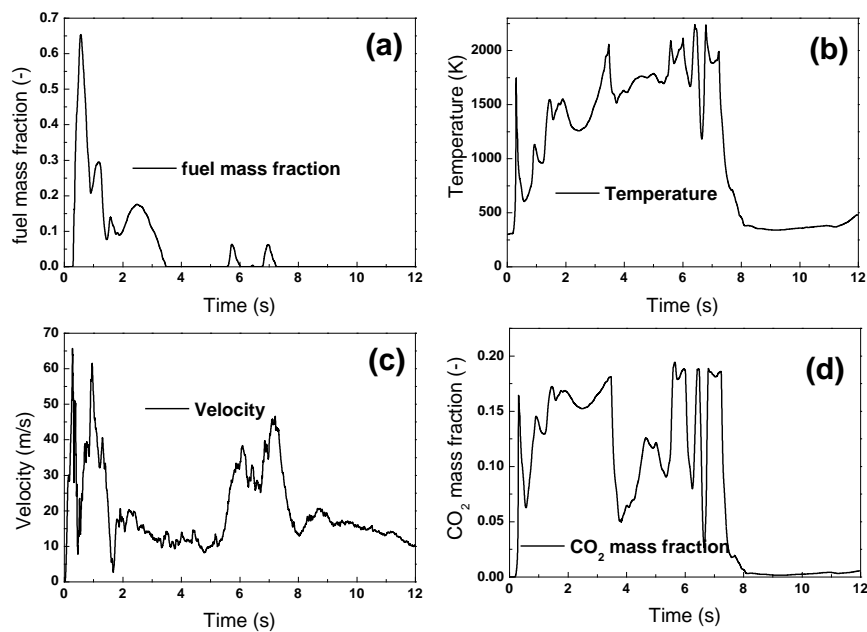
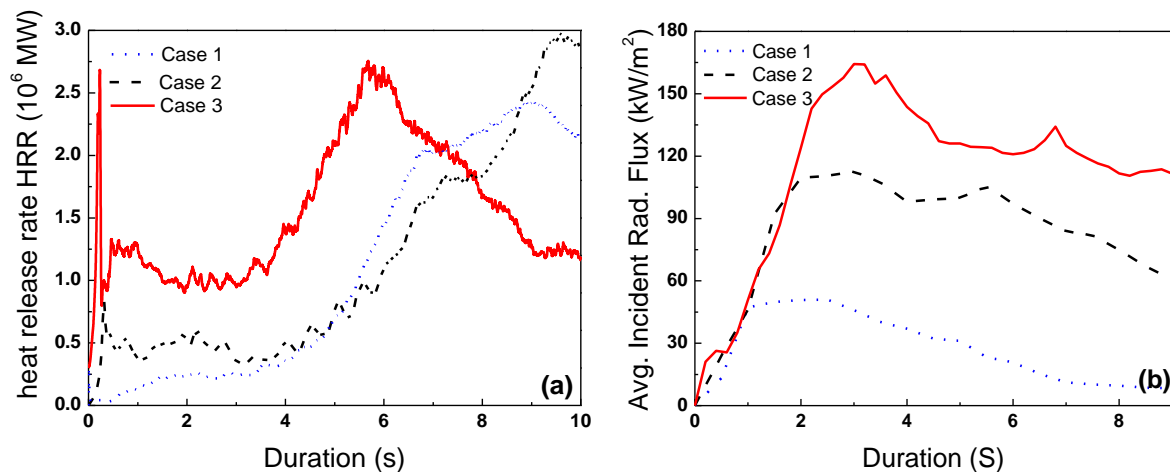


Figure 6.12: Time history of safety relevant parameters calculated at 30m away from the containment building (at the assumed opening of the building).

## 6.8. Effect of structures on fireball evolution

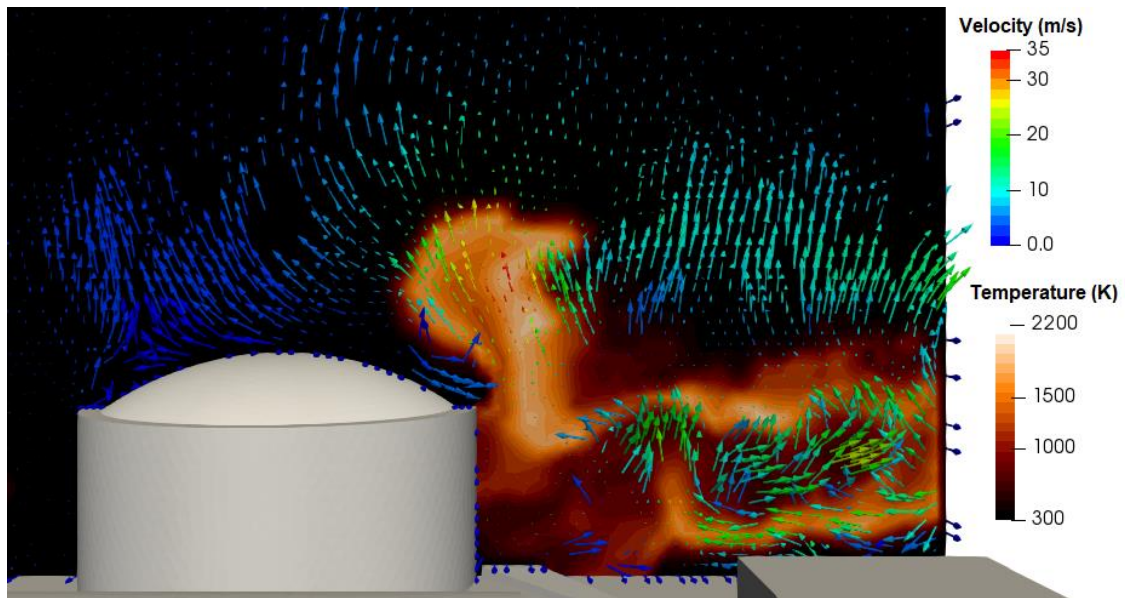
The fireball evolution is affected by the presence of NPP structure. The structures disturb the flame propagation. Again, the droplets in the fuel cloud may stick to the walls of the building structure, which may further affect the evolution of fireball and burning of fuel close to building.

Figure 6.13 shows the global heat release rate (HRR) during the simulations. The fireball for case1, HRR and effect of turbulence due to presence of structure has been discussed below. Combustion of fuel is controlled by the rate of mixing of air and fuel. For the low turbulence, mixing was less and required more time to complete the combustion. This resulted in lower HRR. For case 2, more spreading of fuel has been observed, which leads to better mixing and higher heat release as observed in Figure 6.13(a). Figure 6.13(b) depicts the average radiative flux incident on building surfaces. It has been found that Case 3 shows the higher value of flux during the evolution of fireball as it spreads over the larger area. This can be considered as a worst case amongst all the cases studied.



**Figure 6.13: (a) Global heat release rate (HRR), (b) Average incident radiative heat flux on building surfaces.**

Figure 6.14 depicts the swirl generated around the containment building and development of “hot-spot” at 4 s. The maximum temperature in the fireball is found to be 2200 K. The temperature near the containment building is about 1200 K. In the view of above discussion, it can be said that the radiation received in the vicinity of the structures is maximum for case 3.



**Figure 6.14: local velocity vectors and temperature distribution near containment wall**

The lifting of the fireball is another important phenomenon which can also indicate heat transfer from the fireball. The average lifting velocity is calculated from **equation 3.27** in the **Chapter 3**. Average lifting velocities of fireball calculated from the CFD analysis for case 1, case 2 and case 3 and calculated from equation (3.27) are depicted in Table 6.3. The calculated upward velocity is 15.9 m/s using equation (3.27). For case 1, the lifting velocity is 16.18 m/s. In this case, the fireball evolution takes place in almost unconfined manner. For other cases, the flame remains attached to the wall of NPP structure for longer duration. This again leads to more heat transfer to the structure walls.

**Table 6.3: Average Uplifting velocity of fireball**

<b>Parameters</b>	<b>Average Lifting Velocity</b>
Impact Condition 1	16.18 m/s
Impact Condition 2	13.50 m/s
Impact Condition 3	12.01 m/s
Calculated from equation (3.27)	15.9 m/s

## 6.9. Closure

The safety assessment due to impact of aircraft with nuclear power plant (NPP) structure resulting fuel dispersion, fireball evolution and its progression is carried out using three-dimensional computational fluid dynamics code. In the CFD simulation, the time history of local and global safety relevant parameters provides the necessary input data for potential hazard assessment. The simulation with dynamic spray model gives new insight into the evolution and combustion of fireball in presence of building structures. Fireball evolution is affected by the building structure. The fireballs spread over a diameter of 80 m and remained close to the building structures for a longer duration. The average temperature near the containment building reaches near 1200 K during the fireball evolution. Since these buildings should be to 3 Hr. rated construction, a few seconds of flame exposure won't compromise the building structures, but may create injuries to personals.

## CHAPTER 7: CONCLUSION AND FUTURE WORK

---

In the current work, the hydrocarbon fireballs have been analysed using CFD simulations for their detailed characterization including diameter, lifetime, flame and internal structure to reveal inherent assumptions and limitation made in empirical models. To study the fireball associated with aircraft crash using CFD simulation using dynamic fuel spray, the detail spray characterization is needed. A Mathematical model is developed for prediction of droplet sizes and distribution associated with the impact of a liquid-containing projectile. The velocity and droplet distribution of dispersed fuel have been used as inputs to CFD code and simulations have been performed with dynamic fuel spray to analyse the formation of fireball associated with aircraft crash. Further, for a hypothetical aircraft crash on nuclear power plant (NPP) structure, the engulfment of fireball and the effect of building structures on fireball evolution are studied for safety assessment using dynamic fuel spray model.

This chapter represents the summary and conclusions of the current work. Recommendations for future work are also described in this chapter.

### **7.1. Summary, conclusions and recommendations**

In the first part, fireball resulting from fuel vapour is studied and analysed using CFD simulations. The Eddy Dissipation Concept (EDC) combustion model and single step reaction coupled with LES turbulence model provides the reliable results. The spatial distribution of fuel and product concentrations, as well as the temperature, helped to understand the internal structures of fireball at its evolution. The inner zone of a fireball does not lose heat through radiation/convection, hence, the temperature of the inner zone of a fireball (1900 K for Propane) is found close to adiabatic flame temperature.

The parametric studies on fireball from a vertically released fuel are conducted by varying the mass of fuel, inlet velocity and inlet opening diameter. In the parametric studies, it has been found that the heat release ratio reduces with increase in the fuel mass (for constant velocity and injection time) as the larger fireball burns slowly. With increasing injection velocity (with constant fuel mass), the heat release rate is increases and this is due to better mixing of fuel with air. The fireball lifting height is higher for higher velocity as the initial momentum is high but no substantial change is observed in thermal dose at the calculated locations on ground. The effect of inlet opening diameter is found insignificant on the fireball shape (for constant fuel mass and inlet velocity). New correlations have been proposed for fireball diameter and duration based on the mass of fuel participated in fireball. The proposed correlations predict the fireball diameter within 13% and duration of fireball in 18% of the previously published accidental/ experimental data.

The inlet fuel area, fuel velocity and the direction of fuel injection are the key factors for initial momentum input affecting the fireball evolution. Since all the parameters cannot be determined in case of aircraft crash due to its complexity and distinct nature. The fuel dispersion and fireball associated with aircraft impact can be modelled in the computational fluid dynamics using fuel droplet spray as it introduces both momentum and fire load into initially resting atmosphere. The input data and boundary conditions are needed to study fire dynamics.

In the second part, a mathematical model is developed to investigate the transientbehaviour of liquid slug emerging out from the impacting vessel filled with a liquid which can predict the transientbehaviour of droplet cloud. This involves spreading, ligament formation, droplet formation, and secondary breakup, droplet sizes and distribution. The characteristic diameters and velocities of final droplets estimated are compared with the experiments available in the literature (performed using impact of water-filled-projectiles). Parametric studies are also

performed to study the effects of impacting velocity on final droplet sizes and distribution for different liquids. It has been found from the analysis that droplet formed are of smaller size when impact velocity is high. The maximum velocity of spreading film is 2 to 2.5 times of the impacting velocity of the vessel. The size of secondary droplets is less for kerosene than that of water for same impacting conditions. This developed mathematical model is further used to analyse the liquid dispersion associated with aircraft crash.

The evolution of fireball associated with aircraft impact has been studied using dynamic fuel spray in the third part. An accident case of Boeing 747-400 is analysed using fuel vapour inlet and dynamic fuel spray. The inputs to the dynamic spray have been calculated using the above mentioned mathematical model. It has been found that both methods give similar predictions for fireball diameter and lifting height though other parameters like pressure developed, radiative heat flux and temperature are predicted differently. Parametric studies are also performed to analyse the effects of fuel mass of fireball parameters using vapour fuel inlet and dynamic fuel spray methods. In this study, the time-averaged temperature predicted around the area engulfed by fireball up to a distance of 20 m from the centre of wings has been observed to be greater than 400 K, which is high enough for causing human fatalities as well as spalling of concrete structures.

For a hypothetical aircraft crash with NPP structure resulting in a fuel dispersion and fireball formation, safety assessment has been carried out using CFD simulations. It is found that the fireball evolution is affected by the building structures. The fireball of fuel mass 90 tone spreads over a diameter of 80 m. The highest temperature of fireball (2200 K) is reached when fireball lifts above NPP and leaves the structures. The average temperature of the wall structure is found 1200 K for 10 s.

It is recommended to carry out the experiments to get more insight the various phenomena of fireball formation. Studies can also be performed with a large amount of liquid pool engulfed in a fire.

## APPENDIX A

### A-1. Experimental data considered for validation of Mathematical Model

As discussed earlier, Hostikka et al.(2015)performed experiments on impacting of water filled metal projectile on a hard wall. They investigated the spray behaviour using high speed cameras and droplet size and velocity distribution using ultra high speed cameras. The experimental data given by them have been used for validating the above mentioned methodology. Table A.1gives the specifications of selected tests for the model validation from the study of Hostikka et al. (2015).

**Table A.1:Specifications of tests (Hostikka et al., 2015)**

<b>Test ID</b>	<b>Wall thickness (m)</b>	<b>Inner diameter (m)</b>	<b>water tank length (m)</b>	<b>mass (kg)</b>	<b>Water Mass (kg)</b>	<b>Impact Velocity (m/s)</b>
SFP 2	0.0015	0.15	2.155	50.52	37.1	97
SFP 3	0.0015	0.15	2.155	38.09	24.69	97
SFP 4	0.0015	0.15	1.204	38.4	24.81	99
SFP 5	0.0015	0.15	1.204	38.38	24.74	99
SFP 7	0.0015	0.2	1.204	49.75	36.82	103
SFP 8	0.002	0.2	1.204	51.05	37.24	100
SFP 11	0.0015	0.2	1.204	49.9	36.96	126
SFP 12	0.002	0.2	1.204	51.5	37	122

Here for sample calculation, case SFP-7 from the experimental data has been selected.

***Kinetic energy of cylinder***

Total weight of cylinder	49.75 kg
Weight of water in the cylinder	36.82 kg
impact velocity	103 m/s
Total Kinetic Energy (Cylinder + Containing water)	263898.9 J

***Energy of crushing cylinder***

The crushing energy is calculated by the following equation,

$$E_{crushing} = F_{crush} \times L_{cyl} \quad (\text{A.1})$$

Where the expression for the crushing force is given by,

$$F_{crush} = 7.96\sigma_{cyl} t_{cyl}^{1.5} D_{cyl}^{0.5} \quad (\text{A.2})$$

Here,  $\sigma_{cyl}$ ,  $t_{cyl}$ , and  $D_{cyl}$  are stress induced in cylinder, thickness of cylinder and inner diameter of cylinder and length of cylinder is given by  $L_{cyl}$ , Crushing energy of this case is found to be

Thickness of impacting cylinder	0.0015 m
Diameter of impacting cylinder	0.2 m
Flow stress, $\sigma_{cyl}$	250 MPa
Length of impacting cylinder	1.204 m
Crushing force, $F_{crush}$	51.70172 J
Energy of crushing cylinder, $E_{crush}$	62248.86 J

## A-2. Energy remained in the water column (liquid slug)

Energy remained in the water column inside the impacting cylinder is calculated by subtracting crushing energy of impacting cylinder from the total Kinetic energy. (i.e. Kinetic Energy of impacting cylinder containing liquid). It is assumed that the target on which the cylinder is impacted absorbed no energy. The secondary metallic missiles that are resulting from impacting cylinder and their energy has also been neglected in this calculations.

Energy remained in water Column	201650.01	<i>J</i>
Energy Fraction	1.016	-
velocity of impacting water	104.65	<i>m/s</i>

This velocity of impacting slug of water has been used in following calculation of velocity of spreading. This total mass of liquid has been emerging out from the impacting cylinder within a critical time,  $t_c$ . This critical time is characteristic spreading time of liquid slug and calculated as,

$$t_c = \frac{L_{slug}}{V_n} \quad (\text{A.3})$$

Here the impacting velocity of liquid slug is 140.65 m/s and length of slug is 1.204 m (water tank length, mentioned in Table A.1). Therefore, the characteristic time is 0.0115 s i.e. 11.5 ms. For this time only, the liquid will emerging out. To study and find the characteristics of liquid sheets emerging from the impacting cylinder, this process is Quasi-Statically analysed and formulated for each time step. Here the time step has been selected as 0.001 ms (that is 1.0  $\mu$ s). At each of these time steps liquid film formation, breakup of liquid film, ligament formation, primary droplet, secondary droplets and evaporation have been calculated. The data

of the entire duration is used in combined manner to determine the characteristic droplet diameters and characteristic droplet velocities to analyse the droplet cloud. The acceleration due to gravity is incorporated in a spreading of liquid front/ droplets in the vertically downward direction. The spreading velocity of each film at particular tie instant and specific direction is calculated in following manner,

Time (s)	Velocity of spreading film (Ligament)				
	90° upside	45° upside	0° (Horizontal)	45° downside	90° downside
0.000001	203.351623	203.351623	203.3516234	203.3516234	203.3516234
0.000002	195.239358	195.2392993	195.2394091	195.239471	195.2394714
0.000003	188.044773	188.0447674	188.0449871	188.0451108	188.0451117
...	...	...	...	...	...
...	...	...	...	...	...
...	...	...	...	...	...
0.011498	25.74915	25.801913	25.910338	25.971380	25.9718166
0.011499	25.73835	25.791174	25.899709	25.960813	25.961249
0.0115	25.72758	25.780450	25.889095	25.950261	25.950698

Spreading velocity of liquid film is further used to determine to the ligament properties and sizes of primary droplets. The sample calculations are shown below for the stream of liquid emerging out from 90° upside. Similar calculations have been performed for all considered angles. The velocity of primary droplets is calculated by the conservation kinetic energy and surface energy of ligament and primary droplets.

### A.3 Primary droplet formation

The diameter of primary ligament calculated by using following equation,

$$d_{lig} = \sqrt{\frac{16h_l}{K_s}} \quad (\text{A.4})$$

$K_s$  is the wave number of fastest growing surface wave. Since the sheet become thinner as it departs from the source, the position of first breakup determines the ligament diameter. Here  $h$  is film thickness and have been calculated using  $\sqrt{\nu t}$ , where  $\nu$  is kinematic viscosity of liquid and  $K_s$  is calculated from the following equation,

$$K_s = \frac{2v_s^2 \rho_g}{3\sigma_l} \quad (\text{A.5})$$

The wave number for fastest growing ligament,  $K_{lig}$ , has been calculated using,

$$K_{lig} = \frac{1}{d_{lig}} \left[ 0.5 + \frac{3\mu}{2\sqrt{\rho\sigma_l d_{lig}}} \right]^{-1/2} \quad (\text{A.6})$$

Where  $d_{lig}$  is diameter of ligament. The primary drop diameter,  $d_{drop}$  is determined as

$$d_{drop} = \sqrt[3]{\frac{3\pi d_{lig}^2}{K_{lig}}} \quad (\text{A.7})$$

Following calculations shows the values of ligament characteristics and primary droplet sizes at given time instances.

Time (s)	Velocity (m/s)	$K_s$	$h$	$d_{lig}$ (m)	$K_{lig}$	$v_{lig}$ (m/s)	$d_{drop}$ ( $\mu\text{m}$ )	$V_{drop}$ (m/s)
0.000001	203.35	459465.4	1.06e-05	1.92e-05	48535.2	203.35	41.54	203.36
0.000002	195.23	423537.9	1.11e-05	2.05e-05	45690.36	195.23	44.19	195.25
0.000003	188.04	392898.2	1.15e-05	2.17e-05	43214.54	188.04	46.78	188.05
...	...	...	...	...	...	...	...	...

---

...	...	...	...	...	...	...	...	...
0.011498	25.74	7366.876	0.000101	0.000469	2103.63	25.74	994.34	25.75
0.011499	25.73	7360.702	0.000101	0.000469	2102.23	25.73	995.00	25.74
0.0115	25.72	7354.539	0.000101	0.000469	2100.84	25.72	995.66	25.731

---

## A.4 Calculations for Secondary break up

The secondary breakup due to aerodynamic forces and the secondary droplets are calculated. The numbers of child droplet are calculated using mass balancing. The gas phase Weber number has been calculated for each droplet by  $We_g = \rho_g U_{rel}^2 d_{drop} / \sigma l$ . Based on the Weber number, the different breakup modes and mechanisms of droplets exist which are shown in Table A. 2.

**Table A.2: Criteria for secondary breakup of droplet (Arcoumanis et al., 1997).**

Sr. No.	Weber Number	Breakup mode	Breakup time ( $\tau_{break}$ )
1	$We_g \approx 12$	Vibrational	$\frac{\pi}{4} \left[ \frac{\sigma}{\rho_l d_{drop}^3} - 6.25 \frac{\mu}{\rho d^2} \right]$
2	$12 \leq We_g < 18$	Bag	$6(We_g - 12)^{-0.25}$
3	$18 \leq We_g < 45$	Bag and streamer	$2.45(We_g - 12)^{0.25}$
4	$45 \leq We_g < 100$	Chaotic	$14.1(We_g - 12)^{-0.25}$
5	$100 \leq We_g < 350$	Sheet stripping	$14.1(We_g - 12)^{-0.25}$

Using the following phenomenological relations, the product droplet sizes are checked from distribution functions and the Sauter mean diameters (SMD) are estimated. According to Arcoumanis et al. (1997), the SMD of the first three modes (vibrational, bag and bag-and-streamer) is

$$SMD_{1,2,3} = \frac{4d_{drop}}{4 + 0.5(1 + 0.19\sqrt{We_g})} \quad (\text{A.8})$$

Prefix 1, 2 and 3 gives the serial numbers in Table 4.1, while for the chaotic breakup mode (serial number 4 in Table 4.1) following relation is used.

$$SMD_4 = 6.2 \frac{\sigma_l}{\rho_g U_{rel}^2} \left( \frac{\rho_l}{\rho_g} \right)^{1/4} \left( \frac{\mu l}{\rho_l d_{drop} U_{rel}} \right)^{1/2} \cdot We \quad (\text{A.9})$$

By considering the modes of breakup, secondary droplet diameters have been calculated in following manner.

Time (s)	$We$	$We_g$	Breakup criteria	Breakup	$D_{32}$ ( $\mu\text{m}$ )
0.000001	22795.25	27.44017	$18 \leq We_g < 45$	bag & streamer	32.46
0.000002	22351.65	26.90624	$18 \leq We_g < 45$	bag & streamer	34.57
0.000003	21949.45	26.42214	$18 \leq We_g < 45$	bag & streamer	36.63
...	...	...	...	...	...
...	...	...	...	...	...
0.011498	8749.402	10.53426	$We_g < 12$	No breakup	970.16
0.011499	8747.917	10.53247	$We_g < 12$	No breakup	970.81
0.0115	8746.434	10.53069	$We_g < 12$	No breakup	971.46

## A.5. Calculation of droplet Evaporation

There is a strong linking of evaporation rate and gas conditions and for this reason; a combined calculation of heat and mass transfer processes have been deliberated. The evaporation of secondary droplets is calculated using the following correlations.

$$\dot{m}_{evp} = d_{drop} \pi \rho D_f \ln \left[ \frac{1 - Y_{f,\infty}}{1 - Y_{f,R}} \right] Sh \quad (\text{A.10})$$

$$Sh = 2.0 + 0.6 Re^{1/2} Sc^{1/3} \quad (\text{A.11})$$

Liquid vapour mass outside boundary,  $Y_{f,\infty}$  is calculated by considering 40% relative humidity assumed has been considered for calculations. The value of liquid vapour mass outside boundary is given in Table A.3.

**Table A.3: Liquid vapor mass outside the boundary**

Relative Humidity (%)	Liquid vapour mass outside the boundary, $Y$
10	0.002152083
20	0.0043045
30	0.00645675
40	0.008609167
50	0.010760833
60	0.012913333
70	0.015065833

To calculate liquid vapour mass at droplet surface,  $Y_{f,R}$  is calculated for 20°C. It is calculated using saturation pressure, maximum humidity ratio and molecular mass of air and water given in Table A.4. The following expression has been used to calculate vapour mass at droplet surface.

$$Y_{f,R} = \frac{P_{vap}(T_1)}{P_{out}} \frac{Mw_{liq}}{Mw_{mix,R}} \quad (\text{A.12})$$

**Table A.4: Saturation vapour pressure**

<b>Temperature (°C)</b>	<b>Saturation Pressure of Water Vapour(Pa)</b>
0	609.9
5	870
10	1225
15	1701
20	2333
25	3130
30	4234

The effect of an increased mass transfer due to relative velocity between the droplets and surrounding gas has been calculated and the final droplet sizes that are remained in the domain are presented here.

$V_{drop}$ (m/s)	$Re$	$Sh$	$\dot{m}_{evp}$	Remaining mass (kg)	$d_{drop}$ ( $\mu\text{m}$ )
100.7273	194.1073026	8.206789	3.51E-12	8.55E-13	11.77
96.70915	198.238389	8.27249	4.11E-12	1.15E-12	12.95
93.14552	202.1195824	8.333595	4.75E-12	1.49E-12	14.172
...	...	...	...	...	...
...	...	...	...	...	...
12.76217	588.1413864	12.80406	1.19E-08	4.78E-08	450.49
12.75683	588.2877257	12.8054	1.19E-08	4.79E-08	450.80
12.7515	588.4339552	12.80675	1.19E-08	4.8E-08	451.11

## **A.6. Characteristic diameters, characteristic velocities**

For spray characterization purpose, Sauter Mean Diameter  $d_{32}$ , volumetric mean diameter  $d_{43}$  are defined as:

$$d_{32} = \frac{\sum_{i=1}^N d_i^3}{\sum_{i=1}^N d_i^2} \quad \text{and} \quad d_{43} = \frac{\sum_{i=1}^N d_i^4}{\sum_{i=1}^N d_i^3} \quad (\text{A.13})$$

Here, the Sauter mean diameter (SMD) and Volumetric mean diameters have been calculated by considering the secondary droplets after evaporation for whole spray (spray in all considered directions). Table A.5 shows the comparison of experimental values of Sauter mean diameter and characteristic velocities with that of calculated using above mentioned model.

**Table A.5: Comparison of experimental and Calculated values**

Parameters	Experimental	Calculated
Sauter Mean Diameter (SMD), $d_{32}$	344 $\mu\text{m}$	340.62 $\mu\text{m}$
Maximum velocity, $V_{\text{max}}$	116 m/s	100.72 m/s
Root mean square velocity, $V_{\text{r.m.s}}$	19.4 m/s	24.45 m/s

## A.7. Spreading of droplet front

To determine the spreading of droplet

$$\frac{dv}{dt} = \frac{3}{8} C_D \frac{\rho_g}{\rho_D} \frac{|U_{rel}|}{r_{drop}} U_{rel} + g_{component} \quad (\text{A.14})$$

Calculations for each considered angle is done and average distance covered by droplet's spray fronts are shown as following;

Duration	0.1 s	0.2 s	0.4 s	0.6 s	0.8 s	1.0 s
90° upside	1.27	2.289	2.9956	3.3716	3.5172	3.535
45° upside	1.27	2.317	3.1085	3.6255	3.9686	4.1764
0° horizontal	1.27	2.379	3.3555	4.1788	4.9285	5.6186
45° downside	1.279	2.414	3.4879	4.4073	5.1999	5.866
90° downside	1.279	2.4143	3.4956	4.4966	5.517	6.596

Spreading of liquid fronts for selected experimental case is visualized in transient manner in Figure A.1.

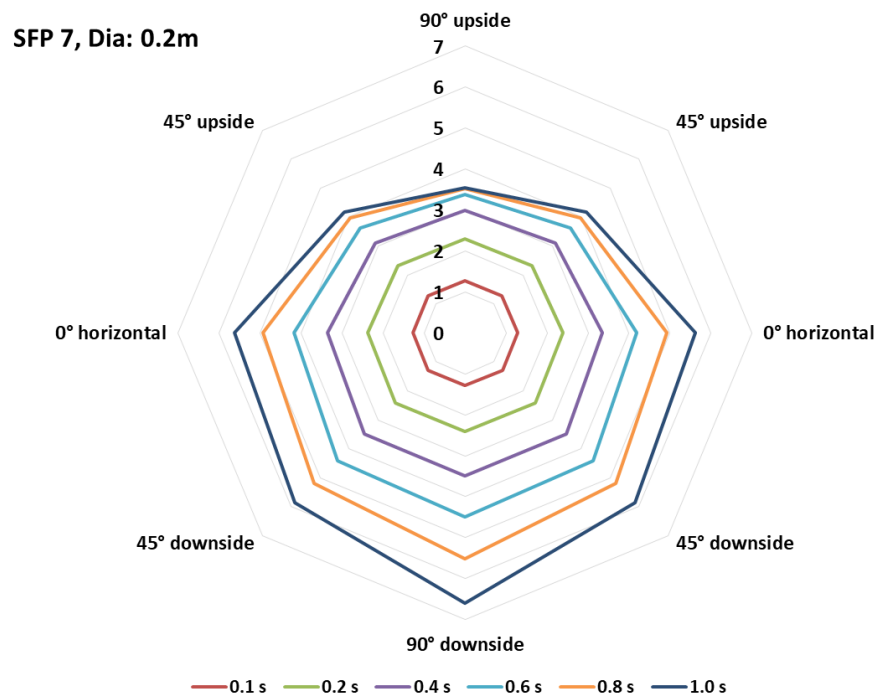


Figure A.1: Transient behaviour of liquid spary fronts



## REFERENCES

---

- Abbasi, T., Abbasi, S.A., 2007. The boiling liquid expanding vapour explosion (BLEVE): Mechanism, consequence assessment, management. *J. Hazard. Mater.* 141, 489–519.
- Abbott, J.A., 1990. *Prevention of Fires and Explosions in Dryers: A User Guide*. IChemE.
- Arcoumanis, C., Gavaises, M., French, B., 1997. Effect of fuel injection processes on the structure of diesel sprays. *SAE Technical Paper*.
- Armenio, V. and Fiorotto, V., 2001. The importance of the forces acting on particles in turbulent flows. *Physics of Fluids*, 13(8), pp.2437-2440.
- Arturson, G., 1981. The Los Alfaques disaster: a boiling-liquid, expanding-vapour explosion. *Burns* 7, 233–251.
- Ashgriz, N., 2011. *Handbook of Atomization and Sprays, Theory and*. ed. Springer. <https://doi.org/10.1007/978-1-4419-7264-4>
- Bader, B.E., Donaldson, A., Hardee, H.C., 1971. Liquid-propellant rocket abort fire model. *J. Spacecr. Rockets* 8, 1216–1219.
- Baker, W.E., Kulesz, J.J., Ricker, R.E., Westine, P.S., Parr, V.B., Vargas, L.M., Moseley, P.K., 1978. *Workbook for estimating effects of accidental explosions in propellant ground handling and transport systems*.
- Baum, H.R., Rehm, R.G., 2005. A simple model of the World Trade Center fireball dynamics. *Proc. Combust. Inst.* 30, 2247–2254. <https://doi.org/10.1016/j.proci.2004.08.125>
- Baumgarten, C., 2006. *Mixture Formation in Internal Combustion Engine*. Springer-Verlag Berlin Heidelb. 294. <https://doi.org/10.1007/3-540-30836-9>
- Bird R B, Stewart W E, L.E.N., 1974. *Transport phenomena, Heat and Mass Transfer*.
- Branch, G.B.D. of T.A.A.I., 1990. *Report on the accident to Boeing 747-121, N739PA at Lockerbie, Dumfriesshire, Scotland on 21 December 1988*. HMSO.
- Brennen, C.E., 2005. *Fundamentals of Multiphase Flow*. Cambridge university press, Cambridge. <https://doi.org/10.1017/CBO9780511807169>
- Carlsson, J., 1999. *Fire Modeling Using CFD-An introduction for Fire Safety Engineers*.
- CCPS, 1999. *Guidelines for consequence analysis of chemical releases*. Wiley-AIChE.
- Chase, M., 1998. *NIST-JANAF Thermochemical Tables, NIST Chemistry WebBook, NIST Stand. ed.*
- Coppalle, A., Vervisch, P., 1983. The total emissivities of high-temperature flames. *Combust. Flame* 49, 101–108.
- Cruz, A.M., Steinberg, L.J., Luna, R., 2001. Identifying hurricane-induced hazardous material release scenarios in a petroleum refinery. *Nat. Hazards Rev.* 2, 203–210.
- CSB, 1998. *U.S. Chemical Safety Board , Investigation Report Propane Tank Explosion (2*

Deaths, 7 Injuries).

- Dombrowski, N., Johns, W.R., 1963. The aerodynamic instability and disintegration of viscous liquid sheets. *Chem. Eng. Sci.* 18, 203–214. [https://doi.org/10.1016/0009-2509\(63\)85005-8](https://doi.org/10.1016/0009-2509(63)85005-8)
- Droste, B., 1999. Die Untersuchung extremer Unfalleinwirkungen auf Transportbehälter für radioaktive Stoffe.
- Droste, B., Probst, U., Heller, W., 1999. Impact Of An Exploding Lpg Rail Tank Car Onto A Castor Spent Fuel Cask. *Nucl. Technol. Publ.* 10, 231–240.
- Engel, O.G., 1955. Waterdrop collisions with solid surfaces. *J. Res. Natl. Bur. Stand.* (1934). 54, 281. <https://doi.org/10.6028/jres.054.033>
- Ertesvåg, I.S., Magnussen, B.F., 2000. The eddy dissipation turbulence energy cascade model. *Combust. Sci. Technol.* 159, 213–235.
- Fay, J.A., Lewis, D.H., 1977. Unsteady burning of unconfined fuel vapor clouds, in: *Symposium (International) on Combustion*. Elsevier, pp. 1397–1405.
- FEMA, 2001. World Trade Center Building Performance Study, Executive Summary.
- Forasassi, G., Lofrano, R., 2010. Preliminary analysis of an aircraft impact (CERSI-UNIPRI RL 1059/2010) 31.
- Gouse, S.W., Brown, G.A., Brown, G., 1964. A survey of the velocity of sound in two-phase mixtures. ASME.
- Gupta, A., Kumar, R., 2010. Droplet impingement and breakup on a dry surface. *Comput. Fluids* 39, 1696–1703. <https://doi.org/10.1016/j.compfluid.2010.06.006>
- Hardee, H.C., Lee, D.O., 1975. Expansion of clouds from pressurized liquids. *Accid. Anal. Prev.* 7, 91–102.
- Hardee, H.C., Lee, D.O., Benedick, W.B., 1978. Thermal hazard from LNG fireballs. *Combust. Sci. Technol.* 17, 189–197.
- Harlow F.H. and Shenon, 1967. Splash of liquid Droplet. *J. Applphys* 38, 3855–3866.
- Hasegawa, K., Sato, K., 1977. Study on the fireball following steam explosion of n-pentane. *Second Int. Symp. Loss Prev. Saf. Promot. Heidelb.* 297–304.
- Haworth, D.C., 2005. A review of turbulent combustion modeling for multidimensional in-cylinder CFD. SAE Technical Paper.
- Hayden, M.S., Shanahan, D.F., Chen, L.-H., Baker, S.P., 2005. Crash-resistant fuel system effectiveness in civil helicopter crashes. *Aviat. Space. Environ. Med.* 76, 782–785.
- High, R.W., 1968. The saturn fireball. *Ann. N. Y. Acad. Sci.* 152, 441–451.
- Hirt, C.W., Nichols, B.D., 1981. Volume of fluid (VOF) method for the dynamics of free boundaries. *J. Comput. Phys.* [https://doi.org/10.1016/0021-9991\(81\)90145-5](https://doi.org/10.1016/0021-9991(81)90145-5)
- Horton, T.W., Kempel, R.W., 1988. Flight test experience and controlled impact of a remotely piloted jet transport aircraft. NASA Tech. Memo. 4084.

- Hostikka, S., Silde, A., Sikanen, T., Vepsä, A., Paajanen, A., Honkanen, M., 2015. Experimental characterisation of sprays resulting from impacts of liquid-containing projectiles. *Nucl. Eng. Des.* 295, 388–402. <https://doi.org/10.1016/j.nucengdes.2015.09.008>
- Hu, Z., Trouve, A., 2008. Numerical simulation of explosive combustion following ignition of a fuel vapor cloud. *Fire Saf. Sci.* 9, 1055–1066. <https://doi.org/10.3801/IAFSS.FSS.9-1055>
- Hymes, I., 1983. The physiological and pathological effects of thermal radiation, SRD R275. UK At. Energy Authority, Culcheth.
- Imsen, B.C., Wierzbicki, T., 1997. Plasticity, fracture and friction in steady state plate cutting. *Int. J. Impact Eng.* 19, 667–691.
- Jackson, K.E., Boitnott, R.L., Fasanella, E.L., Jones, L.E., Lyle, K.H., 2004. A History of Full-Scale Aircraft and Rotorcraft Crash Testing and Simulation at NASA Langley Research Center.
- Jepsen, R., Jensen, K., Hern, T.O., 2004. Water Dispersion Modeling and Diagnostics for Water Slug Impact Test, in: SEM X International Congress. pp. 1–8.
- Johnson, D.M., Pritchard, M.J., 1991. Large Scale Experimental Study of Boiling Liquid Expanding Vapour Explosions (BLEVEs). British Gas plc, Research and Technology Division.
- Joseph M., K., Aldo L., F., George H., M., Agnes C., I., 1969. Crash Fire Hazard Rating System For Controlled Flammability Fuels.
- Keller, W., Modarres, M., 2005. A historical overview of probabilistic risk assessment development and its use in the nuclear power industry: a tribute to the late Professor Norman Carl Rasmussen. *Reliab. Eng. Syst. Saf.* 89, 271–285.
- Kodur, V.K.R., 2002. World Trade Center Building Performance Study: Data Collection, Preliminary Observations, and Recommendations.
- Kuchta, J.M., 1985. Investigation of fire and explosion accidents in the chemical, mining, and fuel-related industries. *Bull./US. Dep. Inter. Bur. mines.*
- Kuchta, J.M., 1973. Fire And Explosion Manual For Aircraft Accident Investigators (No. PMSRC-4193). Bureau Of Mines Pittsburgh Pa Pittsburgh Mining And Safety Research Center.
- Kuo, K.K., 1996. Recent advances in spray combustion: Spray atomization and drop burning phenomena. AIAA.
- Large, J.H., 2003. The implications of 11 September for the nuclear industry, in: Disarmament Forum. pp. 29–38.
- Lees, F., 2012. Lees' Loss prevention in the process industries: Hazard identification, assessment and control, Volume No. ed. Butterworth-Heinemann.
- Lees, F.P., 1996. Loss Prevention in the Process Industries, volume 2. ed.
- Li, X., Koseki, H., Mannan, M.S., 2015. Case study: Assessment on large scale LPG BLEVEs in the 2011 Tohoku earthquakes. *J. Loss Prev. Process Ind.* 35, 257–266.

- Lihou, D.A., Maund, J.K., 1982. Thermal radiation hazard from fireballs, in: IChemE Symp. Series. pp. 191–224.
- Lipton, E., Glanz, J., 2002. First Tower to fall was hit at higher speed, study finds. New York Times, [www.nytimes.com](http://www.nytimes.com) 2, 2.
- Liu, J., Vu, H., Yoon, S.S., Jepsen, R., Aguilar, G., 2010. Splashing Phenomena During Liquid Droplet Impact 20, 297–310.
- Loth, E., 2000. Numerical approaches for motion of dispersed particles, droplets and bubbles. *Progress in energy and combustion science*, 26(3), pp.161-223.
- Luther, W., Müller, W.C., 2009. FDS simulation of the fuel fireball from a hypothetical commercial airliner crash on a generic nuclear power plant. *Nucl. Eng. Des.* 239, 2056–2069. <https://doi.org/10.1016/j.nucengdes.2009.04.018>
- Makhviladze, G., Roberts, J., Yakush, S., 1997. Modelling The Fireballs From Methane Releases. *Fire Saf. Sci.* 5, 213–224. <https://doi.org/10.3801/IAFSS.FSS.5-213>
- Makhviladze, G.M., Roberts, J.P., 2000. Modelling and Scaling of Fireballs from Single-and Two-Phase Hydrocarbon Releases. *Fire Saf. Sci.* 6, 1125–1136.
- Makhviladze, G.M., Roberts, J.P., Yakush, S.E., 1999. Combustion of Two-phase Hydrocarbon Fuel Clouds Released into the Atmosphere. *Combust. Flame* 2180, 583–605.
- Makhviladze, G.M., Yakush, S.E., 2002. Large-scale unconfined fires and explosions. *Proc. Combust. Inst.* 29, 195–210. [https://doi.org/10.1016/S1540-7489\(02\)80028-1](https://doi.org/10.1016/S1540-7489(02)80028-1)
- Makhviladze, G.M., Yakush, S.E., 2000. Combustion of unconfined hydrocarbon vapor-droplet clouds 28, 2851–2858.
- Marshall, V.C., 1987. *Major chemical hazards*. Chichester: Ellis Horwood.
- Martinsen, W.E., Marx, J.D., 1999. An improved model for the prediction of radiant heat from fireball.
- Maurer, B., Hess, K., Giesbrecht, H., Leu~Kel, W., 1977. K. Hess, H. Giesbrecht and W. Leu kel. 2nd Int. Syrup. Loss Prev. Eur. Fed. Chem. Eng. Heidelberg, 305–321.
- McGrattan, K., Hostikka, S., McDermott, R., Floyd, J., Weinschenk, C., Overholt, K., 2013. *Fire dynamics simulator, user's guide*. NIST Spec. Publ. 1019, 20.
- Miguel, A.S., 1978. Antimisting fuel kinematics related to aircraft crash landings. *J. Aircr.* 15, 137–142.
- Mishra, K.B., Wehrstedt, K.D., Krebs, H., 2015. Boiling Liquid Expanding Vapour Explosion (BLEVE) of Peroxy-fuels: Experiments and Computational Fluid Dynamics (CFD) Simulation, in: *Physics Procedia*. Elsevier B.V., pp. 149–152. <https://doi.org/10.1016/j.egypro.2015.02.082>
- Mishra, S.C., Roy, H.K., 2007. Solving transient conduction and radiation heat transfer problems using the lattice Boltzmann method and the finite volume method. *J. Comput. Phys.* 223, 89–107.
- Mlakar, P.F., Dusenberry, D.O., Harris, J.R., Haynes, G., Phan, L.T., Sozen, M.A., 2003. *The*

- Pentagon building performance report. ASCE Reston, VA.
- Modest, M.F., 2003. Narrow-band and full-spectrum k-distributions for radiative heat transfer—correlated-k vs. scaling approximation. *J. Quant. Spectrosc. Radiat. Transf.* 76, 69–83.
- Moorhouse, J., Pritchard, M.J., 1982. Thermal radiation hazards from large pool fires and fireballs—a literature review. *ICHEME Sym Ser Assess. Major Hazards* 397–428.
- Moussa, N.A., 1990. Flammability of aircraft fuels. SAE Technical Paper.
- Mozingo, D.W., Barillo, D.J., Holcomb, J.B., 2005. The Pope Air Force Base aircraft crash and burn disaster. *J. Burn Care Res.* 26, 132–140.
- Muto, K., Sugano, T., Tsubota, H., Kasai, Y., Koshika, N., Suzuki, M., Ohrui, S., Von Rieseemann, W.A., Bickel, D.C., Parrish, R.L., 1989. Full-Scale Aircraft Impact Test for Evaluation of Impact Forces, Part 2: Analysis of the Results.
- NTSB, 2015. Steep Climb and Uncontrolled Descent During Takeoff National Air Cargo, Inc., dba National Airlines Boeing 747 400 BCF, N949CA Bagram, Afghanistan April 29, 2013. 490 L'Enfant Plaza, S.W. Washington, D.C. 20594.
- Park, K., Mannan, M.S., Jo, Y.-D., Kim, J.-Y., Keren, N., Wang, Y., 2006. Incident analysis of Bucheon LPG filling station pool fire and BLEVE. *J. Hazard. Mater.* 137, 62–67.
- Pasandideh-Fard, M., Pershin, V., Chandra, S., Mostaghimi, J., 2002. Splat shapes in a thermal spray coating process: Simulations and experiments. *J. Therm. Spray Technol.* 11, 206–217. <https://doi.org/10.1361/105996302770348862>
- Piers, M., 1998. Methods and models for the assessment of third party risk due to aircraft accidents in the vicinity of airports and their implications for societal risk, in: *Quantified Societal Risk and Policy Making*. Springer, pp. 166–204.
- Pietersen, C., 1985. Analysis of the LPG Accident in San Juan Ixhuatepec, Mexico City, November 19, 1984. TNO. Technical Report. The Hague.
- Piomelli, U., 1999. Large-eddy simulation: achievements and challenges. *Prog. Aerosp. Sci.* 35, 335–362. [https://doi.org/10.1016/S0376-0421\(98\)00014-1](https://doi.org/10.1016/S0376-0421(98)00014-1)
- Pitts, W.M., 1991. Wind effects on fires. *Prog. Energy Combust. Sci.* 17, 83–134.
- Planas-Cuchi, E., Gasulla, N., Ventosa, A., Casal, J., 2004. Explosion of a road tanker containing liquified natural gas. *J. Loss Prev. Process Ind.* 17, 315–321.
- Poinsot, T., Veynante, D., 2001. *Theoretical and Numerical Combustion* (Philadelphia, PA: Edwards).
- Powell, A.E., 2001. September eleventh: The days after, the days ahead. *Civ. Eng.* 71, 36.
- Rajendram, A., Khan, F., Garaniya, V., 2015. Modelling of fire risks in an offshore facility. *Fire Saf. J.* 71, 79–85. <https://doi.org/10.1016/j.firesaf.2014.11.019>
- Ranz, W.E., Marshall, W.R., 1952. Evaporation from drops. *Chem. Eng. Prog* 48, 141–146.
- Raoult, F.M., 1887. General law of the vapor pressure of solvents. *Comptes Rendus* 104, 1430–1433.

- Rehm, R., Pitts, W., Baum, H., Evans, D., Prasad, K., Mcgrattan, K., Forney, G., 2003. Initial Model For Fires In The World Trade Center Towers. *Fire Saf. Sci.* 7, 25–40. <https://doi.org/10.3801/IAFSS.FSS.7-25>
- Reporter Daily Mail, 2013. Did cargo shift cause Bagram 747 crash? Straps that tied down 16-ton MRAP vehicles “broke before plane plummeted to Earth.” Mail Online.
- Roberts, A.F., 1982a. The effect of conditions prior to loss of containment on fireball behaviour. *Assess. major hazards*, (Rugby Instn Chem. Engrs).
- Roberts, A.F., 1982b. Thermal radiation hazards from releases of LPG from pressurised storage. *Fire Saf. J.* 4, 197–212.
- Roberts, T., Gosse, A., Hawksworth, S., 2000. Thermal Radiation from Fireballs on Failure of Liquefied Petroleum Gas Storage Vessels, *Process Safety and Environmental Protection - PROCESS SAF ENVIRON PROT.* <https://doi.org/10.1205/095758200530628>
- Roper, F., Arno, J., Jagers, H.C., 1991. The effect of release velocity and geometry on burning times for non-premixed fuel gas clouds. *Combust. Sci. Technol.* 78, 315–338.
- Saarenheimo, A., Tuomala, M., 2009. Experimental and numerical studies on projectile impacts. *Raken. Mek. (Journal Struct. Mech.* 42, 1–37.
- Sakai, N., Shoji, Y., Jimbo, M., Tanaka, N., 2014. Development of Evaluation Method for Impact of Aircraft Fuel Explosion and Fire on BWR Reactor Building, in: 2014 22nd International Conference on Nuclear Engineering. American Society of Mechanical Engineers, p. V004T10A030-V004T10A030.
- Shelke, A., Maheshwari, N.K., Gera, B., Singh, R.K., 2017. CFD Analysis of Hydrocarbon Fireballs. *Combust. Sci. Technol.* 189, 1440–1466. <https://doi.org/10.1080/00102202.2017.1296433>
- Shentsov, V., Cirrone, D.M.C., Makarov, D., Molkov, V., 2016. Simulation Of Fireball And Blast Wave From A Hydrogen Tank Rupture In A Fire, in: 7th International Symposium on Non-Equilibrium Processes, Plasma, Combustion, and Atmospheric Phenomena, At Sochi, Russia.
- Shih, T.H., Liou, W.W., Shabbir, A., Yang, Z., Zhu, J., 1995. A new  $k-\epsilon$  eddy viscosity model for high reynolds number turbulent flows. *Comput. Fluids.* [https://doi.org/10.1016/0045-7930\(94\)00032-T](https://doi.org/10.1016/0045-7930(94)00032-T)
- Siegel, R., 1992. J. R, Howell. *Therm. Radiat. heat Transf.*
- Silde, A., Hostikka, S., Kankkunen, A., 2011. Experimental and numerical studies of liquid dispersal from a soft projectile impacting a wall. *Nucl. Eng. Des.* 241, 617–624. <https://doi.org/10.1016/j.nucengdes.2010.07.033>
- Skřínská, J., Tetub, G., Skřínkác, M., Marekd, J., Slukae, V., Pražáková, M., Malý, S., 2013. Validation possibilities of the BLEVE thermal effects. *JOSRA* 2.
- Smith, T.F., Shen, Z.F., Friedman, J.N., 1982. Evaluation of coefficients for the weighted sum of gray gases model. *J. Heat Transfer* 104, 602–608.
- Sugano, T., Tsubota, H., Kasai, Y., Koshika, N., Orui, S., von Riesemann, W.A., Bickel, D.C., Parks, M.B., 1993. Full-scale aircraft impact test for evaluation of impact force. *Nucl.*

- Eng. Des. 140, 373–385. [https://doi.org/10.1016/0029-5493\(93\)90119-T](https://doi.org/10.1016/0029-5493(93)90119-T)
- The Guardian, 2015. Crash of Boeing 747 in Afghanistan caused by shifting cargo.
- Thomson, R.G., Caiafa, C., 1982. Designing for aircraft structural crashworthiness. *J. Aircr.* 19, 868–874.
- Tieszen, S.R., 1995. Fuel Dispersal Modeling for Aircraft-Runway Impact Scenarios. Sandia Natl. Labs., Albuquerque, NM (United States).
- TNO Yellow Book, 1989. Methods for the calculation of the physical effects of the escape of dangerous material, Rijswijk, The Netherlands: TNO. Chapter 6.
- Utilities, 2018. All India installed capacity (in mw) of power stations [WWW Document]. URL [http://www.cea.nic.in/reports/monthly/installedcapacity/2018/installed\\_capacity-03.pdf](http://www.cea.nic.in/reports/monthly/installedcapacity/2018/installed_capacity-03.pdf) (accessed 8.17.18).
- Vander Wal, R.L., Berger, G.M., Mozes, S.D., 2006. The splash/non-splash boundary upon a dry surface and thin fluid film. *Exp. Fluids* 40, 53–59.
- Versteeg, H.K., Malalasekera, W., 2005. *An Introduction to Computational Fluid Dynamics - The Finite Volume Method*, Science. <https://doi.org/10.2514/1.22547>
- Von Riesenmann, W.A., Parrish, R.L., Bickel, D.C., Heffelfiner, S.R., Muto, K., Sugano, T., Tsubota, H., Koshika, N., Suzuki, M., Ohri, S., 1989. Full-scale aircraft impact test for evaluation of impact forces, Part 1: Test plan, test method, and test results.
- Wang, K., Liu, Z., Qian, X., Huang, P., 2017. Long-term consequence and vulnerability assessment of thermal radiation hazard from LNG explosive fireball in open space based on full-scale experiment and PHAST. *J. Loss Prev. Process Ind.* 46, 13–22. <https://doi.org/10.1016/j.jlp.2017.01.001>
- Wang, Y., Meredith, K., Chatterjee, P., Krishnamoorthy, N., Zhou, X., Dorofeev, S., 2011. Status of FireFOAM development and future plan, in: 3rd FM Global Open Source CFD Fire Modeling Workshop, Norwood, MA, USA.
- Wierzbicki, T., Hendry-brogan, M., 2002. Aircraft Impact Damage. Access. online <http://web.mit.edu/civenv/wtc/PDFfiles> 31–64.
- Wolfson, M., Klinge-Wilson, D., Donovan, M., Cullen, J., Neilley, D., Liepins, M., Hallowell, R., DiStefano, J., Clark, D., Isaminger, M., 1990. Characteristics of thunderstorm-generated low altitude wind shear: a survey based on nationwide Terminal Doppler Weather Radar testbed measurements, in: *Decision and Control, 1990.*, Proceedings of the 29th IEEE Conference On. IEEE, pp. 682–688.
- Xu et al, 2005. Drop splashing on dry and smooth surface. *phys Rev lett* 94, 505–516.
- Yakush, S.E., Makhviladze, G.M., 2005. Large Eddy Simulation of Hydrocarbon Fireballs Institute for Problems in Mechanics 1–6.
- Yeoh, G.H., Yuen, K.K., 2009. *Computational fluid dynamics in fire engineering: theory, modelling and practice*. Butterworth-Heinemann.